U.PORTO
FEUP FACULDADE DE ENGENHARIA
UNIVERSIDADE DO PORTO

# 3DArm
# Inertial sensor-based 3D upper limb motion tracking and trajectories reconstruction

**Ana Cristina Campos Pereira**

Supervisor at FEUP: Miguel Velhote Correia, PhD

Supervisor at FhP-AICOS: Vânia Guimarães, MSc

Integrated Master in Bioengineering

June, 2016

Faculdade de Engenharia da Universidade do Porto

# 3DArm
# Inertial sensor-based 3D upper limb motion tracking and trajectories reconstruction

**Ana Cristina Campos Pereira**

Dissertation submitted to Faculdade de Engenharia da Universidade do Porto
to obtain the degree of

**Master in Bioengineering**

June, 2016

# Abstract

Upper limb motion tracking plays a major role in several applications such as movement evaluation of workers, gaming, human-machine interaction and medical rehabilitation. There are many systems to perform upper limb tracking - they can be non-visual (inertial), visual (with markers or marker-free) or robot-aided. Despite this variety of tracking systems, they have limitations and some of these systems also consist of specifically designed sensors and tend to be designed for a specific goal, making them unsuitable for acting in all the applications mentioned above. This way, the need for a global upper limb motion tracking solution arises.

For that purpose, the 3DArm - Upper Limb Inertial Tracking System was developed. Based on literature review, this system was built in order to track the upper limb for various applications. In order to do that, two inertial sensors were placed on the upper and lower arms and the upper limb was modeled so that the joints and movements could be described in a global body reference frame. Then, data from inertial sensors were combined through an Extended Kalman Filter sensor fusion method with biomechanical constraints, in order to obtain orientation. The sensors were aligned with each other and with the global body reference frame so that the upper limb position could be described in the global body frame. After finding sensor orientation relative to the global body frame, the upper limb kinematic model was used to reconstruct upper limb motion.

To evaluate the system, 3DArm was compared to Kinect and, in spite of the small deviation between them - a maximum mean error of 10,60 centimeters and 16,33 centimeters for the elbow and wrist joints, respectively - the experimental results demonstrated that the proposed tracking system had an acceptable performance, in different movements. Therefore, 3DArm can be considered a viable tracking system with the advantages of being portable, without occlusion problems, small-sized, unobtrusive, low-cost and lightweight.

Moreover, it was difficult to guarantee that the two sensors were aligned with each other. To overcome this problem, a sensor-to-body frame transformation, without the need of aligning the sensors with each other and with the global body reference frame, was developed. With a calibration movement, each axis of the global body reference frame was defined. The results of the sensor-to-body frame transformation showed that the calculated elbow and wrist positions resulted in errors in the same order as the ones reported when sensors were manually aligned on each arm segment.

Although results were promising, further development of this project is required to potentially improve upper limb motion tracking.

**Keywords:** Upper Limb. Inertial Tracking. Sensor Fusion. Orientation Estimation. Quaternions. Extended Kalman Filter. Trajectory Reconstruction.

# Resumo

O *tracking* do movimento do membro superior tem uma grande importância em várias aplicações, como a avaliação do movimento de trabalhadores, jogos, interacções homem-máquina e reabilitação médica. Existem muitos sistemas de *tracking* do membro superior; estes podem ser não-visuais (inerciais), visuais (com ou sem marcadores) ou assistidos por robôs. Apesar desta variedade de sistemas de *tracking*, estes têm limitações e alguns utilizam sensores específicos concebidos para objectivos muito restritos, tornando-os inadequados para todas as aplicações. Assim, surge a necessidade de uma solução global de *tracking* do movimento do membro superior.

Com isso em mente, foi desenvolvido o *3DArm - Upper Limb Inertial Tracking System*. Baseado numa revisão da literatura, este sistema foi construído de forma a fazer o *tracking* do membro superior para qualquer aplicação. Para isso, foram colocados dois sensores inerciais nos segmentos superior e inferior e o membro superior foi modelado de forma a que as articulações e movimentos pudessem ser descritos num sistema corporal global. De seguida, os dados dos sensores inerciais foram combinados através de um método de *sensor fusion Extended Kalman Filter* com restricções biomecânicas, para obter a sua orientação. Os sensores foram alinhados um com o outro e com o sistema corporal global, de forma a que a posição do membro superior pudesse ser descrita nesse mesmo sistema. Após calculada a orientação relativamente ao sistema corporal global, o modelo cinemático do membro superior foi utilizado para fazer a reconstrução do movimento.

Para avaliar o sistema, o *3DArm* foi comparado com o *Kinect* e, apesar do pequeno desvio entre eles - um erro médio máximo de 10,60 centímetros e de 16,33 centímetros para o cotovelo e pulso respectivamente - os resultados experimentais demonstraram que o sistema de *tracking* proposto tinha uma prestação aceitável, com diferentes movimentos. Desta forma, o *3DArm* pode ser considerado um sistema de *tracking* viável com as vantagens de ser portátil, sem problemas de oclusão, pequeno, não-obtrusivo, barato e leve.

Foi difícil garantir que os dois sensores estavam efectivamente alinhados um com o outro. Para ultrapassar este problema, foi desenvolvida uma transformação de sistema sensor-para-corpo que não requer o alinhamento dos sensores consigo próprios nem com o sistema corporal global. Com um movimento de calibração, cada eixo do sistema corporal global foi definido. Os resultados da transformação de sistema sensor-para-corpo mostraram que as posições do cotovelo e pulso calculadas originaram erros da mesma ordem que os erros quando os sensores eram manualmente alinhados em cada segmento do braço.

Apesar de os resultados serem promissores, é necessário mais desenvolvimento deste projecto de forma a potencialmente melhorar o *tracking* do membro superior.

**Keywords:** Membro Superior. *Tracking* Inercial. *Sensor Fusion*. Estimação da Orientação. Quaterniões. *Extended Kalman Filter*. Reconstrução de Trajectórias.

# Acknowledgments

Em primeiro lugar, gostaria de agradecer à Faculdade de Engenharia da Universidade do Porto por toda a educação e conhecimento que me proporcionou ao longo destes cinco anos. Ao professor Miguel Velhote Correia, pela orientação na minha dissertação, pelo seu apoio e experiência. À Fraunhofer Portugal AICOS, pelas instalações e equipamento que tornarem possível a realização do meu trabalho. À minha orientadora Vânia Guimarães, pelo apoio, conhecimento, sugestões, motivação e esforço para que tudo corresse sempre da melhor maneira, pela disponiblidade para todos os assuntos, desde os mais simples aos mais complexos.

Um grande obrigada a todos os meus amigos que marcaram estes cinco anos e os tornaram no mínimo inesquecíveis.

O obrigada ao Miguel, por tudo e mais alguma coisa. Pelos conselhos, avisos, pela grande força e motivação incondicionais. Por ter-me feito acreditar em mim e no meu trabalho. Por ser tão chato e tão preocupado e por estar motivado a aprender as lides da casa.

Um último obrigada, mas não menos importante, aos meus pais, irmão e infinita família. Aos meus pais por terem permitido tudo isto ser possível e apoiarem-me em todos os momentos. Ao João, por termos crescido juntos e continuarmos a crescer. À família toda, aos grandes Santas, aos meus avôs que estão lá a olhar por mim, e às minhas avós, as mulheres mais fortes que conheço.

Ana Pereira

# Contents

# List of Figures

# List of Tables

# List of Abbreviations

| | |
|---|---|
| CF | Complementary Filter |
| DOF | Degree of Freedom |
| EKF | Extended Kalman Filter |
| FEUP | Faculdade de Engenharia da Universidade do Porto |
| FhP-AICOS | Fraunhofer Portugal Research Center for Assistive Information and Communication Solutions |
| GB | Global Body |
| IMU | Inertial Measurement Unit |
| ISP | Integrated Sensor Pack |
| KF | Kalman Filter |
| MMSE | Minimum Mean Square Error |
| VR | Virtual Reality |

# Chapter 1

# Introduction

Upper limb motion tracking has become an extensive research topic in the human motion tracking studies. This is due to its broad range of applications, including movement evaluation of workers, gaming, human machine interaction and medical rehabilitation [1].

Movement evaluation of workers takes place in the factories and it is most needed for workers who execute repetitive tasks during their working day. Many industrial work tasks involve extensive arm and hand movements (e.g. short-cyclic assembly and packaging tasks), which are associated with an increased prevalence of musculoskeletal disorders on the neck, shoulders, arms and hands [2]. Thus, an upper limb tracking system can evaluate the worker's movements and obtain several metrics, such as movement amplitude, in order to understand the prevalence of these disorders [3].

Moreover, a new generation of video game consoles enables video gamers to employ active body movements as interaction mode. To achieve a movement-based interaction, the interfaces have to analyze the movement patterns of their users in order to identify them. This is not a trivial task as the human body, in particular the upper limb, is complex and has a large number of degrees of freedom [4]. Tracking the upper limb is one of the main objectives of these video consoles, which is achieved through different techniques, like video and inertial tracking.

Besides this, the study of automatic and natural modes of interaction between humans and machines is an important field of research. For this purpose, it is clearly important not only to locate potential users but also to obtain information about their body posture and arm configurations. This task can be complicated due to the high dimensionality of the upper-body and the often unpredictable motion of the arms, so a tracking system is necessary to continuously monitor the upper limb motion [5]. One application of human machine interface is the use of robotics in rehabilitation therapies, since robots are certainly well suited to precisely perform repetitive and mechanically power consuming rehabilitation tasks [6].

Furthermore, major disabilities require extensive rehabilitation programmes in order to treat disabled individuals and prepare them for independent living. The intense repetitions of coordinated motor activities during rehabilitation constitute a significant burden for the therapists assisting patients. In addition, and due to economical reasons, the duration of primary rehabilitation is

becoming increasingly shorter, since rehabilitation in a hospital-based environment is very expensive to the National Health Service and health insurers due to specialists, therapy staffs and the time required. To address this problem, trajectories during rehabilitation have to be quantified and the need for a motion tracking system emerges to allow a rehabilitation process at home. Data on the progress of the patient undertaking home-based rehabilitation could be then passed onto therapists or experts remotely for evaluation. The patients could then adjust their exercises based on the feedback from the therapists or expert systems [7, 8]. Additionally, new rehabilitation tools based on Virtual Reality (VR) and serious games are being developed and have recently gained significant interest in the physical therapy area. These tools also rely on an upper limb tracking system [9].

## 1.1 Problem Identification

There are many methods and systems to perform upper limb tracking; they can be non-visual (inertial), visual (with markers or marker-free) or robot-aided. Despite this variety of tracking systems, they have some limitations. In summary, an inertial system suffers from drift, a visual system is space-limited, which means that the tracking only occurs within the space where the camera is, and the robot-aided system cannot allow a subject to freely move his/her arm [10]. Another challenge is cost, since people tend to build complicated tracking systems in order to satisfy multiple purposes. These require expensive components on designed systems. Some of these systems also consist of specifically designed sensors, which limit the further development and broad application of the designed systems [7].

The problem identified is the non-existence of an unique portable low-cost system that can be worn in a non-intrusive way by people, allowing a real time upper limb tracking. This happens because the existing systems are focused on a single application, making it difficult for its re-utilization in other contexts.

This way, the problem relies on the need for an upper limb tracking system that can be used by all people in several different contexts, like the applications mentioned above. The system needs to be low-cost and wearable in different environments, allowing a real time tracking.

## 1.2 Motivation and Objectives

Movement can be measured using a wide variety of techniques and sensors. Several successful examples have existed in literature for the application of inertial sensor based systems in the measurements of upper limb movements [11].

Considering the problem mentioned above and the drawbacks of the current tracking techniques, an inertial low-cost tracking system should be the solution. Wearable inertial sensors have the advantages of being small-sized, unobtrusive, low-cost, lightweight and self-contained. Despite the drift problem, once it is corrected, inertial sensors are well suited for recording long-term

monitoring procedures while the subject performs normal activities of daily life at home or at work [11].

Developing an inertial tracking system can have numerous applications in different fields: movement evaluation of workers, gaming, human machine interaction and medical rehabilitation. This is possible because an inertial system can undergo a process of sensor-to-body frame transformation, enabling every person to place the sensors on the arm in a correct way. With an inertial tracking system, it is possible to obtain the upper limb movement and its trajectories, which can be evaluated in real time, enabling the extraction of distinct characteristics (for instance, the movement amplitude, the angle between segments, the movement velocity, etc.) each one more suitable for distinct applications.

In the movement evaluation of workers, an inertial system would be useful to track the movements during the different tasks, since it is a portable system that can follow all the worker's movements. In gaming, an inertial tracking system overcomes the problem of the user being limited to a certain space in front of the console (like in the Xbox) or having to hold a remote control (like in Nitendo Wii). For a human-machine interaction, an inertial system provides a real-time tracking, allowing for a real time interaction. In rehabilitation, a system like this will provide a home-based rehabilitation, allowing the patient to perform upper limb exercises at home and, at the same time, to be followed by the therapists without the need to go to the medical facilities.

As it can be seen, the development of an inertial motion tracking system can be useful for a variety of applications and not specifically or exclusively for any of them. The tracking system could be used in every situation and can accompany the person's upper limb movement during the day [12].

Therefore, the main objective of this dissertation is to develop a wearable inertial tracking system to estimate orientation and find the motion trajectories of the humam upper limb. The motion trajectories will be estimated by combining sensor fusion and orientation tracking with biomechanical constraints of the upper limb that will take into account the relationships between each arm segment and the human motion limitations. To avoid the burden of manually aligning the sensors to each other and with the mounted arm segment, an automatic method to discover the alignment of the sensors relative to the arm segments will be studied.

## 1.3 Dissertation Structure

This dissertation is organized in chapters, each one covering a specific topic, and these are subdivided in sections that focus on specific subjects of the said topic.

In Chapter 1 – Introduction, the main purpose is making a first approach of the context and objectives that will be fulfilled in this dissertation and also describing its structure.

In Chapter 2 – Background and Literature Review, the objective is to present an extended overview on upper limb motion tracking and trajectory reconstruction is made. Firstly, there is a description of the modeling of the upper limb movement, based on the joints and range of motion and the kinematic model itself. Secondly, there is a description of inertial measurement unit sensor

fusion, based on the sensors and the orientation representation. Lastly, there is also a strong focus on how inertial upper limb tracking and sensor-to-body processes have been applied in research studies by several authors.

In Chapter 3 – 3DArm - Upper Limb Inertial Tracking System, the work developed in order to obtain an upper limb inertial tracking system will be described. There is a description of the methods implemented and how the system was evaluated, presenting its results and introducing future improvements.

In Chapter 4 – Sensor-to-Body Frame, the objective is to develop a sensor-to-body frame process in order to avoid the burden of manually aligning sensors. Here, the methodology implemented is described and the results are discussed also introducing future improvements.

In Chapter 5 – Conclusions and Future Work, a description of what was achieved in this dissertation is shown and future developments are referenced.

# Chapter 2

# Background and Literature Review

This Chapter provides a review of the fundamental topics regarding the upper limb motion tracking and its trajectories reconstruction. Firstly, the modeling of the upper limb is described considering its anatomy and representation in a coordinate frame. Then, inertial tracking is presented as an efficient option to measure upper limb movements and positions. Inertial sensors are described, sensor fusion for orientation estimation is explained based on these sensors, and the methods to represent the orientation output from sensor fusion are presented. With the orientation of each arm segment and with the kinematic model considered before, the upper limb trajectories can be reconstructed. In this part, a review of the work developed in this area is described. Lastly, a sensor-to-body frame process is presented in order to avoid the burden of manually aligning the sensors with each arm segment.

## 2.1 Modeling of the Upper Limb Movement

Compared to lower limb activity monitoring, the upper limb is more difficult due to a number of complications. Firstly, the higher number of degrees of freedom (DOF) of the upper limb joints means that different people can exhibit entirely different motions for the same activity, and within-subject motions may vary for the same activity. Secondly, the activity may be performed differently depending on physical conditions and surroundings. Lastly, there are no strong, identifiable signatures that distinguish upper body motions. Therefore, few research has been published on activity classification in the domain of upper limb motion, since it is difficult to classify a healthy or unhealthy movement, except those aimed at classifying a strictly defined activity set [13].

The main purpose of modeling the upper limb movement is to define an upper limb model and a reference frame where the positions, and consequently the trajectories of the upper limb movement, will be described.

### 2.1.1 Upper Limb Joints and Movements

The upper limb skeletal system is divided in four main structures: pectoral girdle, arm, forearm and hand, depicted in Figure 2.1 [14]. Since the first three structures are the ones involved in the

movement of the arm and forearm, those are the most relevant for upper limb motion tracking, which will be developed in the dissertation. The hand is the most distal part of the upper limb and its movement does not influence upper limb motion tracking.

In order to perform the tracking of its movement, it is important to understand which movements the upper limb can execute and which joints are involved in those movements.

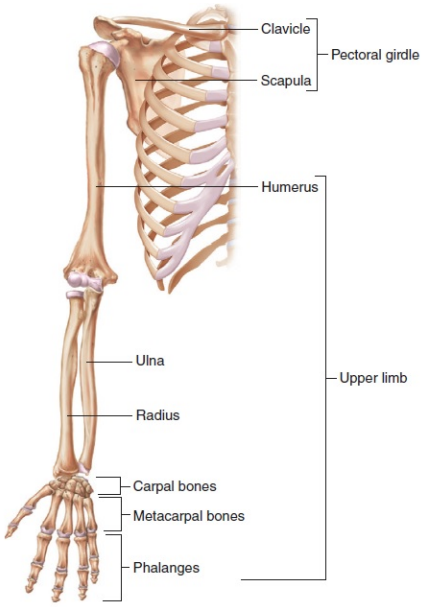


Figure 2.1: Representation and bone configuration of the four structures (pectoral girdle, arm, forearm and hand) of the upper limb [14].

#### 2.1.1.1 Joints

Muscles pull on bones to make them move, but movement would not be possible without the joints between the bones. A joint is a place where two or more bones come together. The joints are commonly named according to the bones or portions of bones that join together [14]. Regarding the upper limb, there are two fundamental joints:

- **Shoulder Joint** - the shoulder joint, or *glenohumeral joint*, is a ball-and-socket joint (Figures 2.2a and 2.2b) in the arm segment. The rounded head of the humerus articulates with the shallow glenoid cavity of the scapula.

- **Elbow Joint** - the elbow joint is a compound hinge joint (Figures 2.2c and 2.2d) consisting of the **humeroulnar joint**, between the humerus and ulna, and the **humeroradial joint**, between the humerus and radius. The elbow joint is surrounded by a joint capsule.

(a) Ball and socket

(b) Glenohumeral

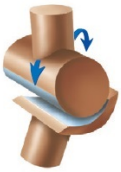

(c) Hinge

(d) Cubital

Figure 2.2: Upper Limb Joints [14].

#### 2.1.1.2 Movements

A joint's structure relates to the movements that occur at that joint. Different basic movements occur in different combinations in the body joints. Regarding the upper limb, two types of movements can be considered:

- **Angular Movements** - in angular movements, one part of a linear structure, such as the trunk or a limb, bends relatively to another part of the structure, thereby changing the angle between the two parts. The most common angular movements are **flexion** and **extension** and **abduction** and **adduction**. Flexion is a bending movement in which the relative angle of the joint between two adjacent segments decreases. Extension is a straightening movement in which the relative angle of the joint between two adjacent segments increases as the joint returns to the zero or reference position. Abduction is a movement away from the midline of the body or the segment. Lastly, adduction is the return movement of the segment back toward the midline of the body or segment [14, 15].

- **Circular Movements** - Circular movements involve rotating a structure around an axis or moving the structure in an arc. The most common circular movements are **supination** and **pronation**, **rotation** and **circumduction**. Supination and pronation refer to the unique rotation of the forearm. Supination is the movement of the forearm in which the palm rotates to face forward from the fundamental starting position. Pronation is the movement in which the palms face backwards. Rotation is the turning of a structure around its long axis, as in rotating the head, the humerus, or the entire body. Medial rotation of the humerus with the forearm flexed brings the hand toward the body. Lateral rotation of the humerus moves the hand away from the body. Lastly, circumduction is a combination of flexion, extension, abduction, and adduction [14, 15].

The range of motion describes the amount of mobility that can be demonstrated in a certain joint [14]. As mentioned before, the most important joints when studying the movement of the

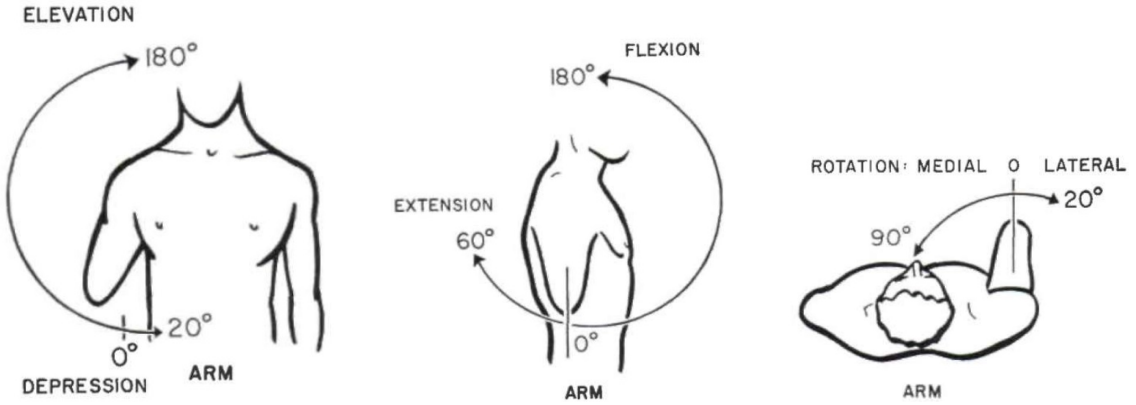


(a) Elevation and depression (b) Flexion and extension (c) Medial and lateral rotation

Figure 2.3: Simplified movement system in the arm [16].

upper limb are the shoulder joint and the elbow joint, since they determine the range of motion of the arm and forearm. The following values of range of motion in each type of movement are relative to the anatomical position (the position where it is not exerted any force to move it). Those values were estimated from average body measurements [16], on which the shoulder-elbow length was estimated at 36,33 centimeters and the elbow-hand length was estimated at 47,49 centimeters.

**Shoulder Joint**

The shoulder or glenohumeral joint can perform several types of movements, such as flexion, extension, abduction, adduction, rotation and circumduction [14]. The glenohumeral joint is responsible for the movement of the arm. The arm is able to elevate itself up to 180° and suffer a depression of 20° (in this case, elevation and depression corresponds to adduction and abduction, respectively), while its flexion movement may reach 180° and its extension may reach 60°. The arm is also able to perform rotation movements of 90° to the medial side and 20° to the lateral side [16]. All this type of movements and range of motion are depicted in Figure 2.3.

**Elbow Joint**

The radiohumeroulnar joint is able to move itself through flexion, extension, pronation and supination, since it is a combination of both the humeroulnar joint, responsible for flexion and extension, and the humeoradial joint, that allows pronation and supination. This joint is responsible for the movement of the forearm [14]. The forearm is able to withstand flexions up to 140° , but the extension capacity is close to 0°. Additionally it can perform a supination of 80° and pronation of 90° [16]. These movements and range of motion are depicted in Figure 2.4.

#### 2.1.1.3 Bio-mechanical Constraints

As mentioned before, each of the upper limb joints has its range of motion, so a constraint to the upper limb movement could be the range of motion for each movement.


(a) Supination and Pronation (b) Flexion and extension

Figure 2.4: Simplified movement system in the forearm [16].

Another constraint is based on the fact that the elbow of a healthy subject can only admit two DOFs, namely, flexion/extension and pronation/supination, so abduction/adduction of the elbow is nearly impossible [17].

These restrictions will be later useful to define the upper limb model.

### 2.1.2 Kinematic Model

To describe joint movements, a reference system where the movements will be represented is necessary. Also, in order to describe the movements performed by the upper limb it is necessary to consider a model which corresponds to the upper limb, taking into account the concepts described above. The next sections will explain how the movements are characterized and how the upper limb is modeled.

#### 2.1.2.1 Joint Reference Systems

To specify the position of the body, segment, or object, a reference system is necessary so as to describe motion or identify whether any motion has occurred. The reference frame or system is arbitrary and may be within or outside of the body. The reference frame consists of imaginary lines called axes that intersect at right angles at a common point termed the origin. The origin of the reference frame is placed at a designated location such as a joint center. The axes are generally given letter representations to differentiate the direction in which they are pointing. Any position can be described by identifying the distance of the object from each of the axes. In a three-dimensional movement, there are three axes, two horizontal axes that form a plane and a vertical axis. It is important to identify the frame of reference used in the description of motion.

The universally used method of describing human movements is based on a system of planes and axes. A plane is a flat, two-dimensional surface. Movement is said to occur in a specific plane if it is actually along that plane or parallel to it. Movement in a plane always occurs about an axis of rotation perpendicular to the plane, which is depicted in Figure 2.5. These planes allow full description of a motion.

The movement in a plane can also be described as a single DOF. This terminology is commonly used to describe the type and amount of motion structurally allowed by the anatomical joints. A

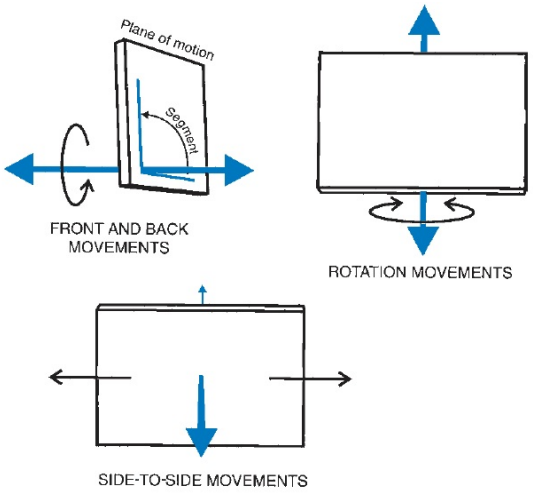


Figure 2.5: The plane and axis. Movement takes places in a plane about an axis perpendicular to the plane [15].

joint with one DOF indicates that the joint allows the segment to move through one plane of motion. A joint with one DOF is also termed uniaxial because one axis is perpendicular to the plane of motion about which movement occurs [15].

In summary, anatomical movement descriptors should be used to describe segmental movements. This requires the knowledge of the starting position (anatomical), standardized use of segment names (arm, forearm, hand, thigh, leg, and foot), and the correct use of movement descriptors (flexion, extension, abduction, adduction, and rotation).

All movements, joints, DOFs and related structures are summarized in Table 2.1.

Table 2.1: Movement Review

| Segment | Joint | Stuctures Joined | DOF | Movements |
|---|---|---|---|---|
| Arm | Glenohumeral | Scapula<br>Humerus | 3 | Flexion, extension, abduction, adduction, medial and lateral rotation and circumduction |
| Forearm | Humeroulnar | Humerus<br>Ulna | 1 | Flexion and extension |
| | Humeoradial | Humerus<br>Radius | 1 | Pronation and supination |

#### 2.1.2.2 Upper Limb Model

An upper limb model is necessary to model the upper limb segments, joints and movements. The definition of the upper limb model sightly varies from author to author, although, in general, all authors apply the same principles.

Zhou et al. in [18, 19, 20], assume that the human arm motion could be approximated as an articulated motion of rigid body parts. Regardless of its complexity, human arm motion can still be characterized by a mapping describing the generic kinematics of the underlying mechanical

structure. In other words, one assumption to model upper limb motions is to characterize the human arm as two rigid segments, the upper arm and the lower arm. Each of the segments can only rotate about its preceding joints, the shoulder joint or the elbow joint.

The referenced literature states that human arm motions can be represented by kinematic chains. Usually, a 7-DOF model is utilized to kinematically describe the transformation of human arm movements. In this case, the shoulder joint is assumed with three DOFs; the elbow with one DOF, and the wrist with three DOFs [21]. However, in some articles [20] the kinematic chain consists of six joint variables, i.e. three for the shoulder and the others for the elbow, where in the latter the motion of the elbow joint only has one DOF. This assumption of one DOF may not be realistic. For example, it has been discovered that rotation of the forearm (supination/pronation) accompanies regularly repetitive movements.

One example of an upper limb kinematic model is depicted in Figure 2.6, where a 5-DOF model is considered.

In a 5-DOF model there are two frames: the shoulder and elbow frames. Considering an initial posture of standing with arm falling down, for the shoulder and elbow frames, Z axis is from posterior to anterior, X is from left to right and Y axis is from inferior to superior. Considering the DOF of each joint, for the shoulder there will be movement around the three axes (movement around the X axis corresponds to flexion/extension, movement around the Y axis to medial/lateral rotation and movement around the Z axis to elevation/depression) and for the elbow there will be movement around two axes (movement around the X axis corresponds to flexion/extension and movement and movement around Z axis corresponds to pronation/supination).

The kinematic model described will be useful for describing the position and orientation of the upper limb segments, discussed in Section 2.3.

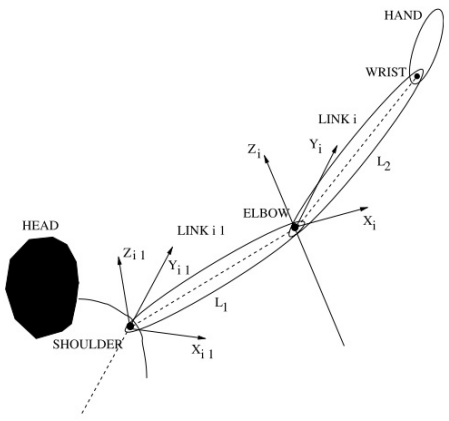


Figure 2.6: Upper limb model [18]. The right arm is depicted viewed from the back, where $L_1$ and $L_2$ represent the upper and lower segments' length, respectively.

## 2.2 Inertial Tracking

Many successful examples exist in literature for the applications of inertial sensor-based systems in the measurement of upper limb movements. Inertial sensors are able to provide accurate readings without inherent latency. They are able to cope with the occlusion problem found in the optical tracking systems. However, accumulating errors (or drifts) are usually found in the measurements by inertial sensors [22]. Wearable inertial sensors have the advantages of being simple, unobtrusive, self-contained, with fewer costs, compact sized, lightweight and no motion constraint. They are well suited to record long term monitoring while the subject performs normal activities of daily life at home [11]. Wearable inertial sensors have become an efficient option to measure the movements and positions of a person [23].

Inertial sensors are described below and, due to their advantages, they have been widely used in upper limb motion tracking, which is described in Section 2.3. Taking into account the main objective of this dissertation, an inertial tracking system will be developed in order to be applied in different contexts and environments (at home or at work) by any person, using a sensor-to-body frame transformation process that will be also developed, which is described in Section 2.4. This way, an inertial tracking system is essential for monitoring upper limb movement and its trajectories in real time, which allows different feature extraction.

This section will enable a better understanding of how an Inertial Measurement Unit operates through its inertial sensors and how it can provide an estimation of orientation by sensor fusion methods.

### 2.2.1 Inertial Measurement Unit

Inertial sensors were first used in the detection of human movements in the 1950s. However, these sensors were not commercially available until, in recent years, their performance had been dramatically improved [24].

Inertial systems normally consist of gyroscopes, accelerometers and magnetometers, whereas a device containing gyroscopes and accelerometers, is commonly called Inertial Measurement Unit (IMU). IMU's are usually used to determine orientation through sensor fusion techniques, which will be discussed in Section 2.2.2. Next, a brief description of each sensor is described.

#### 2.2.1.1 Accelerometers

Usually, an IMU contains a 3 axis accelerometer sensor. A 3 axis accelerometer sensor gives the acceleration measurements in meters per second squared ($m/s^2$) along each of X, Y, Z axes, including the force of gravity. It can be used to recognize the motion activities. The most important source of error of an accelerometer is the bias. The bias of an accelerometer is the offset of its output signal from the true value. It is possible to estimate the bias by measuring the long term average of the accelerometers output when it is not undergoing any acceleration [25].

#### 2.2.1.2 Gyroscopes

A gyroscope sensor provides the angular velocities[1] in radians per second (rad/sec) along each one of the three axes. It can be used to get the orientation of the device while in motion.

However, the problem with gyroscope is that there are bias and numerical errors. The bias of a gyroscope is the average output from the gyroscope when it is not undergoing any rotation. The bias shows itself after integration as an angular drift, increasing linearly over time. Another error arising in gyroscopes is the calibration error, which refers to errors in the scale factors, alignments, and linearities of the gyroscopes. Such errors are only observed whilst the device is turning. Such errors lead to the accumulation of additional drift in the integrated signal, the magnitude of which is proportional to the rate and duration of the motions [25].

#### 2.2.1.3 Magnetometers

Magnetic sensors provide stability in the horizontal plane by sensing the direction of the earth magnetic field like a compass. A magnetometer sensor measures the magnetic field, usually in micro Tesla ($\mu$T), in X, Y, Z axes. It can be used in combination with accelerometer to find the direction with respect to North when linear acceleration is zero. The main source of measurement errors are magnetic interference in the surrounding environment and in the device [25].

### 2.2.2 Sensor Fusion for Orientation Estimation

In geometry, the orientation, also called angular position or attitude, of an object, such as a line, plane or even a human body, is part of the description of how this object is placed in space. By combining the information provided by the IMU, through sensor fusion methods, one is able to calculate and estimate the orientation of an object [26]. The task of a sensor fusion filter is to compute a single estimate of orientation through the optimal fusion of gyroscope, accelerometer and magnetometer measurements [27].

Sensor Fusion is the combination of sensory data or data derived from sensory data such that the resulting information is in some sense better than would be possible when these sources were used individually. The term better in this case can mean more accurate, more complete, or more dependable, or refer to the result of an emerging view, such as orientation estimation [28].

If the gyroscopes would provide perfect measurements of the IMU turn motions, then simple integration of the gyroscope's signal would give the attitude. But since IMUs gyroscopes suffer substantially from noise and drift, other sensors like accelerometers and magnetometers are needed to correct this imperfectness. So to get the best estimate of the IMU attitude, a sensor fusion algorithm as shown in Figure 2.7 is needed to combine the measurements from the different sensors [29].

[1] The angular velocity is the ratio of the angle traversed to the amount of time required to traverse that angle. It can also be measured as the ratio of the velocity to the distance covered.

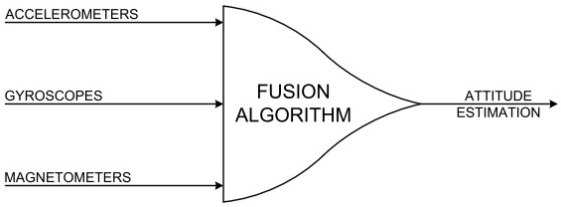


Figure 2.7: Fusion of the different sensor readings in order to get the best attitude estimation [29].

In literature, the orientation estimation using inertial sensors is done mainly using a Kalman Filter (KF) approach. Perez-D'Arpino et al. [29] state that there is an extensive volume of literature considering the solution of the attitude determination problem using Kalman Filter.

The Kalman Filter has become the accepted basis for the majority of orientation filter algorithms and commercial inertial orientation sensors: xsens, micro-strain, VectorNav, Intersense, PNI and Crossbow all produce systems founded on its use [27].

Besides the orientation estimation through accelerometers, gyroscopes and magnetometers measurements, the use of biomechanical geometrical constraints has been explored in the upper limb orientation estimation algorithm. Since the sensors are placed on anatomical structures, with known movement constraints, orientation estimation through sensor fusion can be improved with the incorporation of this information. One example is shown by Veltink et al. [12] that proposed a method for drift-free estimate of the orientations of the two arm segments using inertial sensors. The anatomical elbow constraint of no adduction in elbow joint (explained in Section 2.1.1.3) was considered to compensate drift and revise the orientation estimation.

Therefore, the Kalman Filter is a popular choice for estimating movement in different applications. Since position information is linear, standard Kalman filtering can be easily applied to the tracking problem without much difficulty. However, human pose information also contains nonlinear orientation data, requiring a modification of the KF. The extended Kalman Filter (EKF) provides this modification by linearizing all nonlinear models (i.e., process and measurement models) so the traditional KF can be applied [30].

In order to better understand the behavior of Extended Kalman Filter, its mathematical formulations are explored below. A particular focus is given to the EKF, since it is the appropriated filter for upper limb orientation estimation with bio-mechanical constraints.

#### 2.2.2.1 Kalman Filter

The Kalman filter is essentially a set of mathematical equations that implement a predictor-corrector type estimator that is optimal in the sense that it minimizes the estimated error covariance—when some presumed conditions are met [31]. From a theoretical standpoint, the Kalman filter is an algorithm that allows for an exact inference in a linear dynamical system, which is a Bayesian model, but where the state space of the latent variables is continuous and where all latent and observed variables have a Gaussian distribution [32].

This type of filter is capable of estimating past, present or future states, even if the totality of the model which describes the system is unknown. The algorithm is based in a linear measurement model which operates in two different phases: a prediction phase, in which it conducts a state extrapolation to future time step based on the current step and on the measurements until the moment; and the correction or observation phase, in which a new measurement is added to minimize the estimated error covariance of the estimated current state [33].

It is shown that the Kalman filter is a linear, discrete time, finite dimensional time-varying system that evaluates the state estimate that minimizes estimated error covariance. When either the system state dynamics or the observation dynamics is nonlinear, the conditional probability density functions that provide the minimum error covariance estimate are no longer Gaussian. A non optimal approach to solve the problem, in the frame of linear filters, is the Extended Kalman filter (EKF). The EKF implements a Kalman filter for a system dynamics that results from the linearization of the original non-linear filter dynamics around the previous state estimates[31].

**Extended Kalman Filter**

The Kalman filter addresses the general problem of trying to estimate the state $x \in \Re^n$ of a discrete-time controlled process that is governed by the linear stochastic difference equation 2.1 with a measurement $z \in \Re^m$ that is defined in equation 2.2 [34]:

$$x_k = Ax_{k-1} + w_{k-1} \tag{2.1}$$

$$z_k = Hx_k + v_k \tag{2.2}$$

The random variables $w_k$ and $v_k$ represent the process and measurement noise (respectively). They are assumed to be independent (of each other), white, and with normal probability distributions, described in equations 2.3 and 2.4 where $Q$ and $R$ represent the *process* and *measurement noise covariance*, respectively [34].

$$p(w) \sim N(0, Q) \tag{2.3}$$

$$p(v) \sim N(0, R) \tag{2.4}$$

What happens if the process to be estimated and (or) the measurement relationship to the process is non-linear is the following: in something similar to a Taylor series, the estimation around the current estimate could be linearized using the partial derivatives of the process and measurement functions to compute estimates, even in the face of non-linear relationships. Let's assume that the process has a state vector $x \in \Re^n$, but is now governed by the *non-linear* stochastic difference equation 2.5, with a measurement $z \in \Re^m$ defined by equation 2.6 [34],

$$x_k = f(x_{k-1}, w_{k-1}) \tag{2.5}$$

$$z_k = h(x_k, v_k) \tag{2.6}$$

where the random variables $w_k$ and $v_k$ again represent the process and measurement noise as in equations 2.1 and 2.2. In this case, the *non-linear* function in the difference equation 2.5 relates the state at the previous time step $k-1$ to the state at the current time step $k$. It includes as parameters any driving function $u_k$ and the zero-mean process noise $w_k$. The *non-linear* function in the measurement equation equation 2.6 relates the state $x_k$ to the measurement $z_k$ [34].

In practice of course, the individual values of the noise and at each time step are not known. However, the state and measurement vector can be approximated without them as in equations 2.7 and 2.8:

$$x_k{}^- = f(\hat{x}_{k-1}, 0) \tag{2.7}$$

$$z_k{}^- = h(x_k{}^-, 0) \tag{2.8}$$

where $\hat{x}_k$ is some a *posteriori* estimate of the state (from a previous time step $k$). To estimate a process with non-linear difference and measurement relationships, the new governing equations that linearize an estimate about equation 2.7 and equation 2.8 are described in equations 2.9 and 2.10 [34]:

$$x_k \approx x_k{}^- + A(x_{k-1} - \hat{x}_{k-1}) \tag{2.9}$$

$$z_k \approx z_k{}^- + H(x_k - x_k{}^-) \tag{2.10}$$

where

- $x_k$ and $z_k$ are the actual state and measurement vectors,
- $x_k{}^-$ and $z_k{}^-$ are the approximate state and measurement vectors from equations 2.7 and 2.8,
- $\hat{x}_k$ is an *a posterior* estimate of the step $k$,
- the random variables $w_k$ and $v_k$ represent the process and measurement noise as in equations 2.1 and 2.2,
- $A$ is the Jacobian matrix of partial derivatives of $f$ with respect to $x$, that is

$$A_{[i,j]} = \frac{df_{[i]}}{dx_{[j]}}(\hat{x}_{k-1}, 0) \tag{2.11}$$

- $H$ is the Jacobian matrix of partial derivatives of $h$ with respect to $x$, that is

$$H_{[i,j]} = \frac{dh_{[i]}}{dx_{[j]}}(x_k^-, 0) \tag{2.12}$$

Note that, for simplicity in the notation, it is not used the time step subscript $k$ with the Jacobians $A$ and $H$, even though they are in fact different at each time step [34].

Then, the notation for the *priori* and *posterior* estimate errors is defined as

$$e_k \equiv x_k - \hat{x}_k^- \; and \tag{2.13}$$

$$e_k \equiv x_k - \hat{x}_k \tag{2.14}$$

The a *priori* estimate error covariance and the *a posteriori* estimate error covariance are described in equations 2.15 and 2.16:

$$P_k^- = E[e_k^- e_k^{-T}] \tag{2.15}$$

$$P_k = E[e_k e_k^T] \tag{2.16}$$

In deriving the equations for the Kalman filter, the goal is to find an equation that computes an *a posteriori* state estimate $\hat{x}_k$ as a linear combination of an *a priori* estimate $\hat{x}_k^-$ and a weighted difference between an actual measurement $z_k$ and a measurement prediction $H\hat{x}_k^-$ as shown below in equation 2.17.

$$\hat{x}_k = \hat{x}_k^- + K(z_k - h(\hat{x}_k^-, 0)) \tag{2.17}$$

The difference $(z_k - h(\hat{x}_k^-, 0))$ in equation 2.17 is called the measurement *innovation*, or the *residual*. The residual reflects the discrepancy between the predicted measurement $h(\hat{x}_k^-, 0)$ and the actual measurement $z_k$. A residual of zero means that the two are in complete agreement. The $n \times m$ matrix $K$ in equation 2.17 is chosen to be the gain or blending factor that minimizes the *a posteriori* error covariance equation 2.16.

The complete set of EKF equations are shown in Tables 2.2 and 2.3. As with the basic discrete Kalman filter, the time update equations in table 2.2 project the state and covariance estimates from the previous time step $k-1$ to the current time step $k$. Again, $f$ in equation 2.18 comes from equation 2.7, $A_k$ and $W_k$ are the process Jacobians at step $k$, and $Q_k$ is the process noise covariance equation 2.3 at step $k$.

As with the basic discrete Kalman filter, the measurement update equations in table 2.3 correct the state and covariance estimates with the measurement $z_k$. Again, $h$ in equation 2.21 comes from equation 2.8, $H_k$ is the measurement Jacobian at step $k$, and $R_k$ is the measurement noise covariance equation 2.4 at step $k$.

The basic operation of the EKF is depicted in Figure 2.8. An important feature of the EKF is that the Jacobian $H_k$ in the equation for the Kalman gain $K_k$ serves to correctly propagate or "magnify" only the relevant component of the measurement information. For example, if there is not a one-to-one mapping between the measurement $z_k$ and the state via $h$, the Jacobian $H_k$ affects the Kalman gain so that it only magnifies the portion of the residual $z_k - h(\hat{x}_k, 0)$ that does affect the state. Obviously, if over *all* measurements there is not a one-to-one mapping between the measurement $z_k$ and the state via $h$, then as it might be expected, the filter will quickly diverge. In this case the process is *unobservable* [34].

Table 2.2: EKF time update equations.

| **Update Equations** | |
|---|---|
| $\hat{x_k}^- = f(\hat{x_{k-1}}^-, 0)$ | (2.18) |
| $P_k^- = A_k P_{k-1} A_k^T + Q_{k-1}$ | (2.19) |

Table 2.3: EKF measurement update equations.

| **Measurements Equation** | |
|---|---|
| $K_k = P_k^- H^T (H P_k^- H^T + R_k)^{-1}$ | (2.20) |
| $\hat{x}_k = \hat{x}_k^- + K_k(z_k - h(\hat{x}_k^-, 0))$ | (2.21) |
| $P_k = (I - K_k H_k) P_k^-$ | (2.22) |

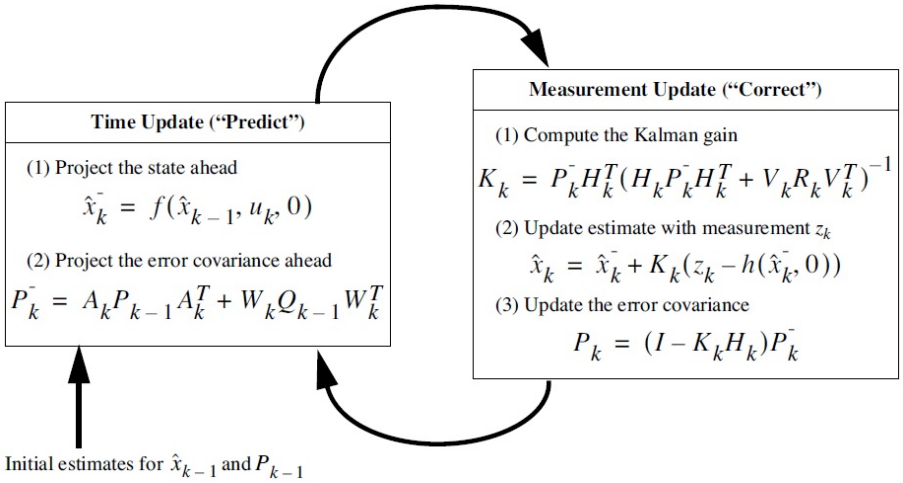


Figure 2.8: A complete description of the operation of the EKF [34].

### 2.2.3 Attitude Representation

The goal of an attitude determination algorithm is to determine the orientation of an object with respect to a reference frame [29, 35]. Thus, two different coordinate frames are considered:

- **Earth Reference Frame** - The earth frame E is represented by the orthogonal vector basis $x_0$, $y_0$, $z_0$ and is attached to the earth. Therefore, $x_0$ points north, $y_0$ points east and $z_0$ points toward the center of earth as shown in Figure 2.9. This coordinate system is always static independently of the orientation of the body.
- **Sensor Frame** - The sensor frame S is rigidly attached to the object whose attitude we would like to describe. This frame is fixed to the sensor, but varies relative to the Earth reference frame due to the sensor movement.

In the literature, there are different ways of representing the attitude between two coordinate frames and transforming vectors and coordinates from one coordinate frame to another [35]. The most efficient method to represent upper limb segments orientation is Quaternions [26].

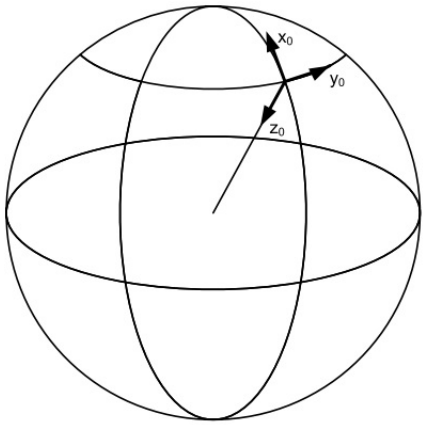


Figure 2.9: Earth Reference Frame [29].

#### 2.2.3.1 Quaternions

A quaternion is a four-dimensional complex number that can be used to represent the orientation of a rigid body or coordinate frame in three-dimensional space. An arbitrary orientation of frame $B$ relative to frame $A$ can be achieved through a rotation of angle $\theta$ around an axis ${}^{A}\hat{\mathbf{r}}$ defined in frame $A$.

This is represented graphically in Figure 2.10 where the mutually orthogonal unit vectors $\hat{x}_{\mathrm{A}}$, $\hat{y}_{\mathrm{A}}$ and $\hat{z}_{\mathrm{A}}$, and $\hat{x}_{\mathrm{B}}$, $\hat{y}_{\mathrm{B}}$ and $\hat{z}_{\mathrm{B}}$ define the main axis of coordinate frames $A$ and $B$ respectively. The quaternion describing this orientation, ${}^{A}_{B}\hat{\mathbf{q}}$, is defined by equation (2.23) where $r_x$, $r_y$ and $r_z$ define the components of the unit vector ${}^{A}\hat{\mathbf{r}}$ in the $x$, $y$ and $z$ axes of frame $A$ respectively. A leading subscript denotes the frame being described and a leading superscript denotes the frame this is

with reference to. For example, ${}^{A}_{B}\hat{\mathbf{q}}$ describes the orientation of frame $B$ relative to frame $A$ and ${}^{A}\hat{\mathbf{r}}$ is a vector described in frame $A$ [27].

Quaternion arithmetics often requires that a quaternion describing an orientation is first normalized. It is therefore conventional for all quaternions describing an orientation to be of unit length. A quaternion with unity norm is referred to as unit quaternion and can be used to represent the attitude of a rigid body [27]. Therefore, the unit quaternion is represented in equation 2.23.

$$ {}^{A}_{B}\hat{\mathbf{q}} = \begin{bmatrix} q_1 & q_2 & q_3 & q_4 \end{bmatrix} = \begin{bmatrix} \cos\frac{\theta}{2} & -r_x \sin\frac{\theta}{2} & -r_y \sin\frac{\theta}{2} & -r_z \sin\frac{\theta}{2} \end{bmatrix} \tag{2.23} $$

The quaternion conjugate, denoted by *, can be used to swap the relative frames described by an orientation. For example, ${}^{B}_{A}\hat{\mathbf{q}}$ is the conjugate of ${}^{A}_{B}\hat{\mathbf{q}}$ and describes the orientation of frame $A$ relative to frame $B$. The conjugate of ${}^{A}_{B}\hat{\mathbf{q}}$ is defined by equation (2.24).

$$ {}^{A}_{B}\hat{\mathbf{q}}^{*} = {}^{B}_{A}\hat{\mathbf{q}} = \begin{bmatrix} q_1 & -q_2 & -q_3 & -q_4 \end{bmatrix} \tag{2.24} $$

The quaternion product, denoted by $\otimes$, can be used to define compound orientations. For example, for two orientations described by ${}^{A}_{B}\hat{\mathbf{q}}$ and ${}^{B}_{C}\hat{\mathbf{q}}$, the compounded orientation ${}^{A}_{C}\hat{\mathbf{q}}$ can be defined by equation (2.25).

$$ {}^{A}_{C}\hat{\mathbf{q}} = {}^{B}_{C}\hat{\mathbf{q}} \otimes {}^{A}_{B}\hat{\mathbf{q}} \tag{2.25} $$

For two quaternions, $\boldsymbol{a}$ and $\boldsymbol{b}$, the quaternion product can be determined using the Hamilton rule and defined as equation (2.26). A quaternion product is not commutative; that is, $\boldsymbol{a} \otimes \boldsymbol{b} \neq \boldsymbol{b} \otimes \boldsymbol{a}$.

$$ \begin{aligned} \boldsymbol{a} \otimes \boldsymbol{b} &= \begin{bmatrix} a_1 & a_2 & a_3 & a_4 \end{bmatrix} \otimes \begin{bmatrix} b_1 & b_2 & b_3 & b_4 \end{bmatrix} \\ &= \begin{bmatrix} a_1 b_1 - a_2 b_2 - a_3 b_3 - a_4 b_4 \\ a_1 b_2 + a_2 b_1 + a_3 b_4 - a_4 b_3 \\ a_1 b_3 - a_2 b_4 + a_3 b_1 + a_4 b_2 \\ a_1 b_4 + a_2 b_3 - a_3 b_2 + a_4 b_1 \end{bmatrix}^{T} \end{aligned} \tag{2.26} $$

A three dimensional vector can be rotated by a quaternion using the relationship described in equation (2.27). ${}^{A}\mathbf{v}$ and ${}^{B}\mathbf{v}$ are the same vector described in frame $A$ and frame $B$ respectively where each vector contains a 0 inserted as the first element to make them 4 element row vectors.

$$ {}^{B}\mathbf{v} = {}^{A}_{B}\hat{\mathbf{q}} \otimes {}^{A}\mathbf{v} \otimes {}^{A}_{B}\hat{\mathbf{q}}^{*} \tag{2.27} $$

The orientation described by ${}^{A}_{B}\hat{\mathbf{q}}$ can be represented as the rotation matrix ${}^{A}_{B}\mathbf{R}$ defined by equation (2.28) [27].

$$ {}^{A}_{B}\mathbf{R} = \begin{bmatrix} 1-2q_3^2-2q_4^2 & 2(q_2q_3-q_1q_4) & 2(q_2q_4+q_1q_3) \\ 2(q_2q_3+q_1q_4) & 1-2q_2^2-2q_4^2 & 2(q_3q_4+q_1q_2) \\ 2(q_2q_4-q_1q_3) & 2(q_3q_4+q_1q_2) & 1-2q_2^2-2q_3^2 \end{bmatrix} \tag{2.28} $$

Therefore, by transposing this explanation to the orientation estimation of a sensor, with equation (2.27) a three dimensional vector that could be the IMU output, described in sensor frame, can be rotated by a quaternion, giving the same vector but described in the earth reference frame.

Quaternions are used to represent orientation to improve computational efficiency and avoid singularities. In addition, the use of quaternions eliminates the need for computing trigonometric functions [36]. However, the main disadvantages of using unit quaternions are: that the four quaternion parameters do not have intuitive physical meanings, and that a quaternion must have unity norm to be a pure rotation. The unity norm constraint, which is quadratic in form, is particularly problematic if the attitude parameters are to be included in an optimization, as most standard optimization algorithms cannot encode such constraints [35].

To conclude, human body tracking using inertial sensors requires an attitude estimation filter capable of tracking in all orientations. Singularities associated with Euler angles[2] make them unsuitable for use in body tracking applications. So, quaternions are an alternate method of orientation representation, gaining popularity in the graphics community. Quaternion rotation is more efficient than the use of rotation matrices and does not involve the use of trigonometric functions [37].

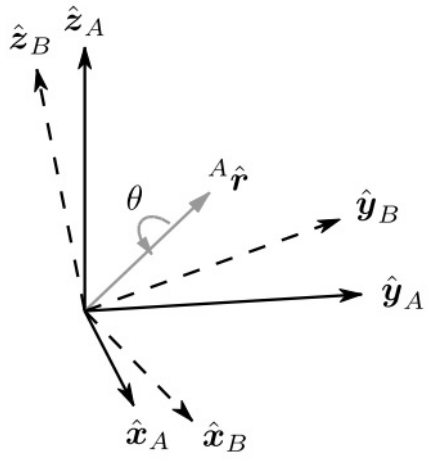


Figure 2.10: The orientation of frame $B$ is achieved by a rotation, from alignment with frame $A$, of angle $\theta$ around the axis ${}^{A}\mathbf{r}$ [38].

[2]The transformation from the body frame to the Earth frame is based on three angular rotations. These angular rotations can be represented as the Euler angles: rotation $\psi$ around $X$-axis (yaw angle), rotation $\theta$ around $Y$-axis (pitch angle) and rotation $\phi$ around $Z$-axis (roll angle).

## 2.3 Position and Trajectory Reconstruction

Measurements of movement of body segments need to be performed outside the laboratory, with body mounted sensors like accelerometers, gyroscopes and magnetometers. This means that IMUs are suitable for measuring arm movements, since they are small enough to be attached to the upper and forearm without interfering with the subject's movement [39].

A fundamental question is defining the places and parts of the body where the sensors are placed. One very common solution is applying the sensors in joints of interest, for instance, the ones explained in Section 2.1.1.1. Additionally, it has been observed that significant errors, e.g. rapid variations, quite often appeared in the measurements. This mainly results from the soft tissue effects and inertial properties, where the relative movements between the sensors and the rigid structures (i.e. bones) are sampled [40].

There is a considerable amount of studies that have used sensor fusion with accelerometers, gyroscopes, magnetometers or combinations of these in the determination of orientation and position of upper limb anatomical segments with the purpose of tracking upper limb movement and reconstruct its trajectories. After finding the sensors orientations using sensor fusion techniques, the biomechanical models for the upper limb are used to reconstruct upper limb motion. Also, to determine the position of an arm in an earth reference frame, it is necessary to transform the inertial measurements from the sensor coordinate system to the earth reference frame. Figure 2.11 illustrates a moving inertial sensor and two engaged coordinated systems (or frames). To report positions in the earth reference frame, the orientation of the sensor relative to the earth needs to be known.

In Table 2.4 there is an overview of upper limb tracking related work by several authors. This table presents the work summarized in this section and other examples. The table is organized in terms of author, year, sensors, sensor location, kinematic model, orientation representation, sensor fusion method, position estimation and results. The sensors are the IMU sensors used in each work, and the sensor locations are the place where they are attached. The kinematic model is the upper limb model considered in each work and corresponds to the modeling of its joints and movements. The position estimation is related to the method that is used to obtain the upper limb positions and the reconstruction of its trajectories and is based on the joint orientation and on the kinematic model considered. Lastly, the results are the output from each work.

Considering Table 2.4, regarding the sensors, the MT-9, MT9-B and MT-X are frequent inertial sensors used in the upper limb motion tracking. The MT9 module consists of 3-D gyroscopes and 3-D accelerometers. The MTX and the MT9-B modules consists of 3-D gyroscopes, 3-D accelerometers, 3-D magnetometers, and a temperature sensor. A Sparkfun 9-DOF is composed by a tri-axis accelerometer, a tri-axis micro rate gyro and tri-axis micro magnetometer. In sensor fusion method, N/A means that no sensor fusion method was applied, instead an optimisation approach was used to reduced drift [41] [18]. In [19] a Monte Carlo Sampling based optimisation technique is used to correct drift problems. In the examples presented below, there is no concern in defining an upper limb reference frame because the sensor reference frames are already aligned

with the upper limb reference frame. This problem is only addressed in Section 2.4.

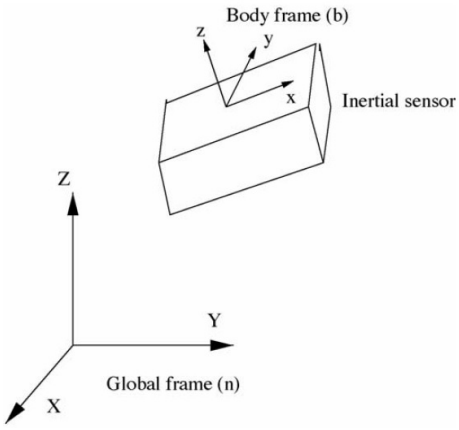


Figure 2.11: Inertial tracking relative to the global frame [18].

Table 2.4: Overview of upper limb motion tracking related work.

| Author | Year | Sensors | Sensor Location | Kinematic Model | Orientation Representation | Sensor Fusion | Position Estimation | Results |
|---|---|---|---|---|---|---|---|---|
| R. Zhu Z. Zhou [22] | 2004 | 2 ISP | Upper and lower arm | 1-DOF elbow | Joint angle and Rotation axis | KF | Global transfer matrix | Lower arm end position |
| H. Zhou H. Hu [42] | 2005 | 1 MT9 | Wrist | 3-DOF shoulder+ 3-DOF elbow | Euler Angles | Extended KF | Inverse kinematics | Elbow and wrist positions |
| H. Zhou et al [41] | 2005 | 1 MT9 | Wrist | Rigid forearm (elbow fixed) | Euler Angles | N/A | Inverse kinematics | Forearm position |
| H. Zhou et al [18] | 2006 | 2 MT9 | Elbow and wrist | 6-DOF shoulder + 1-DOF elbow | Euler Angles | N/A | Wrist and elbow - Euler angles + Kinematic model<br>Shoulder - Lagrange optimisation | Shoulder, elbow and wrist positions |
| H. Zhou et al [19] | 2006 | 1 MT9 | Wrist | 3-DOF shoulder + 1-DOF elbow | Euler Angles | N/A | Wrist - acceleration double integration<br>Elbow -Euler angles + Kinematic model | Elbow and wrist positions |
| H. Zhou et. al [43] | 2007 | 2 MTx | Elbow and wrist | 1-DOF elbow | Quaternions | KF | Elbow and wrist - kinematical modeling<br>Shoulder - acceleration angular changes fusion | Shoulder, elbow and wrist positions |
| H. Zhou H. Hu [40] | 2007 | 2 MTx | Upper arm and wrist | 1-DOF elbow | Euler Angles | KF | Elbow and wrist - kinematical modeling | Elbow and wrist positions |
| H. Zhou et al [24] | 2008 | 2 MT9-B | Elbow and wrist | 1-DOF elbow | Euler Angles | N/A | Wrist and elbow - Euler angles + Kinematic model<br>Shoulder - Lagrange optimisation | Shoulder, elbow and wrist positions |
| C. Chien et. al [44] | 2013 | 2 Sparkfun 9-DOF | Upper and lower arm | 1-DOF elbow | Rotation Matrix | Non-linear CF | Orientation + Kinematic model | Reconstruction of wrist movement |

## 2.4 Sensor-to-Body Frame

Although the motion tracking studies, described in Section 2.3, achieved good experimental results, the relative transformation between the inertial sensor coordinate frames and the segment coordinate frames were ignored. Moreover, they usually require users to align the sensors with each other and with the mounted arm segment, which inhibits their implementation in daily life monitoring. In order to avoid this step, a simple sensor-to-body transformation method could be introduced.

In order for the positions and trajectories tracking to be independent of how the user places the sensors on each segment, it is necessary to define a global reference frame where the positions will be described. After defining this global reference frame, the orientation of each sensor relative to it must be determined.

This way, the final goal of the sensor-to-body transformation process is to find this orientation in order to describe each segment movement in the global reference frame.

Usually, the sensor-to-body transformation consists of defining a set of movements around the upper limb rotation axes for each joint. This procedure is done in order to understand how the sensor is placed and to determine the orientation relative to the defined global coordinate frame where the positions trajectories will be described. Once the global frame is constructed and knowing the orientation of the upper limb segments relative to it, the trajectories can be represented in a unique frame, independent of how the sensors were attached in the first place.

In literature, there are some example of sensor-to-body transformation procedures like the ones reported by H. Wang et al [45] in 2011 and Y. Wang et al [46] in 2014.

In a study developed by H. Wang et al [45] in 2011, the relative orientation between the inertial sensor coordinate frames and the segment coordinate frames were calibrated using the gravity and the sensor data while the subject performs several predefined actions. In the sensor-to-body transformation postures, data from accelerometers and gyroscopes were fused to extract the gravity using Extended Kalman Filter (EKF). Then, the calibrated relative orientation matrix was used to bridge the sensor orientation with the segment orientation, which was then used to track the upper limb motion.

Another sensor-to-body transformation method is presented in the work developed by Y. Wang et al [46] in 2014, where a simple sensor-to-body transformation method was introduced, which effectively avoided the burden of manually aligning the sensors. In addition, the algorithm automatically estimated the arm length so that position trajectories of the elbow and the wrist joints could be reconstructed without manual measurements.

With a sensor-to-body transformation process, it is possible to have a more accurate motion tracking and avoid the burden of manually aligning the sensors, allowing the use of the tracking system in daily life monitoring.

# Chapter 3

# 3DArm - Upper Limb Inertial Tracking System

This Chapter presents the development of an inertial tracking system proposed for this dissertation. The tracking system developed was named 3DArm - Upper Limb Inertial Tracking System. In this Chapter, the methodology and processes for the implementation of this system will be described and it will be presented an evaluation of its performance. All the work developed was to track only the rigth upper limb, to track the left upper limb the methodology is equivalent.

## 3.1 3DArm Overview

The Upper Limb Inertial Tracking System (3DArm) is a sequential algorithm that was developed in order to obtain upper limb joint positions and trajectories in 3D. Based on literature review, a set of steps for 3DArm implementation was defined, which is depicted in Figure 3.1.

Data Acquisition, described in Section 3.2, is related to sensor signal acquisition. The sensors are placed on the upper and lower arm segments, which is explained in Kinematic Model and Global Body Reference Frame Section 3.2.2.

Signal Pre-Processing, explained in Section 3.3, is divided in two different processes: Low-Pass Filter, to remove high frequency noise, and Data Normalization, to define normalized acceleration and angular velocity vectors.

Sensor to Global Body Reference Frame, addressed in Section 3.4, is introduced in order to obtain the orientation between the sensor's local reference frame and the global body reference frame, enabling positions and trajectories to be represented in the global body reference frame. This step is outlined with a different color in the flowchart of Figure 3.1 because it describes a process based on a transformation between reference frames that occurs during the Orientation Estimation phase.

Orientation Estimation, detailed in Section 3.5, presents a sensor fusion method, EKF, that fuses data from accelerometers, gyroscopes and magnetometers, in order to obtain the orientation of each segment relative to the Global Body Reference Frame. This method was developed specif-

ically for upper limb motion tracking, since it fuses a bio-mechanical constraint characteristic of the upper limb movement.

Lastly, Position and Trajectory Reconstruction, addressed in Section 3.6, defines a set of equations to represent the upper and lower segments in the global body reference frame.

The complete methodology explained in this Chapter was implemented in Python with software PyCharm.

Most of the variables will have a left superscript, a right superscript and a right subscript. The left superscript indicates the reference frame for which the variable is calculated. The right superscript indicates the body segment the variable relates to. The right subscript usually represents the time variable. The most used left superscripts are *b* and *s*, which refers to global *b*ody reference frame and *s*ensor local reference frame, respectively; the right most used superscripts are *U* and *L*, which refers to *U*pper and *L*ower segments, respectively; the most used right subscript is *t*, which refers to *t*ime variable.

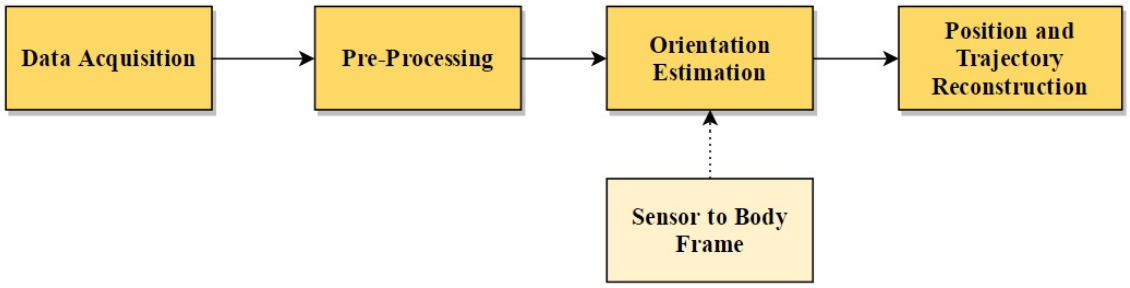


Figure 3.1: 3DArm flowchart.

## 3.2 Data Acquisition

In order to obtain a reliable signal to describe upper limb movement, Data Acquisition defines which sensors were used and how the upper limb was modeled.

### 3.2.1 Inertial Sensors

As mentioned in Section 2.2.1, an IMU is an electronic device that usually combines three sensors - accelerometer, gyroscope and magnetometer. With an IMU, it is possible to measure the gravitational forces acting in the device, usually using three axes. The accelerometer is a sensor that measures the linear acceleration caused by the movement or the earth gravitational acceleration. The gyroscope is a sensor that measures the angular velocity. Lastly, the magnetometer is a sensor that measures local earth magnetic field vector, providing additional information about orientation [27].

Using data from an IMU, it is possible to estimate the posture or movement of the human body. The usage of this device is becoming increasingly popular, due to their low cost, small size,

light weight and limited power requirements compared to traditional approaches of upper limb tracking.

The chosen IMU was the *Pandlets* developed at FhP AICOS, which is depicted in Figure 3.2. This device includes a MPU-9250 Nine-Axis unit, which is from *InvenSense* [47], and has a 3-axis-accelerometer, a 3-axis gyroscope and a 3-axis magnetometer. It consists of a small box with dimensions of 28.4 $\times$ 28.4 millimeters and 10 millimeters height.

The accelerometer, gyroscope and magnetometer signals are sampled at a 50 Hz frequency. This device is connected to a PC via Bluetooth. An application developed by FhP-AICOS allows to record data from Pandlets and store it in a *csv* file.

Two IMUs needed to be placed on the upper and lower segments of the upper limb.


Figure 3.2: Pandlet developed at FhP-AICOS. Sensor's local reference system is presented in orange.

### 3.2.2 Kinematic Model and Global Body Reference Frame

The human arm motion is approximated as an articulated motion of two rigid body parts: the upper and lower segments, where each of the segments can only rotate about its preceding joints, the shoulder and the elbow joint.

The model defined considers the shoulder joint as a fixed joint in space and only the elbow and wrist joints can be tracked. Therefore, the whole model of the upper limb looks like a double pendulum, where the shoulder joint admits abduction/aduction, flexion/extension and medial/lateral rotation (three DOFs), and the elbow joint only admits flexion/extension (one DOF), since the pronation/supination does not influence wrist's position.

The two sensors were placed near the elbow joint, on the upper segment, and near the wrist joint, on the lower segment. The shoulder movements will influence the elbow position and the elbow movements will influence the wrist position. Since the shoulder is fixed, only the elbow and wrist positions are required in order to track upper limb movement.

To describe joint movements, a Global Body (GB) reference frame was defined, with the shoulder joint set as the origin (point O). This frame was constructed by setting the $x$-axis perpendicular to the coronal plane pointing from the chest to the back and the $z$-axis perpendicular to the axial plane pointing from the feet to the head. Using the right-hand rule, the $y$-axis can be constructed accordingly. To represent positions in the GB reference frame, the sensors must be aligned with each other and with this frame. The GB and sensor reference frame is depicted in Figure 3.3.

It is important to notice that this GB reference frame only admits rotations and does not admit translations.

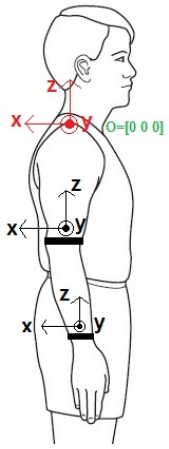


Figure 3.3: Position and orientation of sensors. GB Reference Frame is red and sensors' local reference frame are black. Origin is green.

## 3.3 Signal Pre-Processing

After the raw sensor data have been collected, pre-processing consisted in signal filtering and normalization.

### 3.3.1 Low-Pass Filter

Raw data from accelerometers were low-pass filtered. A first-order low-pass Butterworth filter was adapted to a sampling frequency of 50 Hz with a cutoff frequency of 1 Hz [40, 41, 43].

Since the upper limb movements have a small velocity, this filter rejects linear acceleration and keeps only the gravitational acceleration, which affects orientation.

### 3.3.2 Data Normalization

Most IMUs usually measure non-normalized vectors. For the purpose of representing spatial directions, IMU vectors were normalized. [48].

A simple normalization was applied to filtered IMU data. Taking the vector $v$ as example, its components $v_x$, $v_y$ and $v_z$ were normalized to $v_{x_n}$, $v_{y_n}$ and $v_{z_n}$ by :

$$mag = v_x^2 + v_y^2 + v_z^2 \tag{3.1}$$

$$v_{x_n} = \frac{v_x}{mag} \tag{3.2}$$

$$v_{y_n} = \frac{v_y}{mag} \tag{3.3}$$

$$v_{z_n} = \frac{v_z}{mag} \tag{3.4}$$

## 3.4 Sensor to Global Body Reference Frame

Data from sensors are defined in the sensor's local reference frame. Therefore, to represent positions and trajectories of the upper limb joints, the orientation between the sensor's local reference frame and the GB reference frame must be defined, that is, ${}^{b}q_t^U$ and ${}^{b}q_t^L$.

As mentioned before, two sensors were placed in the upper and lower segments, near the elbow and wrist joints, respectively. In order to define the orientation quaternions ${}^{b}q_t^U$ and ${}^{b}q_t^L$, the user must stand still for a period of 10 seconds before performing any movement, with the arm straight down and with the sensors aligned with each other and with the GB reference frame, as depicted in Figure 3.3.

During this time period, the mean orientation quaternions of ${}^{b}q_t^U$ and ${}^{b}q_t^L$ from time 0 to 10 were defined. The mean orientation quaternions for the upper and lower segment are represented as ${}^{m}q^U$ and ${}^{m}q^L$ (where *m* refers to *mean*). Since the inverse of a quaternion represents the opposite rotation, $\overline{{}^{m}q^U}$ and $\overline{{}^{m}q^L}$ were used to rotate the orientation quaternions $q_t^U$ and $q_t^L$ to ${}^{b}q_t^U$ and ${}^{b}q_t^L$ by:

$${}^{b}q_t^U = \overline{{}^{m}q^U} \otimes q_t^U \tag{3.5}$$

$${}^{b}q_t^L = \overline{{}^{m}q^L} \otimes q_t^L \tag{3.6}$$

where ${}^{b}q_t^U$ and ${}^{b}q_t^L$ represent the upper and lower orientations relatively to the earth reference frame.

The orientation quaternions relative to the earth reference frame were determined by sensor fusion techniques that will be described in the next Section. Then, $q_t^U$ and $q_t^L$ were defined through equations 3.5 and 3.6. In fact, any vector can be substituted into these equations and be defined in the GB reference frame.

The process developed for the 3DArm system to construct the GB reference frame required that the sensors were placed aligned with each other and with the GB reference frame, therefore the GB reference frame is dependent of the sensors' position in the beginning of the data acquisition. This requirement is necessary for describing the elbow and joints' positions in the GB reference frame. If the sensors were not fully aligned with each other, the orientation quaternions ${}^{b}q_t^U$ and ${}^{b}q_t^L$ could not represent the orientation to the GB reference frame defined in Section 3.2.2 and elbow and wrist positions are not described in that GB reference frame.

Since this alignment could be difficult to ensure, the study of the placement of the sensors in any position without being aligned with each other will be addressed in Chapter 4.

## 3.5 Orientation Estimation

Data from inertial sensors were combined through sensor fusion methods in order to obtain orientation. Since the upper limb is represented by a skeleton structure with two segments linked by a revolute joint, each segment's orientation can be represented by a quaternion. Quaternions are computationally effective and avoid problems with singularities such as gimbal lock.

Because of the non-linear dynamics of upper limb motion and the non-linearity of sensor measurements, an Extended Kalman Filter was employed to fuse accelerometer, gyroscope and magnetometer data and recursively estimate the quaternion of each upper limb segment. In this phase, geometric constraint of elbow joint, which was reported in Section 2.1.1.3, was modeled and fused into the EKF framework to improve estimation accuracy.

The goal of Orientation Estimation is to determine ${}^{b}q_{t}^{U}$ and ${}^{b}q_{t}^{L}$, which represent the upper and lower segment orientation relative to the GB reference frame.

In order to compute these quaternions, first, a separate algorithm to find a corresponding quaternion for each set of accelerometer and magnetometer measurements will be followed. At this stage, since sensor data are in the respective local reference frame, the estimated quaternions correspond to the upper and lower orientation relative to the earth reference frame, so they must be rotated to the GB reference frame. Then, the computed quaternions (relative to GB reference frame) will be combined with angular velocity measurements (in GB reference frame), and provided to the EKF as measurements. By doing so, the output equations for the EKF become linear, and the overall EKF design is greatly simplified. Introducing the biomechanical constraint to the EKF design, EKF output quaternions will be ${}^{b}q_{t}^{U}$ and ${}^{b}q_{t}^{L}$.

The scheme presented in Figure 3.4 shows a block diagram of the filter design approach. Acceleration and local magnetic field measurements are used as input to the TRIAD algorithm to produce the computed quaternion $q$. The computed quaternion together with angular velocity measurements is then presented to EKF as measurements.

This section will explain the modeling of the biomechanical constraint and how to incorporate it into sensor fusion to obtain upper and lower segments orientation relative to the GB reference frame.

### 3.5.1 TRIAD Algorithm

The TRIAD algorithm [49] is a single frame deterministic method, which produces a suboptimal orientation estimate in the form of a 3 x 3 rotation matrix. Since the signal acquisition was performed in an environment with different types of electronic and magnetic devices, the magnetic field could be influenced.

Initially, normalized vectors with accelerometers $g$ and magnetometers $m$ readings are defined:

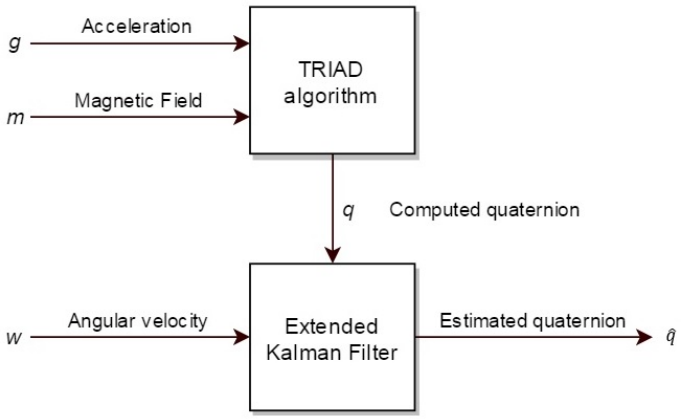


Figure 3.4: Block diagram of EKF design.

$$g = \begin{bmatrix} g_x & g_y & g_z \end{bmatrix} \tag{3.7}$$

$$m = \begin{bmatrix} m_x & m_y & m_z \end{bmatrix} \tag{3.8}$$

Let the cross product between $g$ and $m$ be G and the cross product between $m$ and $g$ be M:

$$G = g \times m = \begin{bmatrix} m_y g_z - m_z g_y & m_z g_x - m_x g_z & m_x g_y - m_y g_x \end{bmatrix} \tag{3.9}$$

$$M = m \times g = \begin{bmatrix} g_y m_z - g_z m_y & g_z m_x - g_x m_z & g_x m_y - g_y m_x \end{bmatrix} \tag{3.10}$$

Now, the rotation matrix $R$ representing the orientation can be defined by:

$$R = \begin{bmatrix} G_x & M_x & g_x \\ G_y & M_y & g_y \\ G_z & M_z & g_z \end{bmatrix} \tag{3.11}$$

Then, the rotation matrix $R$ could be transformed into a computed quaternion $q$ by the process described in Appendix A.

To avoid disturbance from electronic and magnetic devices, the vector $m$ comes from the magnetometers measurements only for the first reading. Then, $m$ vector is defined by earth vector $[0,1,0]$ rotated to sensor local reference frame, that is, multiplied by the last computed quaternion $q$:

$$m = \overline{q} \otimes \begin{bmatrix} 0 & 0 & 1 & 0 \end{bmatrix}^T \otimes q \tag{3.12}$$

Taking into account that the vector $[0,1,0]$ orientation in the earth reference frame, the calculated vector $m$ corresponds to the expected value of the magnetometer in the sensors' reference frame.

This algorithm allows to obtain computed quaternion $q_t^U$ and $q_t^L$ for the upper and lower segment, respectively, which represent the segment orientation relative to earth reference frame. By substituting $q_t^U$ and $q_t^L$ into equations 3.5 and 3.6, ${}^b q_t^U$ and ${}^b q_t$ were obtained.

Computed quaternions from this algorithm do not represent the actual real-time orientation of the body, because accelerometers measure the sum of gravity and motion induced acceleration. This is where angular velocity measurements come to help estimate the orientation of the rigid body. While angular velocity measurements can be integrated to yield an orientation estimate, they are prone to drift over an extended period of time. Acceleration and magnetic field measurements do not drift over time.

Therefore, quaternions ${}^b q_t^U$ and ${}^b q_t^L$ calculated here do not represent final orientation estimation, since their estimation only required accelerometers and magnetometers readings. The quaternions referred in this section will be presented as measurements to EKF in order to obtain the final ${}^b q_t^U$ and ${}^b q_t^L$, which will be described next.

### 3.5.2 Extended Kalman Filter

As stated above, the objective of this step is to design an Extended Kalman Filter for estimation of the upper and lower segments' orientation relative to GB reference frame. Since the data fusion problem in this system is a typical nonlinear problem, an EKF will be developed.

#### 3.5.2.1 Biomechanical Constraints

As studied by Z. Zhang et al [50], sensor data fusion to estimate orientation quaternion for each arm segment does not exclude inevitable motion estimation errors, when using estimation methods with inertial measurements. The accumulation of these errors will result in drift. In order to produce a more reliable motion estimation, biomechanical constraints should be included in sensor fusion.

As mentioned in Section 2.1.1.3, the elbow of an healthy subject can only admit two degrees of freedom: flexion/extension and pronation/supination. The abduction/adduction of the elbow is nearly impossible, which means the adduction angle $\alpha$ is restricted to a very small angle. Considering the GB reference frame, defined in Section 3.2.2, $\alpha$ is defined as the angle between the $z$-axis of the forearm and the $xz$-plane of the upper arm. As $\alpha$ is restricted to a very small angle, the $z$-axis of the lower arm and the normal of the $xz$-plane of the upper arm should be almost orthogonal, which can be represented by dot product as:

$$Y_t^L \cdot Z_t^U = 0 \tag{3.13}$$

Vectors $Y_t^L$ and $Z_t^U$ are the $y$- and $z$-axes of the lower and upper arm coordinate systems, respectively. These vectors are defined in the GB reference frame by:

$$Y_t^L = {}^b q_t^L \otimes \begin{bmatrix} 0 & 0 & 1 & 0 \end{bmatrix}^T \otimes \overline{{}^b q_t^L} \tag{3.14}$$

$$Z_t^U = {}^b q_t^U \otimes \begin{bmatrix} 0 & 0 & 0 & 1 \end{bmatrix}^T \otimes \overline{{}^b q_t^U} \tag{3.15}$$

#### 3.5.2.2 Extended Kalman Filter Process Model

A process model describes the dynamic relation between two successive states.

The relation between the quaternion derivative, $\dot{q}$, and the angular velocity, $w = [w_x, w_y, w_z]^T$, measured by the gyroscope sensor, is as follows:

$$\dot{q} = \frac{1}{2} q \otimes w \tag{3.16}$$

where $\otimes$ represents quaternion multiplication and $q$ is the orientation quaternion to be estimated. To obtain quaternion $q$, the quaternion derivative, $\dot{q}$, needs to be integrated and the resulting quaternion should be normalized to represent rotational relation. A diagram of the process model is depicted in Figure 3.5.

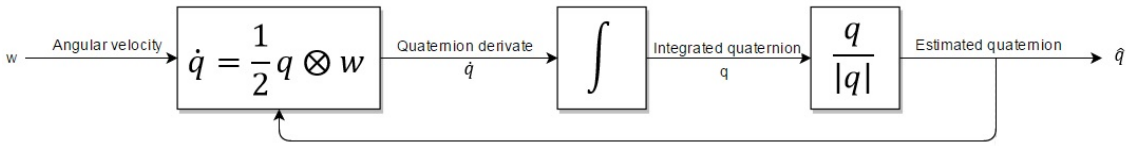


Figure 3.5: Block diagram of the process model for orientation quaternion. $q$ is the orientation quaternion, $\dot{q}$ is the quaternion derivative, $\hat{q}$ is the estimated quaternion and $w$ is the angular velocity.

#### 3.5.2.3 Extended Kalman Filter Design

The orientation with the integrated angular velocity mentioned before can be redesigned by using EKF as follows. Besides orientation quaternions, biomechanical constraints were introduced in order to improve orientation estimation.

The state vector $x$ is a 9-D vector: the first four components are for the upper quaternion $q_t^U$, the next four are for the lower quaternion $q_Y^L$ and the last one is for the biomechanical constraint. The state vector is defined as:

$$\begin{bmatrix} \dot{x}_0 \\ \dot{x}_1 \\ \dot{x}_2 \\ \dot{x}_3 \end{bmatrix} = \frac{1}{2} \begin{bmatrix} x_0 \\ x_1 \\ x_2 \\ x_3 \end{bmatrix} \otimes \begin{bmatrix} 0 \\ {}^{b}w_x^U \\ {}^{b}w_y^U \\ {}^{b}w_z^U \end{bmatrix} \tag{3.17}$$

$$\begin{bmatrix} \dot{x}_4 \\ \dot{x}_5 \\ \dot{x}_6 \\ \dot{x}_7 \end{bmatrix} = \frac{1}{2} \begin{bmatrix} x_4 \\ x_5 \\ x_6 \\ x_7 \end{bmatrix} \otimes \begin{bmatrix} 0 \\ {}^{b}w_x^L \\ {}^{b}w_y^L \\ {}^{b}w_z^L \end{bmatrix} \tag{3.18}$$

$$\dot{x}_8 = x_8 = Y_t^f \cdot Z_t^U \tag{3.19}$$

Equation 3.19 represents the biomechanical constraint introduced as a state variable in order to influence the state of upper and lower quaternions. It is noted that quaternion normalization is not modeled in this state equation, but is carried out in implementation. The angular velocity vectors ${}^{b}w_t^U$ and ${}^{b}w_t^L$ are obtained by:

$${}^{b}w_t^U = {}^{b}q_t^U \otimes \begin{bmatrix} 0 & {}^{s}w_x^U & {}^{s}w_y^U & {}^{s}w_z^U \end{bmatrix}^T \otimes \overline{{}^{b}q_t^U} \tag{3.20}$$

$${}^{b}w_t^L = {}^{b}q_t^L \otimes \begin{bmatrix} 0 & {}^{s}w_x^L & {}^{s}w_y^L & {}^{s}w_z^L \end{bmatrix}^T \otimes \overline{{}^{b}q_t^L} \tag{3.21}$$

where ${}^{b}q^U$ and ${}^{b}q^L$ represent quaternions defined in equations 3.5 and 3.6, and ${}^{s}w^U$ and ${}^{s}w^L$ represent upper and lower angular velocity vectors described in sensor's local reference frame.

The measurement data used in EKF are equal to the result of the TRIAD algorithm, which estimated orientation using accelerometer and magnetometer data. So, the measurement equation $z$ is defined as:

$$z = \begin{bmatrix} x_0 \\ x_1 \\ x_2 \\ x_3 \\ x_4 \\ x_5 \\ x_6 \\ x_7 \end{bmatrix} + \begin{bmatrix} n_0 \\ n_1 \\ n_2 \\ n_3 \\ n_4 \\ n_5 \\ n_6 \\ n_7 \end{bmatrix} \tag{3.22}$$

where $n$ is the measurement noise assumed to be white, zero-mean, uncorrelated. Notice that there are only measurements for state variables $x_0$ to $x_7$. The state variable $x_8$ has no measurement.

Although the measurement equation is linear, an EKF is still required since the state is nonlinear. Nevertheless, linearity in the measurement equation significantly simplifies the filter design

and reduces computational requirements for real-time implementation.

#### 3.5.2.4 Extended Kalman Filter Implementation

Implementation of EKF design will be described next. First, the state equation is linearized and discretized to yield a discrete process model. Second, the modeling of the process noises and measurement noises is presented.

The state variables defined in equations 3.17, 3.18 and 3.19 can be written together in the following form:

$$\dot{x} = f(x) + w \tag{3.23}$$

where $w$ is the process noise and is equal to zero vector. This nonlinear process model can be linearized along the currently estimated trajectory $\hat{x}$:

$$\Delta\dot{x} = \frac{f(x)}{x}\Big|_{x=\hat{x}} \Delta x + w(t) \tag{3.24}$$

The actual trajectory $x$ is the sum of the estimated trajectory $\hat{x}$ and the small increment $\Delta x$:

$$x = \hat{x} + \Delta x \tag{3.25}$$

The next step is to convert the continuous-time model equation 3.24 into a discrete-time model. Let $\Delta t$ be the sampling interval. Then, the difference equation corresponding to the differential equation 3.24 is given by:

$$\Delta x_{k+1} = A_k \Delta x_k + w_k \tag{3.26}$$

where $A_k$ is the discrete state transition matrix. The discrete measurement model is defined by:

$$z_k = H_k x_k + n_k \tag{3.27}$$

where $H_k$ is a $8\times8$ identity matrix, and $n_k$ is the discrete measurement noise. The process noise covariance matrix for the EKF is represented by:

$$Q_k = E\left[w_k {w_k}^T\right] \tag{3.28}$$

where $E$ is the expectation operator, and $w_k$ is the process noise, which is zero, and thus $Q_k$ is a 9×9 zero matrix. The measurement noise covariance matrix for the EKF is defined by:

$$R_k = E\left[n_k n_k{}^T\right] \tag{3.29}$$

where $R_k$ is a 8×8 diagonal matrix, and the elements represent the variance of measurements.

The EKF process is depicted in Figure 3.6. The initial state and covariance are needed to start EKF. Model parameters $A_k$, $H_k$, $R_k$ and $Q_k$ needed to be provided as well. With all this information, the EKF was implemented and the output quaternions ${}^b q_t^U$ and ${}^b q_t^L$ were obtained.

The model parameters, state and measurement equations are extensively detailed in Appendix B.

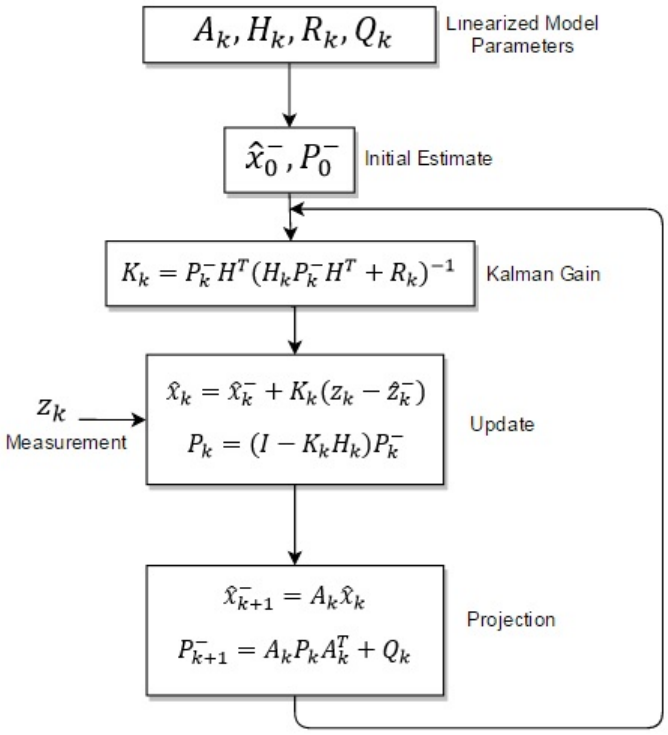


Figure 3.6: Extended Kalman Filter implementation diagram.

## 3.6 Position and Trajectory Reconstruction

After finding sensor orientation through EKF sensor fusion, the upper limb kinematic model was used to reconstruct upper limb motion in GB reference frame.

In order to reconstruct upper limb motion, position of the elbow and wrist joints at time $t$ in GB reference frame, ${}^b p_t^E$ and ${}^b p_t^W$, were tracked, ignoring the movements of the shoulder joint.

Since the shoulder joint was set as the origin of the global reference frame, then:

$$ {}^{b}p_t^S = \begin{bmatrix} 0 & 0 & 0 \end{bmatrix}^T \tag{3.30} $$

so its value does not change with time variable $t$. Considering that the user is initially with the arm straight down, at time 0, vectors describing upper and lower arm posture, ${}^{b}r_0^U$ and ${}^{b}r_0^L$ respectively, were defined by the transformation of vector [0 0 -1], defined in the GB reference frame, to the sensor's initial local reference frame, and then multiplied by $l^U$ and $l^L$ respectively. Vectors ${}^{b}r_0^U$ and ${}^{b}r_0^L$ were obtained by:

$$ {}^{b}r_0^U = (\overline{{}^{m}q^U} \otimes \begin{bmatrix} 0 & 0 & 0 & -1 \end{bmatrix}^T \otimes {}^{m}q^U) \times l^U \tag{3.31} $$

$$ {}^{b}r_0^L = (\overline{{}^{m}q^L} \otimes \begin{bmatrix} 0 & 0 & 0 & -1 \end{bmatrix}^T \otimes {}^{m}q^L) \times l^L \tag{3.32} $$

where $l^U$ and $l^L$ refers to upper and lower segment lengths. Posture vectors ${}^{b}r_0^U$ and ${}^{b}r_0^L$ define a vector from the rotation center (shoulder joint) to the sensor attached on the upper and lower arm, respectively, in the GB reference frame.

By applying the orientation quaternions ${}^{b}q_t^U$ and ${}^{b}q_t^L$, postures at time $t$ are characterized as:

$$ \begin{bmatrix} 0 \\ {}^{b}r_t^U \end{bmatrix} = {}^{b}q_t^U \times \begin{bmatrix} 0 \\ {}^{b}r_0^U \end{bmatrix} \times \overline{{}^{b}q_t^U} \tag{3.33} $$

$$ \begin{bmatrix} 0 \\ {}^{b}r_t^L \end{bmatrix} = {}^{b}q_t^L \times \begin{bmatrix} 0 \\ {}^{b}r_0^L \end{bmatrix} \times \overline{{}^{b}q_t^L} \tag{3.34} $$

Therefore, position of the elbow and wrist joints at time $t$ can be calculated as:

$$ {}^{b}p_t^E = {}^{b}p_t^S + {}^{b}r_t^U \tag{3.35} $$

$$ {}^{b}p_t^W = {}^{b}p_t^E + {}^{b}r_t^L \tag{3.36} $$

## 3.7 3DArm Evaluation

In order to demonstrate the performance of 3DArm, the tracked positions were compared to the ones obtained through a commercially available system: Microsoft Kinect version 2.0.

The Microsoft Kinect incorporates an infrared light and a video camera to capture the user's full body movement in 3D space. It uses an algorithm to automatically determine anatomical landmarks on the body in real time [51]. Therefore, a human body is represented by a number of joints representing body parts such as head, neck, shoulders and arms, as depicted in Figure 3.7. Kinect's output are the 3D coordinates of each joint detected, represented in the Kinect's coordinate system.

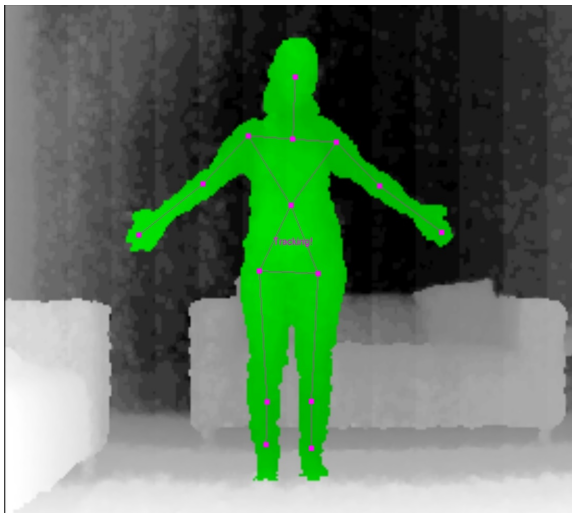

Figure 3.7: Skeletal tracking using a skeletal representation of various body parts. Each part or joint is represent by its correspondent tracking point.

### 3.7.1 Experimental Work

The experimental work is described next. In this section, the experimental setup, protocol and statistics will be presented.

#### 3.7.1.1 Experimental Setup

Before the evaluation begins, the experimental environment requires definition.

The Microsoft Kinect was connected to a PC via USB. The FhP-AICOS application which records the Pandlets' data allows the incorporation of Kinect measurements. Kinect's sample frequency was 30 Hz and the Pandlets' was 50 Hz. In order to compare the two signals, Kinect's outputs were interpolated in order to have the same number of samples as the Pandlets.

To properly compare the two systems, a rotation to align the two coordinate systems is required. To simplify the calculation, the Kinect is located in front of the subject so that the axes ${}^{B}x$, ${}^{B}y$ and ${}^{B}z$ of the GB reference frame are defined in parallel with the Kinect's frame axes ${}^{K}z$, ${}^{K}x$ and ${}^{K}y$. The experimental environment and a schematic of the two coordinate systems are depicted in Figure 3.8.

The relationship between the GB reference frame $O^{B}x^{B}y^{B}z$ and the Kinect frame $O^{K}x^{K}y^{K}z$ can be described as follows:

$$ {}^{B}x = {}^{K}z - z_{shift} \tag{3.37} $$

$$ {}^{B}y = {}^{K}x - x_{shift} \tag{3.38} $$

$$ {}^{B}z = {}^{K}y - y_{shift} \tag{3.39} $$

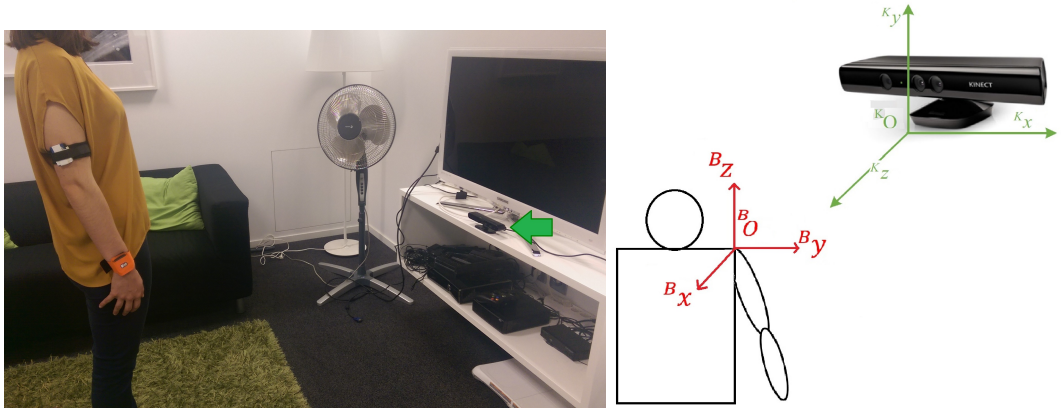


(a) (b)

Figure 3.8: User and Kinect. (a) Experimental environment setup (Kinect system marked with green arrow). (b) The GB reference frame $O^B x^B y^B z$ (seen from the back) and the Kinect frame $O^K x^K y^K z$.

where $[^B x, ^B y, ^B z]$ and $[^K x, ^K y, ^K z]$ are the coordinates in the GB reference frame $O^B x^B y^B z$ and the Kinect frame $O^K x^K y^K z$, respectively. $[x_{shift}, y_{shift}, z_{shift}]$ represent the translation between the origin of the GB reference frame and the origin of the Kinect frame. To measure translation $[x_{shift}, y_{shift}, z_{shift}]$, the position of the GB reference frame origin (that is, the shoulder joint) must be determined in the Kinect's frame. As mentioned above, since the user must remain in the initial position for a time interval of 10 seconds, during this time interval, the mean of the shoulder's position in the Kinect's frame is calculated and it is set to be the translation vector $[x_{shift}, y_{shift}, z_{shift}]$.

Then, to obtain the elbow and wrist joints detected by Kinect described in GB reference frame, the translation vector $[x_{shift}, y_{shift}, z_{shift}]$ is removed from the elbow and wrist joints' Kinect position. Afterwards, the axes are switched as described by equations 3.37, 3.38 and 3.39.

In order to assure that the upper and lower segments' length was the same for the 3DArm system and for the Kinect system, the elbow and wrist Kinect position vectors were normalized and then scaled to the respective upper and lower segment length.

#### 3.7.1.2 Experimental Protocol

Five healthy subjects were selected for the experiments. Before the experiments begin, the length of each segment of upper limbs was measured and then encoded into the computer program to be executed. Lengths of their arm segments are given in Table 3.1.

The two Pandlets were placed at the end of the upper and lower segments, aligned with each other and with the GB reference frame. Each subject was in front of the Kinect performing the requested experiments individually. Before the test begins, each subject has been informed to stay in the initial position for about 10 seconds. For that purpose, a chronometer was used so that only after a command did the users start performing the test.

The experiments are described bellow. Each subject repeated each test three times.

Table 3.1: Segment lengths of individual subjects in the experiments (units:cm).

| Subject | $l^U$ | $l^L$ |
|---|---|---|
| 1 | 30 | 37 |
| 2 | 29 | 34 |
| 3 | 33 | 35 |
| 4 | 34 | 36 |
| 5 | 30 | 35 |

- **Test 1** - subjects were asked to perform shoulder abduction/adduction as described in Figure 3.9. They swang their right arm to the side in the coronal plane keeping the arm straight, and returned to the starting position.

- **Test 2** - subjects were asked to perform shoulder flexion/extension as described in Figure 3.10. They swang their right arm to the front in the sagittal plane keeping the arm straight, and returned to the starting position.

- **Test 3** - subjects were asked to perform shoulder extension, rotation and adduction as described in Figure 3.11. They swang their rigth arm to the front in the sagittal plane keeping the arm straight, rotated to the coronal plane keeping the arm straight and returned to the starting position.

Figure 3.9: Test 1 - shoulder abduction/adduction.

#### 3.7.1.3 Experimental Statistics

Statistics based on the experiments are introduced in order to compare the two systems quantitatively.

The Euclidean distance between the estimated positions of the wrist and elbow joints using 3DArm and by Kinect was analyzed regarding maximum, mean and standard deviation.

Figure 3.10: Test 2 - shoulder flexion/extension.

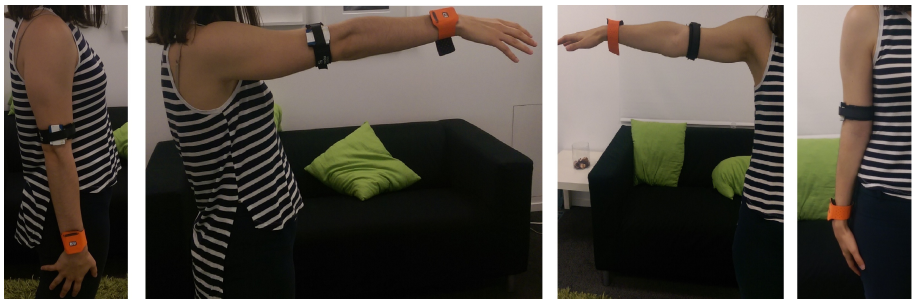

Figure 3.11: Test 3 - shoulder extension, rotation to the coronal side and shoulder adduction.

### 3.7.2 Results and Discussion

This Section describes the results obtained with the proposed methods for 3DArm implementation. These results are relative to the experimental work described in Section 3.7.1 and will provide the necessary information to evaluate the algorithm performance and discuss the possibility to incorporate the system developed into an upper limb tracking system suitable for different applications. This Section also enables the identification of gaps that need improvements. A simultaneous discussion of results is also done in this section.

Considering the overview block diagram depicted in Figure 3.1, after data acquisition, signal was pre-processed in order to obtain the orientation of the upper and lower segments, transforming the data from the sensor to the GB reference frame. Then, position and trajectory of the elbow and wrist joints were tracked.

The proposed experimental work was defined in order to compare the position and trajectory obtained using the 3DArm and using the Kinect. However, intermediate results relative to the orientation estimation are showed, prior to the results for the comparison between the two systems.

#### 3.7.2.1 Orientation Estimation

An Extended Kalman Filter was introduced in order to obtain the orientation between the sensor local reference frame and the GB reference frame. To improve estimation accuracy, the elbow biomechanical constraint was introduced in the EKF framework.

In order to evaluate the reliability of the orientation estimation with biomechanical constraints, the results with 3DArm were compared to the orientation estimation based on Complementary Filter (CF) [29] [52] without biomechanical constraints developed at FhP-AICOS.

For the elbow joint of an healthy subject, the abduction/adduction of the elbow is almost impossible, which means that the adduction angle is restricted to a very small angle. Therefore, the *y*-axis of the forearm and the normal of the *xy*-plane of the upper arm were used to model the constraint: the *y*-axis of the forearm and the *z*-axis of the upper arm, both described in the GB reference frame, should be virtually orthogonal all the time.

To exemplify the effectiveness of the geometrical constraint, the elbow adduction angles and the upper and lower orientation quaternion with the two sensor fusion methods are presented for the three experimental tests.

Figure 3.12 shows the angle between the *y*-axis of the forearm and the *z*-axis of the upper arm in the GB reference frame. In the figure, the blue line represents the result from the EKF sensor data fusion with biomechanical constraint, whereas the green line indicates the result from the CF sensor data fusion without biomechanical constraint. The results represented in Figure 3.12 demonstrate that:

- For **Test 1**, the angle obtained by EKF fusion with constraint deviates from 83 ° to 94 °, which is smaller than the result obtained by CF fusion without constraint, where the angle deviates from 72 ° to 92 °.
- For **Test 2**, the angle obtained by EKF fusion with constraint deviates from 85 ° to 97 °, which is smaller than the result obtained by CF fusion without constraint, where the angle deviates from 66 ° to 91 °.
- For **Test 3**, the angle obtained by EKF fusion with constraint deviates from 83 ° to 97 °, which is smaller than the result obtained by CF fusion without constraint, where the angle deviates from 68 ° to 92 °.

The comparison shows that the constraint can keep the adduction angle near the 90 ° for the three tests, compensating for the drift and improving estimation results. The variation between tests can be explained by the fact that the sensors are in different positions during the movements of the three tests, producing different angles between the *y*-axis of the lower and the *z*-axis of the upper arm. Therefore, the biomechanical constraint introduced can reduce and compensate drift of the inertial sensors, improving orientation estimation.

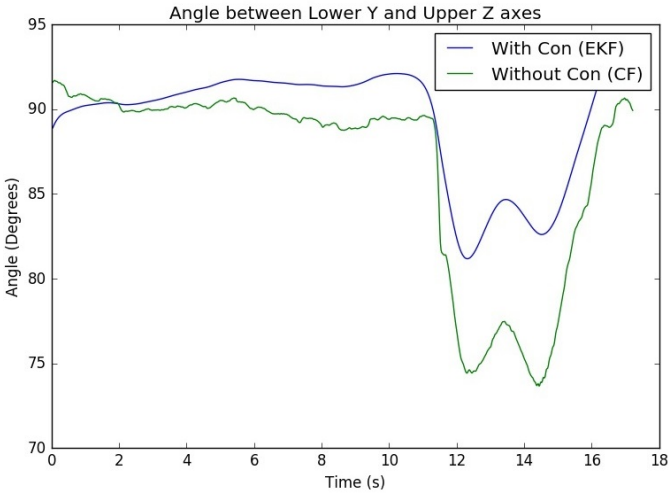


(a) Test 1.

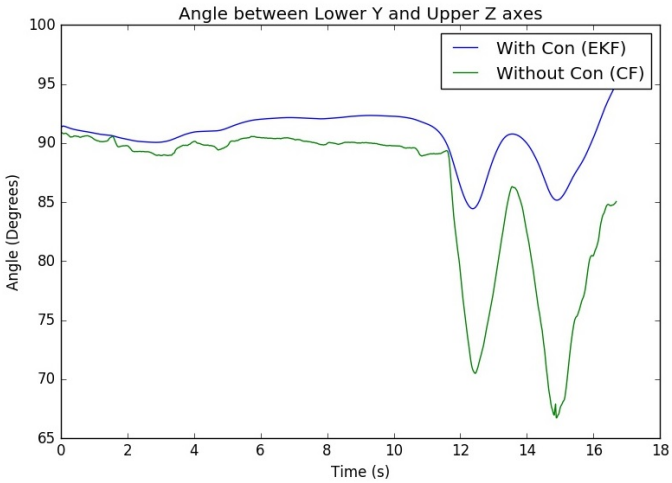


(b) Test 2.

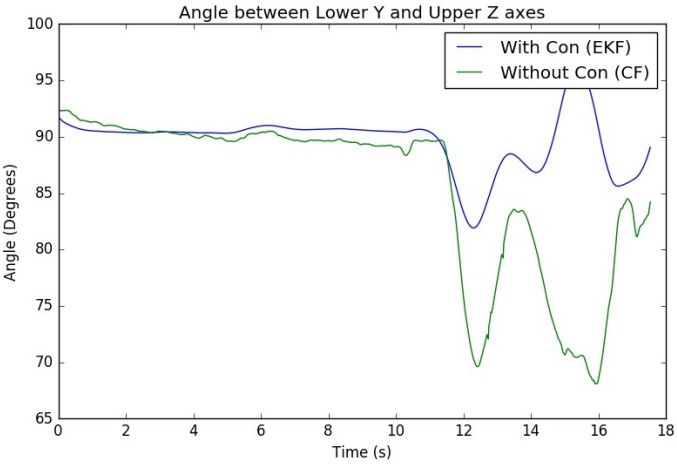


(c) Test 3.

Figure 3.12: Angle related to the abduction/adduction movement of the elbow joint during Test 1, 2 and 3. Blue line represents the result from the EKF sensor data fusion with biomechanical constraint, whereas green line indicates the result from the CF sensor data fusion without biomechanical constraint.

#### 3.7.2.2 Position and Trajectory Reconstruction

As described in Section 3.7.1, a setup with a Kinect system was created in order to compare the position and trajectory obtained using the 3DArm and using the Kinect. Five healthy subjects performed the three tests described. The statistics based on the experiments are introduced in order to compare the two systems quantitatively.

In order to directly compare the positions of the two systems, some procedures were necessary in order to fit the signals. As it can be seen in Figure 3.13, which represents the elbow and wrist joints' position for Test 1, there is an amplitude difference, in this case, in the *y*-axis, when the arm is stationary in the initial position for 10 seconds. This can be explained with the Kinect frame transformation to the GB reference frame: if the Kinect was not parallel to the GB reference frame, the transformation between frames could result in signal amplitude differences at the beginning. A lag between the Kinect signal and the 3DArm signal is also presented, which can be explained by lack of synchronization between signals.

To fit the signals, the amplitude difference in the Kinect signals was removed so that only displacements from an initial position would be evaluated and the signal lag was corrected. The amplitude difference was calculated for the first position and then removed for all the Kinect signals. The lag was calculated by moving the Kinect signal over the 3DArm signal and calculating the Euclidean distance between them: the smaller Euclidean distanced found was the one that provided the best fit. Therefore, the calculated lag was used to synchronize signals.

The results illustrating the upper limb movements during Test 1, 2 and 3, will be presented in terms of elbow and wrist positions (in centimeters) in time (in seconds) for the three axes and in terms of *xy*, *xz* and *yz*-planes, which represent the superior/inferior, rigth/left lateral and front/back views, respectively. Since Test 1 and 2 represent a 2D movement, only two planes are necessary in order to visualize the movement (*xz* and *yz*-planes were used), and since Test 3 represents a 3D movement, the three planes are necessary.

For one example of Test 1, the elbow and wrist positions obtained using the 3DArm and using the Kinect are depicted in Figure 3.14. Despite Test 1 describing a shoulder abduction/adduction, which represents a movement in the *yz*-plane, as it can be seen in Figure 3.14c, the subject did not perform the movement strictly along the coronal plane, since there is movement detection in the *x*-axis, as it can be seen in Figure 3.14b. These results are confirmed by Figure 3.14a. However, the three figures show similarity between the two tracking systems.

Regarding on example of Test 2, the elbow and wrist positions obtained using the 3DArm and using the Kinect are depicted in Figures 3.15. Despite Test 2 describing a shoulder flexion/extension, which represents a movement in the *xz*-plane, as it can be seen in Figure 3.15b, the subject did not perform the movement strictly along the sagittal plane, since there is movement detection in the *y*-axis, as it can be seen in Figure 3.15c. These results are confirmed by Figure 3.15a. However, similarly to Test 1, the three figures show similarity between the two tracking systems.

For Test 3, the elbow and wrist positions obtained using the 3DArm and using the Kinect are depicted in Figure 3.16. Since Test 3 describes a movement in the three planes, movement was

detected around the three axes. Similarly to Test 1 and 2, the three figures show similarity between the two tracking systems.

In order to compare the two systems quantitatively, the Euclidean distance between them was defined in terms of maximum, mean and standard deviation for all the tests performed for the different subjects. These results are summarized in Table 3.2. Five subjects performed each test three times, so after the definition of the mean, standard deviation and maximum Euclidean distance for each test and for each subject, a mean value was presented for the three parameters.

Considering Table 3.2, it is possible to observe that the mean, standard deviation and maximum Euclidean distance were higher for the wrist joint then for the elbow joint. This can be explained because the wrist position is based on the elbow position, therefore the errors for the wrist tracking include the ones for the elbow tracking. Comparing the values for the different tests, there is no significant difference between them.

The values presented in Table 3.2 can be explained by the difficulty of aligning the sensors with each other. As it can be seen in Figures 3.9, 3.10 and 3.11, the upper and lower sensors may not be fully aligned, which translates to a GB reference frame definition that may not correspond to the one defined in Section 3.2.2. This happens because of the upper limb's anatomy, which makes this task extremely difficult: not only the sensors' coordinate system must be aligned with each other and with the GB reference frame (that is, ${}^{s}x$ must be aligned with the ${}^{b}x$ and so one) but also the origin of each reference frame must be the same, which means no translations could happen between them.

Despite the Kinect tracking system being the system chosen to be compared to the 3DArm system, it is known that the Kinect has a "self-occlusion" problem (observation of the movements of upper limb can be obstructed by the body parts) that commonly occurs when tracking movements of the upper limb. Movements like flexing of the shoulder can result in areas on the upper limb that will not be captured by the camera during the movement trajectory. An illustration of this situation is depicted in Figure 3.17, where an example of Test 2 is presented. Test 2 consists in shoulder flexion/extension and as it can be seen, the Kinect signal in the $x$-axis presents a position variation that was not expected. This happened because the wrist tracking point was occluded by the elbow tracking point or vice versa.

This situation results in the increasing of the Euclidean distance between the two systems, which can explain the high values for the maximum Euclidean distance detected. Another problem related to the use of Kinect is the alignment of the two systems in the experimental setup where the Kinect coordinate system could not be fully parallel to the GB reference frame and therefore resulting in a higher Euclidean distance .

All in all, even though small deviations between the Kinect and the 3DArm have been observed in the estimated joints' position (a maximum mean error of 10,60 centimeters and 16,33 centimeters was found for the elbow and wrist joints, respectively), the experimental results demonstrated that the proposed tracking system had an acceptable performance in different movements. The Kinect precision is sufficient for most of the tracking applications (for instance, upper limb tracking in home rehabilitation context), therefore 3DArm could be a viable alternative with the ad-

Table 3.2: Statistical results of the tests performed for elbow and wrist joints, where Std refers to standard deviation and Max to the maximum. All parameters are represented in centimeters (cm).

| Test | Euclidean Distance (cm) | | | | | |
|---|---|---|---|---|---|---|
| | Mean | | Std | | Max | |
| | Elbow | Wrist | Elbow | Wrist | Elbow | Wrist |
| 1 | 1,80 | 3,08 | 2,82 | 4,17 | 9,53 | 14,13 |
| 2 | 1,37 | 2,11 | 1,91 | 2,52 | 8,58 | 10,95 |
| 3 | 1,64 | 2,28 | 2,71 | 4,48 | 10,59 | 16,32 |

vantages of being a portable system, without "self-occlusion" problems, small-sized, unobtrusive, low-cost and lightweight.

In order to reduce errors, future work can be defined to improve 3DArm tracking.

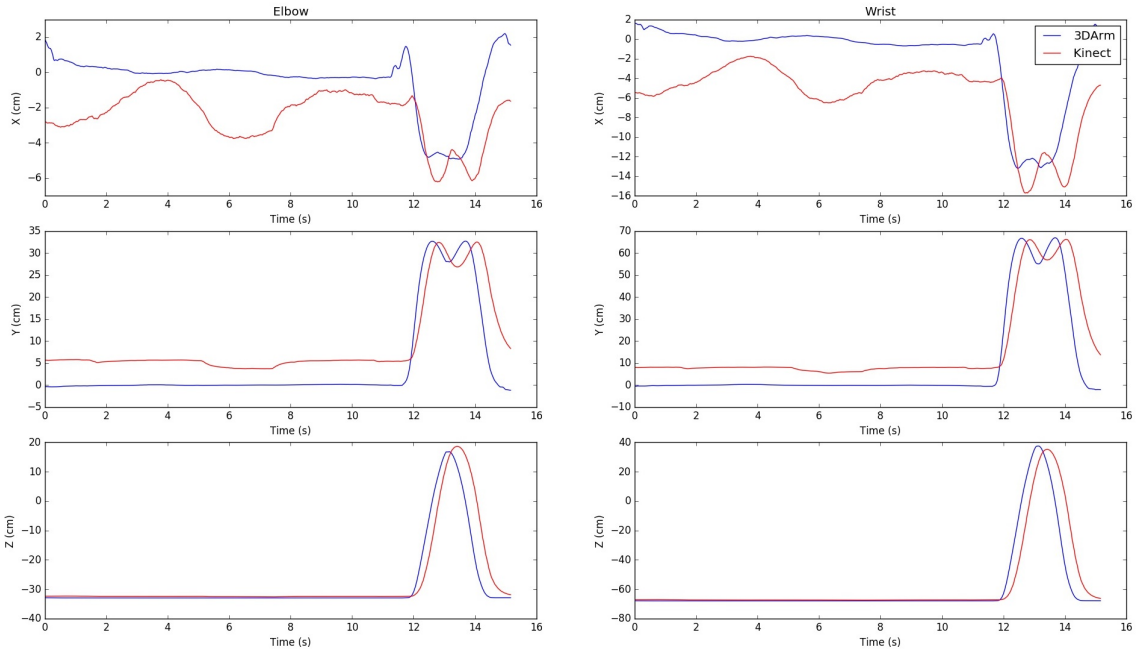


Figure 3.13: Test 1 - Elbow and wirst positions (centimeters) along time (seconds). The blue line represents the 3DArm results and the red line represents the Kinect results. A lag between the 3DArm and the Kinect signal and an amplitude difference are present.

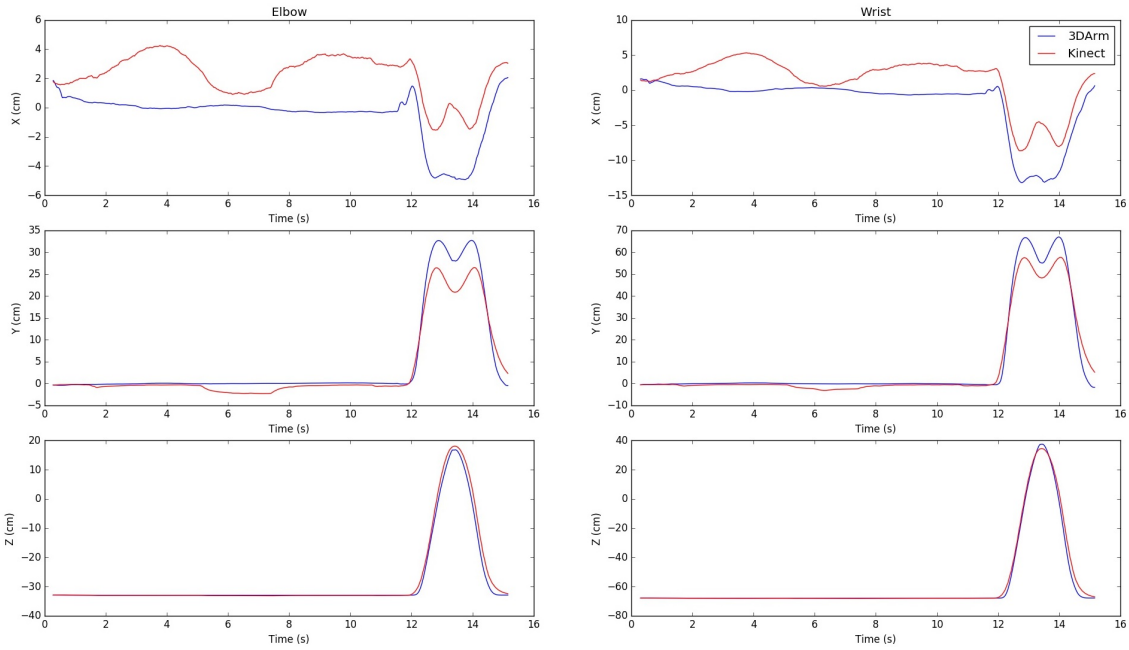


(a) Elbow and wrist positions (centimeters) along time (seconds) in the three axis.

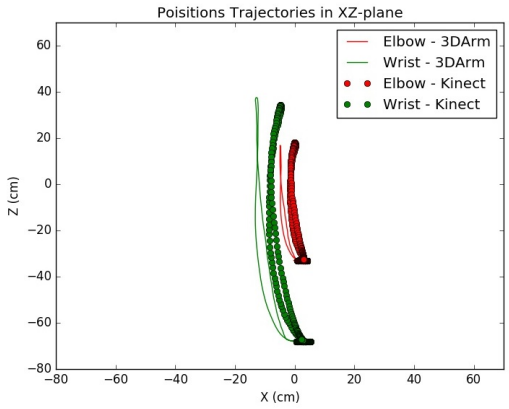


(b) Elbow and wrist positions in the *xz*-plane.

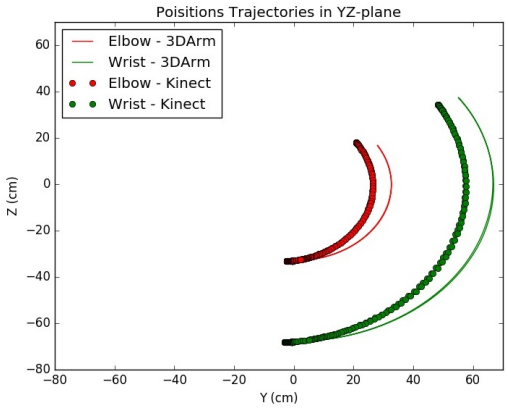


(c) Elbow and wrist positions in the *yz*-plane.

Figure 3.14: Test 1 - Elbow and wrist positions along time (a), in the *xz*-plane (b) and in the *yz*-plane (c). In (a), the blue line represents the 3DArm results and the red line represents the Kinect results. In (b) and (c) the red is for the elbow and green for the wrist; the line represents the 3DArm results and the dots the Kinect results.

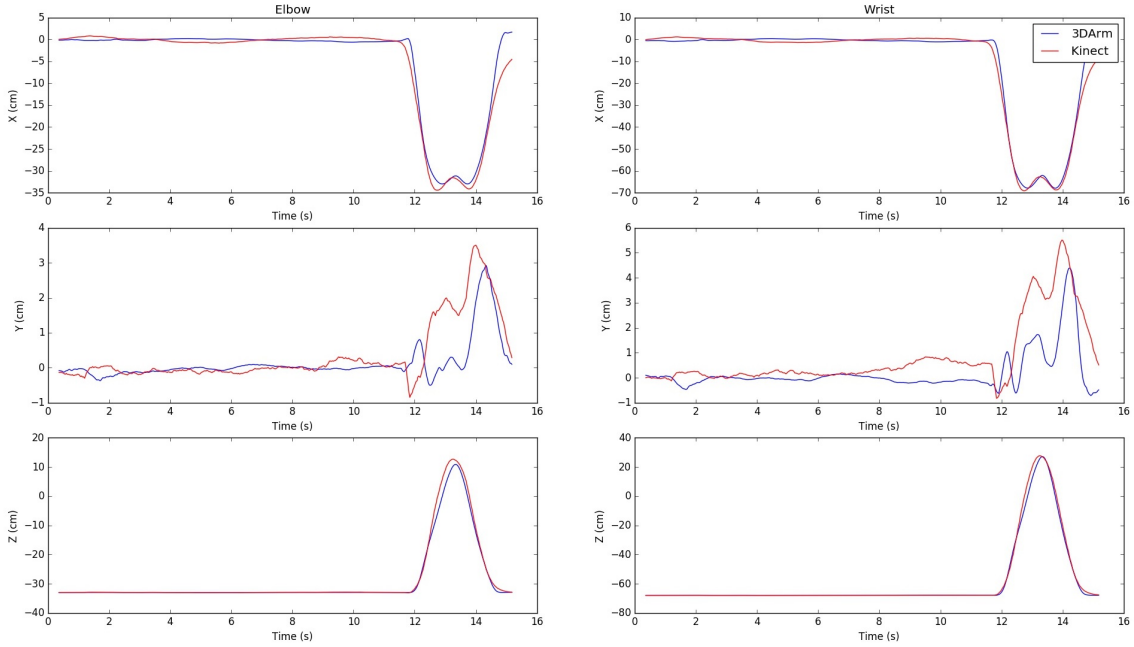


(a) Elbow and wrist positions (centimeters) along time (seconds) in the three axis.

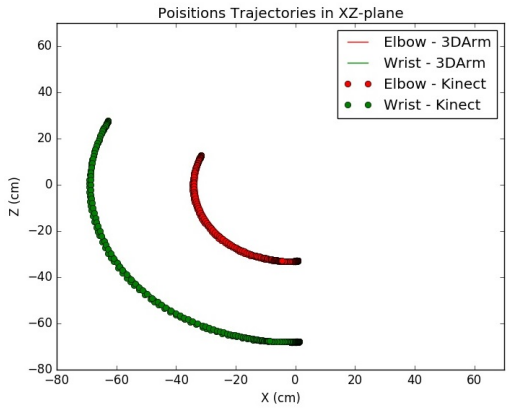


(b) Elbow and wrist positions in the *xz*-plane.

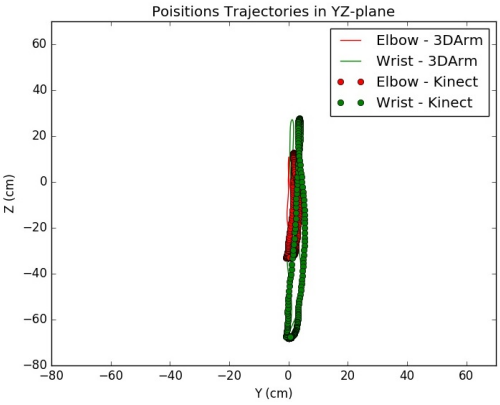


(c) Elbow and wrist positions in the *yz*-plane.

Figure 3.15: Test 2 - Elbow and wrist positions along time (a), in the *xz*-plane (b) and in the *yz*-plane (c). In (a), the blue line represents the 3DArm results and the red line represents the Kinect results. In (b) and (c) the red is for the elbow and green for the wrist; the line represents the 3DArm results and the dots the Kinect results.

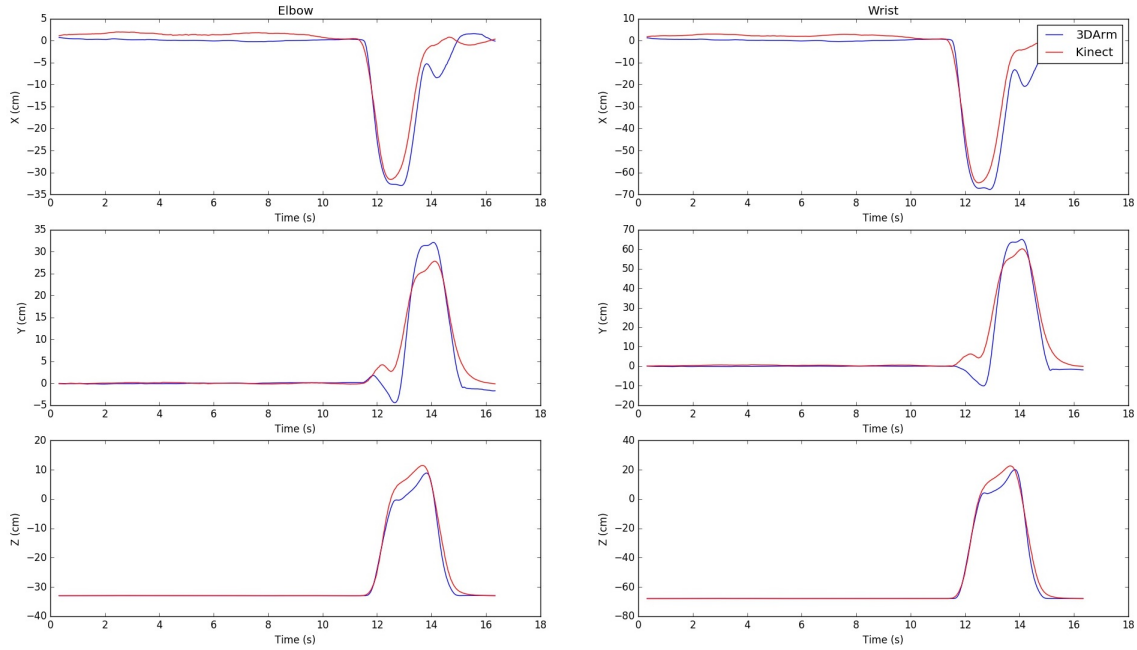


(a) Elbow and wrist positions (centimeters) along time (seconds) in the three axis.

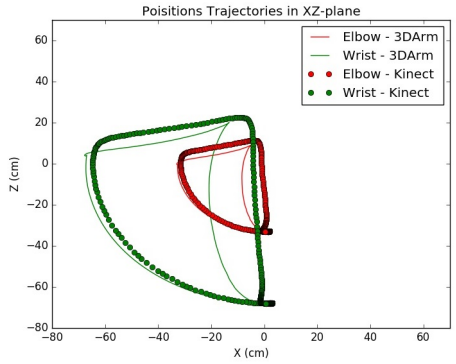


(b) Elbow and wrist positions in the *xz*-plane.

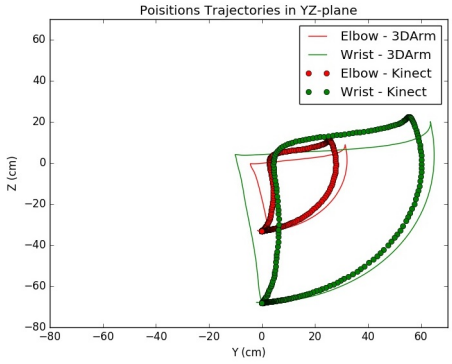


(c) Elbow and wrist positions in the *yz*-plane.

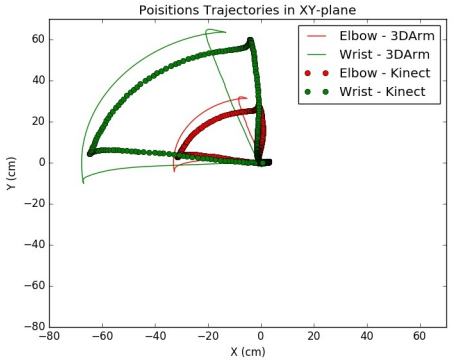


(d) Elbow and wrist positions in the *xy*-plane.

Figure 3.16: Test 3 - Elbow and wrist positions along time (a), in the *xz*-plane (b), in the *yz*-plane (c) and in the *xy*-plane (d). In (a), the blue line represents the 3DArm results and the red line represents the Kinect results. In (b), (c) and (d) the red is for the elbow and green for the wrist; the line represents the 3DArm results and the dots the Kinect results.

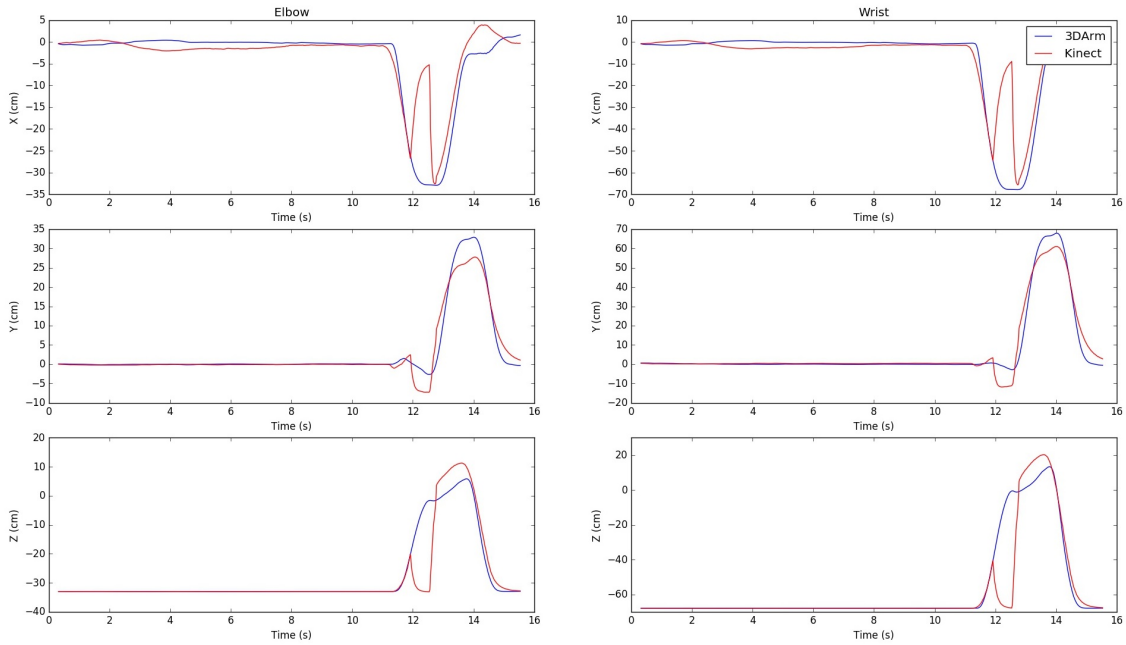


Figure 3.17: Kinect occlusion problem in Test 2 (shoulder flexion/extension).

## 3.8 Proof of Concept

A visualization tool reproducing the movement of the arm in a model was developed as a proof of concept of 3DArm.

The upper limb was modeled as three points, which represent the shoulder, elbow and wrist joints, linked by two lines, which represent the upper and lower segments. The visualization tool was constructed using a 3D graphic where the joints' positions were described in real-time.

To evaluate the performance of the visualization tool, a "free movement" test was performed by a subject for about one minute. No indications of the movements were provided. Some photos were taken to illustrate the visualization tool, which is depicted in Figure 3.18. For comparison with 3DArm, the elbow and wrist positions obtained with Kinect are also illustrated.

As it can be seen in Figure 3.18, the visualization tool is reproducing in real-time the movement that is being executed. Looking at the 3DArm upper limb model, it is possible to conclude that it is correctly reproducing the movement with a slight difference from the Kinect model. These differences were already explained in Section 3.7.2.2, and are mainly due to the misalignment between the Kinect and the GB reference system. It is important to mention that after one minute of tracking, the subject returned to the initial position and so did the joints' positions of the 3DArm model, which means that there was no cumulative errors.

(a)

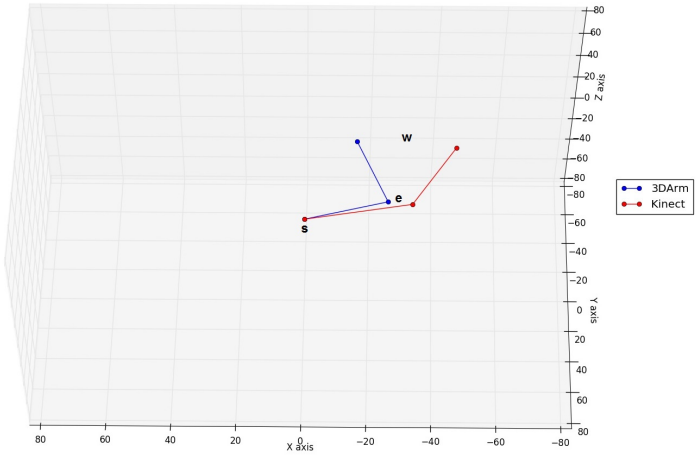


(b)

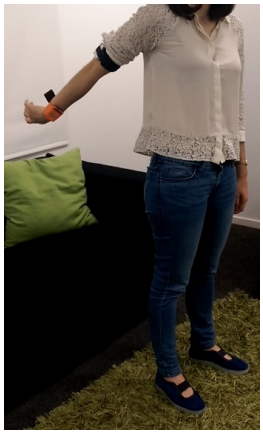

(c)

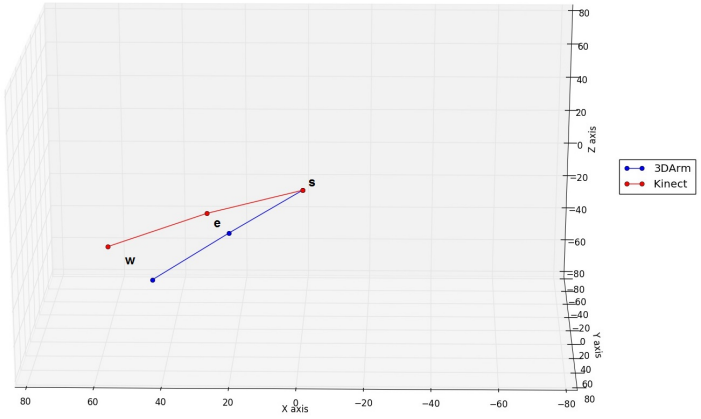


(d)

Figure 3.18: Free movement test: (a) and (c) are photos of the subject performing a free movement, (b) and (d) are the real-time results of the visualization tool reproducing movements (a) and (b). Letters *s*, *e* and *w* represent the shoulder, elbow and wrist joint, respectively.

# Chapter 4

# Sensor-to-Body Frame

As it was discussed in Section 3.7.2.2, it was difficult to guarantee that the two IMUs were aligned with each other and with the mounted arm segment. To overcome this problem, and as it was detailed in Section 2.4, a sensor-to-body frame transformation, without the need of aligning the sensors with each other and with the GB reference frame, was developed.

This transformation was based on the work described in [46], by Y.Wang et al, in 2014. As mentioned in Section 2.4, the final objective of this process is to describe the upper limb trajectories in a GB reference frame defined a priori, without the need for sensor alignment.

Additionally, the algorithm proposed in [46] can also automatically estimate the arm length so that position trajectories of the elbow and the wrist joints are reconstructed without manual measurements.

As the sensors' position in the respective segments is unknown, the use of the biomechanical constraints defined for the 3DArm system cannot be applied in this situation, since the axes which define the elbow adduction/abduction angle are unknown. Therefore, for the sensor-to-body frame transformation, the orientation relative to the earth reference frame was obtained by CF [29, 52] without biomechanical constraints, developed at FhP-AICOS.

Before the development of the sensor-to-body frame algorithm, a preliminary evaluation was conducted in order to evaluate the inherent errors to the sensor-to-body frame transformation process. Then, it is presented the data acquisition, the theoretical formulations and the results and discussion of the sensor-to-body transformation process.

## 4.1 Preliminary Evaluation

A preliminary evaluation was performed in order to evaluate the inherent errors present in the sensor-to-body transformation process when sensors were accurately aligned with the body. The upper limb movement was simulated using a setup with two equal segments linked by a hinge, which is depicted in Figure 4.1. The setup was called *Wodden Arm*, and it was built to replicate a joint with one degree of freedom. This way, the movement of the *Wodden Arm* was completely

controllable. As it can be seen in Figure 4.1, the *Wodden Arm* was placed on a desk over a printed protractor and a sensor was placed at the end of one segment.

Since the *Wodden Arm* has only one joint with one DOF and the movement around that joint is completely controllable, no biomechanical constraints were applied. To track the sensor's position, the orientation was obtained by a CF sensor fusion method [29, 52] developed by FhP-AICOS. This CF sensor fusion method only takes into account the accelerometer and gyroscope measurements.

The orientation obtained was relative to the earth reference frame, so to obtain the orientation relative to the global reference frame and since the sensor was aligned with the global reference frame, sensor-to-body frame transformation (described in Section 3.4) was applied. Then, the sensor's position was tracked based on the methods described in Section 3.6.

The experimental work developed is presented next, where the sensor and the global reference frames are defined.

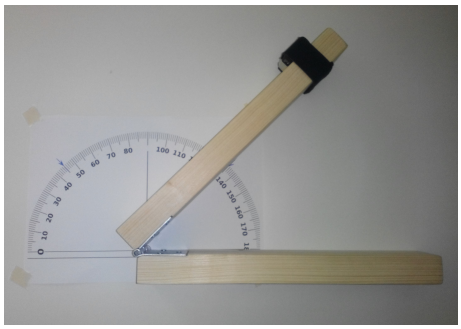

Figure 4.1: *Wodden Arm* placed on the desk.

### 4.1.1 Experimental Work

In order to evaluate the tracking of the sensor placed on the *Wodden Arm*, a protractor was used and movements with known angles were performed. Therefore, to determine the position coordinates of the sensor placed on the *Wodden Arm*, a protractor was used: knowing the angle of the movement and the segment length $L$, it was possible to determine the position of the sensor placed on the *Wodden Arm* in each axis.

Two different tests were performed, varying the position of the *Wodden Arm*. Before starting the movement, the segment with the sensor did not move for about 10 seconds. To identify the movement angle, several stages were defined along the two tests:

1. **Test 1** - The *Wodden Arm* was placed on a desk and then the segment on which the sensor was mounted was moved in the following order: Stage 1 $\rightarrow$ Stage 2 $\rightarrow$ Stage 3 $\rightarrow$ Stage 4, returning to Stage 1 and repeating the sequence 4 times, maintaining each stage for about 10 seconds. In this case, Stage 1 corresponds to a rotation of 0°, Stage 2 to a rotation of 45°, Stage 3 to a rotation of 90° and Stage 4 to a rotation of 180°. The movement sequence is depicted in Figure 4.2a.

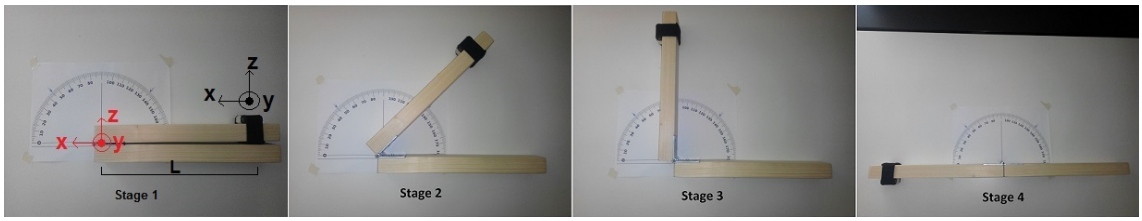


(a)

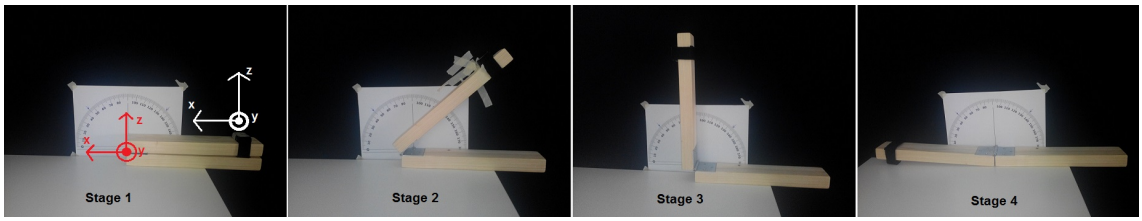


(b)

Figure 4.2: Movement sequence for Test 1 (a) and for Test 2 (b). The black reference system corresponds to the sensor reference frame and the green reference system to the global reference system. $L$ represents the length of the segment, that is, from the origin $O$ to the place where the sensor was mounted, and is the same for Test 1 and 2.

2. **Test 2** - The *Wodden Arm* was placed on a wall and then the segment on each the sensor was mounted was moved in the same order as in Test 1. The movement sequence is depicted in Figure 4.2b.

Since the movement is performed in the $xz$-plane, it corresponds to a rotation about the $y$-axis.

As it can be seen, the test varies in terms of the *Wodden Arm* position. These two positions were evaluated in order to understand the influence of the accelerometer and the gyroscope measurements in the CF fusion. Since the accelerometer reading are used to correct the vertical direction, the *Wodden Arm* could be subject to more errors when it is placed on the desk.

The global reference frame defined is the one where the positions will be represented. Since the *Wodden Arm* is plane, it is easy to correctly align the sensor.

Knowing $L$ and the angle of each stage, it is possible to calculate the expected position at each stage. Based on this information, absolute errors were calculated considering the difference, in absolute value, between the expected position and the one obtained by the algorithm developed.

### 4.1.2 Results and Discussion

The results for the two tests are presented. To obtain the absolute error, the expected position for each axis in each stage was calculated, knowing that $L$=28 centimeters. The expected positions are described in Table 4.1.

For the two tests and for each axis, both the position and the absolute errors are presented in time.

For Test 1, the results are depicted in Figures 4.3a and 4.3b. As depicted in Figure 4.3a, the positions in $x$, $y$ and $z$ are similar to a periodic wave, which is expected since the movement was

Table 4.1: Expected position for each axis in the 4 Stages. Expected positions are represented in centimeters (cm).

| Axis | Expected Position (cm) | | | |
|---|---|---|---|---|
| | Stage 1 | Stage 2 | Stage 3 | Stage 4 |
| x | -28 | -19.8 | 0 | 28 |
| y | 0 | 0 | 0 | 0 |
| z | 0 | 19.8 | 28 | 0 |

cyclic. As it can be seen in Figure 4.3b, the maximum absolute error is about 4 centimeters. In the same stage, the errors do not increase significantly with time, which means that for the acquisition time period, no significant drift occurred.

For Test 2, the results are depicted in Figures 4.4a and 4.4b. The positions in $x$, $y$ and $z$ are also similar to a period wave, as in Test 1. Regarding the absolute errors, the maximum is about centimeters, and the errors do not significantly increase with time.

Comparing Test 1 with Test 2, the results were practically identical, which indicates that the sensor tracking is independent of the position of the *Wodden Arm*. As it can be seen in Figure 4.4b, the errors with higher value can be explained by the position of the sensor in Stage 4. As depicted in Figure 4.2b, at this Stage, the sensor cannot completely rotate 180° because it hits the desk before completing the rotation.

Although the *Wodden Arm* was a controllable object, the tracking positions presented errors. Since the sensor was effectively aligned with the global reference frame, the errors detected in these tests can be due to a misalignment of the IMU inside the Pandlet box and due to the errors inherent to the sensor fusion process and noisy sensor readings.

To conclude, the objective of these preliminary tests was to evaluate the errors of a completely controlled scenario. Therefore, these errors can propagate to the tracking positions even if the sensor is aligned with the global frame and when no external source of correction is considered (for example, a biomechanical restriction). This means that the errors described in this Section are inherent to the sensor-to-body transformation.

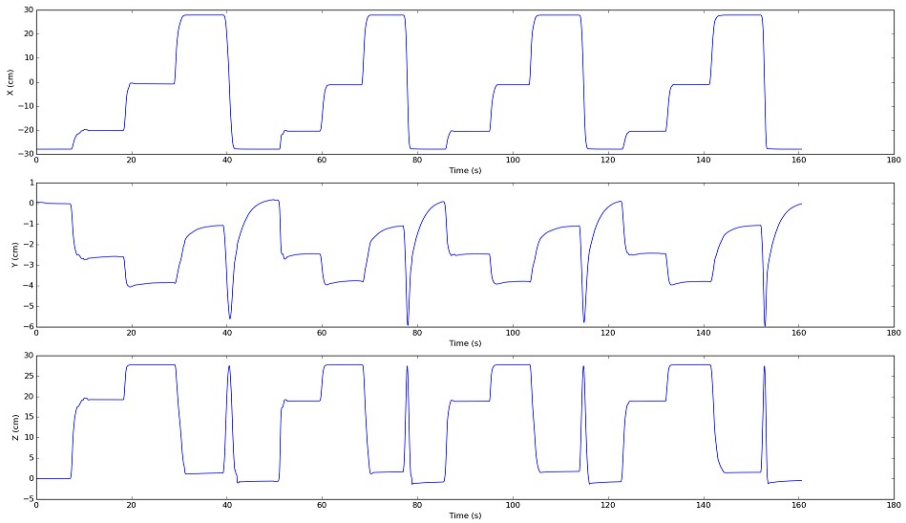


(a) Positions (centimeters) in time (seconds).

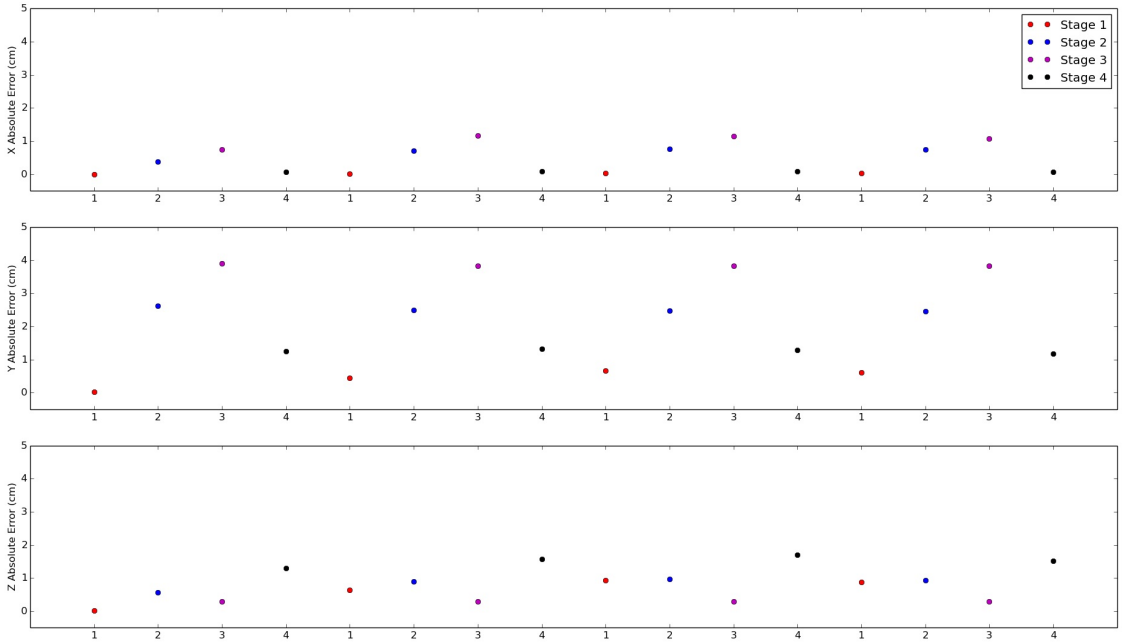


(b) Absolute errors (centimeters).

Figure 4.3: Test 1 results. Positions for each axis are represented in (a) and absolute errors are represented in (b). In (b) the time it is not continuous, instead it is represented by a point that corresponds to the stage where the sensor was in that time.

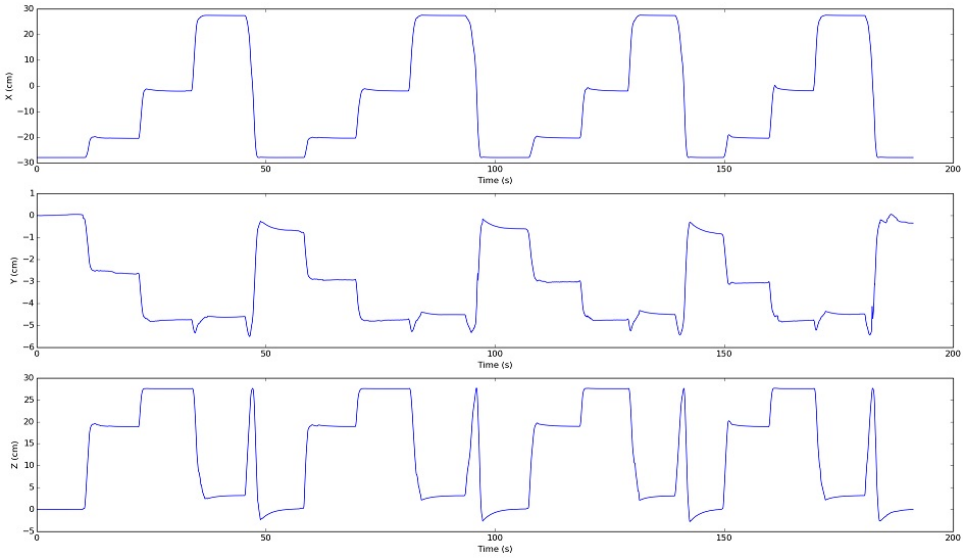


(a) Positions (centimeters) along time(seconds).

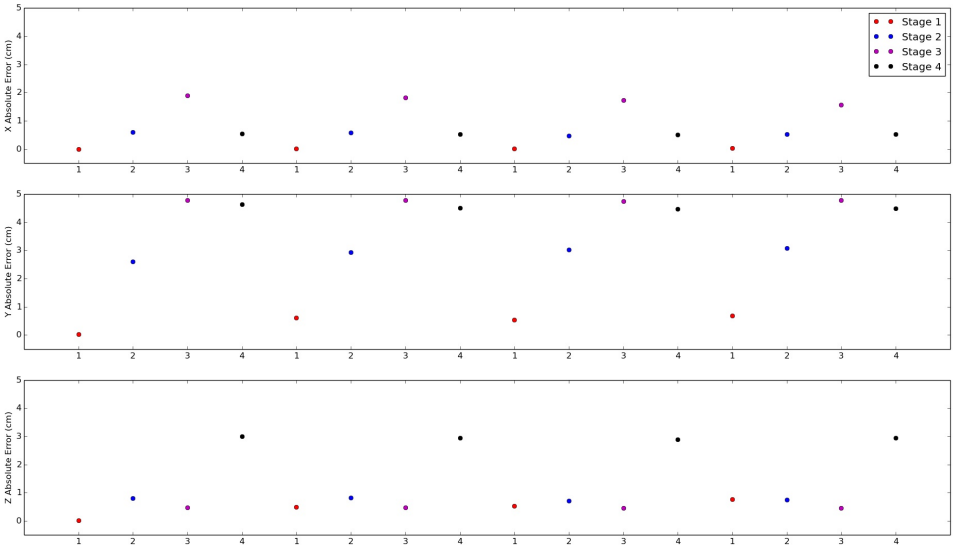


(b) Absolute errors (centimeters).

Figure 4.4: Test 2 results. Positions for each axis is represented in (a) and absolute errors are presented in (b). In (b) the time it is not continuous, instead it is represented by a point that corresponds to the stage where the sensor was in that time.

## 4.2 Data Acquisition

In order to define the sensor-to-body frame transformation, it was necessary to define the GB reference frame, where, independently of the sensor placement, joint positions and trajectories will be described. In this Section, it is also defined a protocol with a calibration movement that allows to find the orientation between the sensors and the GB reference frame.

### 4.2.1 Kinematic Model and Global Body Frame

The Kinematic Model and Global Body Reference Frame defined were the same as in Section 3.2.2. The difference relies on sensor placement: now the sensors are placed at the end of the upper and lower arm and in any orientation, without aligning them with the GB reference frame.

### 4.2.2 Acquisition Protocol

After attaching the IMUs to the upper and lower arm (close to the elbow and wrist joint, respectively), data were acquired in two different configurations, varying the sensor's attachment orientation:

- **Configuration 1** - sensors where aligned with each other as depicted in Figure 4.5a, but were not aligned with the GB reference frame. With this configuration there is only rotation between the sensor frame and the GB reference frame.
- **Configuration 2** - sensors were neither aligned with each other nor with the GB reference frame, as depicted in Figure 4.5b.

The length of each segment was measured with a tape measure (with an uncertainty of $\pm$ 0.5 cm) in order to evaluate the estimation of lengths.

In Configurations 1 and 2, users were asked to keep their right arm (with the sensors attached) straight down for a few seconds, from time 0 to time $t_1$. Then they swang to the side in the coronal plane still keeping their arm straight and returned to the start position. The swing duration was labeled from time $t_1$ to time $t_2$. At the end of the swing, users kept the arm straight down for another few seconds. This movement is depicted in Figure 4.6. Considering the GB reference frame, this movement represents a rotation around the $x$-axis.

(a) Configuration 1. (b) Configuration 2.

Figure 4.5: Sensor's attachment in Configuration 1 (a) and 2 (b).

(a) $Down_1$. (b) *Swing* (c) $Down_2$.

Figure 4.6: Calibration movement sequence: (a) $Down_1$ refers to the initial phase when the arm is stationary, from time 0 to time $t_1$, (b) *Swing* refers to the pahse when the arm is swinging, from time $t_1$ to $t_2$, and (c) $Down_2$ corresponds to the phase when the arm returns to the initial position.

## 4.3 Theoretical Formulations

This section describes the formulations to determine the orientation of each arm segment relatively to the GB reference frame and to estimate the upper limb segment lengths. The variables have the same notations as the ones described in Chapter 3.

The final objective is to determine the upper and lower posture vectors, ${}^{b}r_{0}^{U}$ and ${}^{b}r_{0}^{L}$, and the upper and lower orientation between the segments and the GB reference frame, ${}^{b}q_{t}^{U}$ and ${}^{b}q_{t}^{L}$. Then, these vectors can be substituted into equations 3.33, 3.34, 3.35 and 3.36 to obtain the positions and trajectories in the GB reference frame.

In order to define the vectors described above, the theoretical formulations are divided in three different phases: definition of posture vectors ${}^{s}r_{t}^{U}$ and ${}^{s}r_{t}^{L}$ at time $t$, definition of GB reference frame, and lastly, with the results of the two previous phases, definition of ${}^{b}r_{0}^{U}$, ${}^{b}r_{0}^{L}$, ${}^{b}q_{t}^{U}$ and ${}^{b}q_{t}^{L}$.

### 4.3.1 Definition of posture vectors ${}^{s}r_{t}^{U}$ and ${}^{s}r_{t}^{L}$

The posture vectors ${}^{s}r_{t}^{U}$ and ${}^{s}r_{t}^{L}$ define a vector from the rotation center (the shoulder joint) to the sensor attached on the upper and lower arm, respectively, in the sensor's local reference frame. During the swing phase, since the sensor was rotating, it was its local reference frame. Therefore, ${}^{s}r_{t}^{U}$ and ${}^{s}r_{t}^{L}$ must be constant. The upper and lower arm posture vectors could be estimated through a minimum mean square error (MMSE) method as well as the segments' length, with no previous measurements.

During the swing phase, since the two sensors were going through a circular motion, their instantaneous linear and angular velocities in the sensor's local reference frame are related by

$$ {}^{s}v_{t}^{U} = {}^{s}w_{t}^{U} \times {}^{s}r_{t}^{U} \tag{4.1} $$

where $\times$ represents the cross product between two element column vectors. Considering that ${}^{s}r^{U}$ is constant, it can be estimated by using the MMSE through the following formula:

$$ {}^{s}r^{U} = \underset{{}^{s}r^{U}}{\arg\min} \sum_{t=t_1}^{t_2} \left\| {}^{s}w_{t}^{U} \times {}^{s}r^{U} - {}^{s}v_{t}^{U} \right\|^2 \tag{4.2} $$

To implement equation 4.2, it was necessary to obtain instantaneous angular ${}^{s}w_{t}$ and linear velocities ${}^{s}v_{t}$ in the sensor's local reference frame.

The angular velocity could be directly obtained from the gyroscope measurements, after pre-processing defined in 3.3. To obtain the linear velocity, it was necessary to first determine the linear acceleration. In order to do that, the gravity component needs to be removed from acceleration measurements. Since the gravity component is the result of a low-pass filter, also presented in 3.3, the resulting signal was subtracted to the acceleration measurement, and linear acceleration was obtained. Then, linear acceleration signal could be integrated to obtain linear velocity.

### 4.3.2 Global Body Reference Frame definition

The uniform GB reference frame was constructed from individual sensor's temporary global reference frames. As the sensors can be mounted in any position, a temporary global reference frame was introduced, which is aligned with the sensor's local reference frame when the arm is straight down from time 0 to $t_1$. To construct this frame, ${}^{i}q_t^U$ was projected to the temporary global reference frame as

$$ {}^{t}q_t^U = (\overline{{}^{i}q^U})^{-1} \times {}^{s}q_t^U \tag{4.3} $$

where ${}^{s}q_t^U$ represents the sensor's orientation relatively to the earth reference frame. Here, the orientation employed is the one determine by a Complementary Filter (developed by FhP-AICOS). The quaternion ${}^{i}q^U$ represents the mean of orientation quaternions ${}^{s}q_t^U$ from time 0 to $t_1$ (i.e. when the arm is straight down).

Regarding the right arm, when it is straight down, it is approximately perpendicular to the axial plane. Therefore, $-{}^{t}r_0^U$ can be set as the $z$-axis of the global reference frame pointing from the elbow joint to the shoulder joint. Since at time 0 the sensor's local reference frame was aligned with its temporary global reference frame, $-{}^{t}r_0^U$ was equivalent to $-{}^{s}r^U$.

Meanwhile, since the $y$-axis is parallel to the coronal plane, it can be approximated by finding a vector in the direction of posture vector ${}^{s}r^U$ when the arm is parallel to the ground, that is, in the middle of the swing interval (from $t_1$ to $t_2$) . The swiging plane is defined by ${}^{t}r_t^U$ in equation 4.4.

$$ \begin{bmatrix} 0 \\ {}^{t}r_t^U \end{bmatrix} = {}^{t}q_t^U \times \begin{bmatrix} 0 \\ {}^{s}r^U \end{bmatrix}^T \times \overline{{}^{t}q_t^U} \tag{4.4} $$

The $y$-axis was defined by the ${}^{t}r_{t_{med}}^U$ vector where $t_{med}$ corresponds to the time value in the middle of the swing interval. The remaining $x$-axis was calculated by the cross product between the $z$-axis and $y$-axis.

### 4.3.3 Definition of ${}^{b}r_0^U$, ${}^{b}r_0^L$, ${}^{b}q_t^U$ and ${}^{b}q_t^L$

After having $x$, $y$ and $z$ axes, a rotation matrix $B^U$ was constructed by putting the column vector $x$, $y$ and $z$ together as a $3\times3$ matrix. Then, the rotation matrix $R^U$ representing the orientation of the global reference frame relative to the initialization frame can be calculated as:

$$ R^U = (B^U)^{-1} \tag{4.5} $$

Having the rotation matrix $R^U$, its corresponding quaternion $q^U$ was calculated (Appendix B). After that, it was possible to define

$$ {}^{b}r_0^U = R^U . {}^{s}r^U \tag{4.6} $$

$$ {}^{b}q_t^U = q^U \times {}^{t}q_t^U \times \overline{q^U} \tag{4.7} $$

By applying the same methods, ${}^{b}r_0^W$ and ${}^{b}q_t^L$ could be calculated. ${}^{b}r_0^L$ is obtained by subtracting ${}^{b}r_0^U$ to ${}^{b}r_0^W$.

## 4.4 Results and Discussion

The two Pandlets sensors were placed next to the wrist joints, respectively, where $l^U$ = 24 cm and $l^L$ = 20 cm.

An healthy female subject was asked to perform the calibration motion three times with the sensing boards mounted at Configuration 1 and 2.

This section will present intermediate results of the implementation of the theoretical formulations which are divided in: definition of $t_1$ and $t_2$ and definition of the angular and linear velocities. Then, the position and trajectory reconstruction will be presented for Configuration 1 and 2.

### 4.4.1 Definition of $t_1$ and $t_2$

In order to implement the theoretical formulations, it was necessary to determine the values of $t_1$ and $t_2$ for equations 4.2, 4.3 and 4.4.

The sensor-to-body transformation procedure consists in an upper arm swing, from $t_1$ to $t_2$, to the side in the coronal plane while still keeping the arm straight, and returning to the starting position. A method to determine these time values and to segment the movement phases (when the arm is down, when the arm is in the swing phase, and when the arm is down again) was defined.

Since the sensors could be mounted in any position, it was necessary to find a signal that was independent of the sensors' position: gravitational acceleration variation along the upper and lower orientation relatively to the vertical.

To find the "vertical gravitation acceleration" (quotation marks are used because the vector that will defined the vertical gravitational acceleration is defined by hand), first a mean quaternion was defined, corresponding to the quaternion in the sensors' initial local reference frame from the second and third seconds, ${}^{s}q_{2,3}^U$, that is when the arm is stationary and vertically aligned. This way, the vector ${}^{b}g$=[0 0 -9.8], defined in the GB reference frame, was converted to ${}^{s}g^U$, defined in the sensor's local reference frame, by using equation 4.8. A scheme of the process is represented in Figure 4.7.

$$ \begin{bmatrix} 0 \\ {}^{s}g^U \end{bmatrix}^T = \overline{{}^{s}q_{2,3}^U} \times \begin{bmatrix} 0 \\ {}^{b}g^U \end{bmatrix}^T \times {}^{s}q_{2,3}^U \tag{4.8} $$

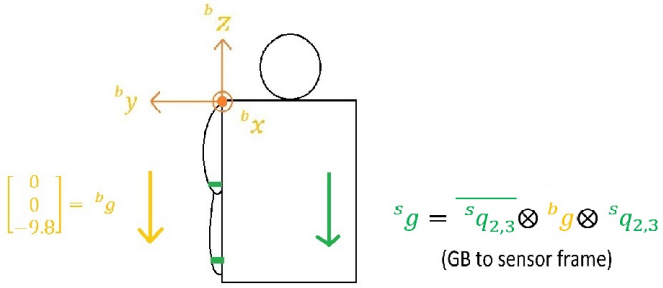


Figure 4.7: Scheme to determine ${}^{s}g$. ${}^{b}x{}^{b}y{}^{b}z$ represent the GB reference frame, ${}^{b}g$ is the gravitational acceleration vector, ${}^{s}q_{2,3}$ is the mean orientation quaternion from seconds 2 to 3, which represent the rotation to the sensor initial reference frame and ${}^{s}g$ is the vector ${}^{b}g$ defined in the sensor' reference frame.

The vector ${}^{s}g^{U}$, described in the sensor's reference frame is constant, but when it is described in the earth reference frame varies with arm movements and represents the vertical gravitational acceleration (which is in the $z$-axis). Therefore, the vector ${}^{s}g^{U}$ was defined in the earth reference frame (E left superscript), where the $z$-axis is pointing down (as depicted in Figure 2.9):

$$\begin{bmatrix} 0 \\ {}^{E}g_{t}^{U} \end{bmatrix}^{T} = {}^{s}q_{t}^{U} \times \begin{bmatrix} 0 \\ {}^{b}g^{U} \end{bmatrix}^{T} \times \overline{{}^{s}q_{t}^{U}} \tag{4.9}$$

where ${}^{s}q_{t}^{U}$ is the sensor orientation relative to the earth reference frame. For the lower arm, the procedure was equivalent. A scheme of the process is depicted in Figure 4.8.

The vertical gravitational acceleration in the earth reference frame ${}^{E}g_{tz}{}^{U}$ is depicted in Figure 4.9. In order to segment the signal in $Down_1$, $Swing$ and $Down_2$, a threshold of $8m/s^2$ was used. After that, the slope of the signals when the arm is straight down ($Down_1$ and $Down_2$ phases) was determined within a window of 0.4 seconds (20 points), which is depicted in Figure 4.10.

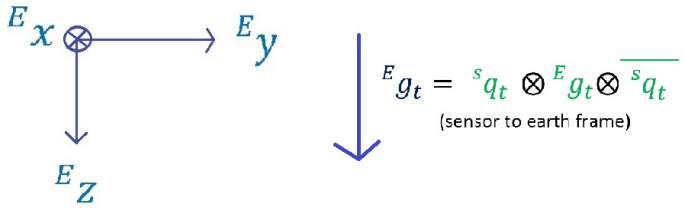


Figure 4.8: Scheme to determine ${}^{E}g_{t}^{U}$. ${}^{E}x{}^{E}y{}^{E}z$ represent the earth reference frame, ${}^{s}g$ is the vector ${}^{b}g$ defined in the sensor' reference frame and ${}^{s}q_{t}$ is the sensor orientation relative to the earth reference frame.

Afterwards, to determine the time value corresponding to $t_1$ and $t_2$, a 0.4 seconds window was defined for each point (where that point is in the middle) of the signal represented in Figure 4.10. For each window, its mean and standard deviation were calculated. Next, for the $Down_1$ phase, each point of the signal was compared to its 20 points window in seconds: if the point had

a higher value then the window mean plus the standard deviation, $t_1$ value was found. For the $Down_2$ phase, the stop criteria was similar, but, in this case, the point had to have a smaller value then the window mean plus the standard deviation, and then $t_2$ value was found. As it can be seen in Figure 4.10 two different values for $t_1$ were found (one for the upper and another for the lower) and two different values for $t_2$ were found (one for the upper and another for the lower). In order to obtain one unique value for $t_1$ and $t_2$, it was calculated the mean value for the two values described previously. These values are depicted in Figure 4.9.

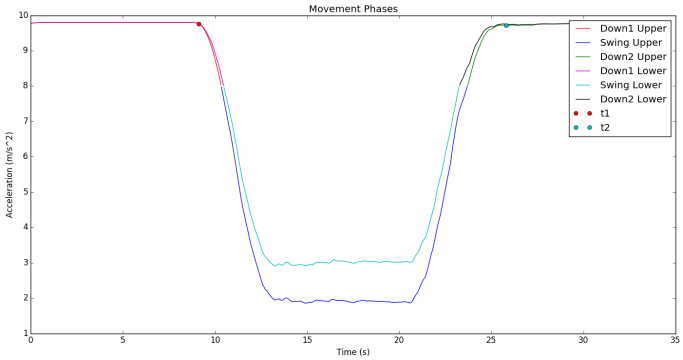


Figure 4.9: Movement phases segmentation with $t_1$ and $t_2$ represented as dots.

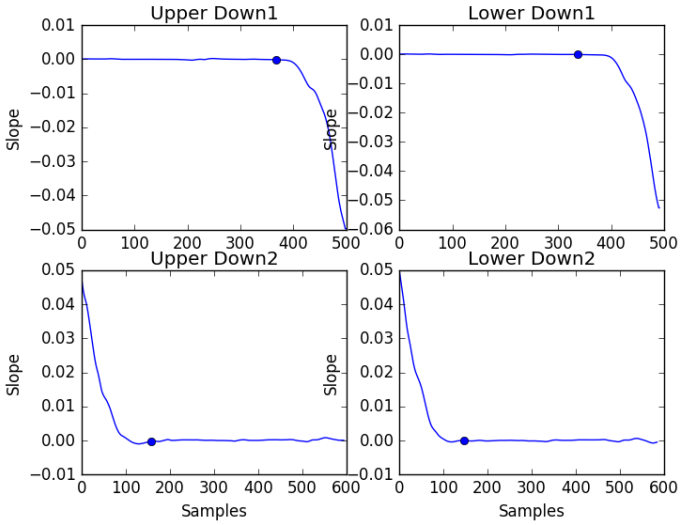


Figure 4.10: Slope of $Down_1$ and $Down_2$ phases within a 0.4 seconds (20 points) window for the upper and lower sensor.

### 4.4.2 Definition of Angular and Linear Velocities

To implement the theoretical formulations, it was necessary to determine linear and angular velocities to be substituted into equation 4.2.

Definition of posture vectors ${}^{s}r_t^U$ and ${}^{s}r_t^W$ was based on a minimization method which required the angular velocity from the gyroscope measurements, and the linear velocity resulting from linear acceleration integration.

The upper and lower gyroscope measurements are depicted in Figure 4.11. As it can be seen, the angular velocity is identical for the upper and lower sensor, since the movement has the same amplitude for the two sensors and, as the arm is straight, it is performed at the same time.

The linear acceleration and velocity, for the upper and lower sensors, are depicted in Figure 4.12. As it can be seen, the linear acceleration integration to obtain velocity produces expected results (i.e. goes to a velocity 0 $cm/s$ when it is expected, that is, when the arm is in $Down_1$ and $Down_2$ phases, and therefore does not accumulate errors). Regarding the upper and lower differences, it is expected that the velocity for the lower sensor will be higher, since the movement is performed at the same time by the two sensors, but the lower one travels a larger distance.

Even so, as it can be seen in Figures 4.12 and 4.13, the linear velocity for the upper and lower arm is almost identical (the velocity in magnitude of the upper sensor is slightly higher than the lower sensor, when it is expected to be the opposite).

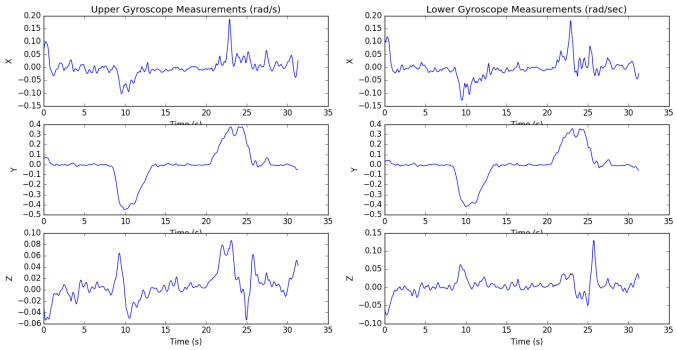


Figure 4.11: Upper and Lower Gyroscope measurements.

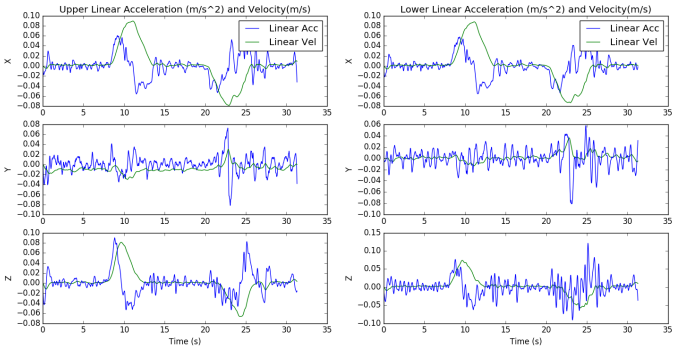


Figure 4.12: Upper and Lower Linear Acceleration and Velocity.

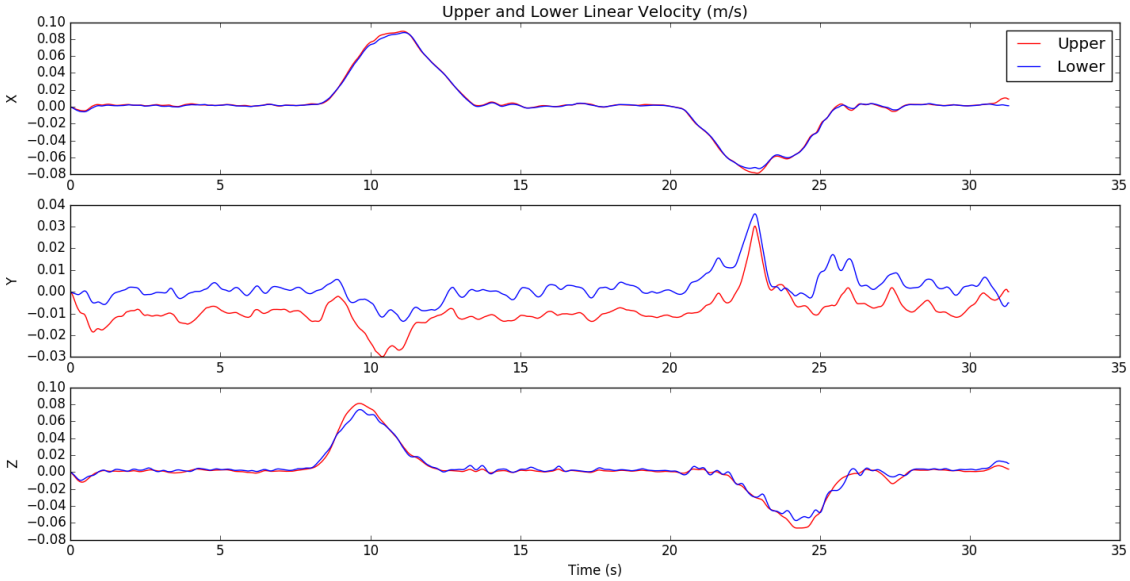


Figure 4.13: Upper and Lower Linear Velocity.

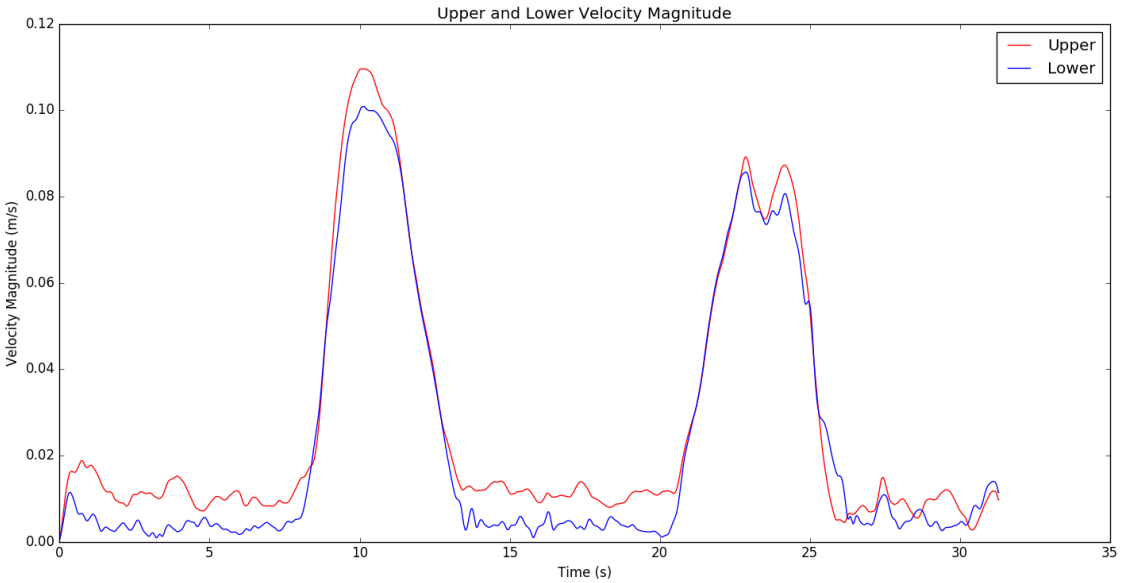


Figure 4.14: Upper and Lower Linear Velocity Magnitude.

### 4.4.3 Position and Trajectory Reconstruction

The results described next represent the calibration movement, which corresponds to the shoulder abduction/adduction after the sensor-to-body transformation process is applied. This means that the movement described will be represented in the defined GB reference frame.

Verification of the sensor-to-body frame algorithm is based on accuracy of the arm length estimation. Length of the upper arm and the lower arm can be estimated from procedures through the following formulas:

$$l_{est}^{U} = \left\| {}^{s}r^{U} \right\| \tag{4.10}$$

$$l_{est}^{L} = \left\| {}^{s}r^{L} \right\| \tag{4.11}$$

For Configurations 1 and 2, the upper and lower lengths were estimated for the three repetitions. The results for the subject in question are summarized in Table 4.2, which corresponds to a mean value of all the estimated lengths.

Table 4.2: Upper and Lower lengths real value $l$, estimation $l_{est}$ and absolute error $e$, in centimeters (cm).

| | $l$ | $l_{est}$ | $\|e\|$ |
|---|---|---|---|
| Upper | 24 | 20 | 4 |
| Lower | 20 | 1 | 19 |

Since the estimation of ${}^{s}r^{U}$ and ${}^{s}r^{W}$ is achieved by equation 4.2, the inputs for that equation are the angular ${}^{s}w_t$ and linear velocities ${}^{s}v_t$. As depicted in Figure 4.11, the gyroscope measurements are identical for upper and lower sensors, and as depicted in Figures 4.12 and 4.13, the linear velocities are almost identical as well.

As explained before, it was expected that angular velocity was the same for the upper and lower arm segment, but the linear velocity should be different. One possible explanation for this could be the latent errors of the accelerometer measurements, that could be masking the differences between the accelerations for the upper and lower sensors. Since the distance between the two sensor is not too large, the differences in accelerations could not be distinguishable.

A possible solution to this problem is to repeat the acquisition movement multiple times, so that better estimations could be obtained. Another solution could rely on the improvement of the signals pre-processing, employing other filters to reduce errors.

Since $l_U$= 24 cm and $l^W$= 20 cm, the estimation algorithm did not produce reliable results. Thus, vectors ${}^{s}r^{U}$ and ${}^{s}r^{L}$ were manually input, as described in Section 3.6 by equations 3.31 and 3.32. The rest of the sensor-to-body frame algorithm was described as presented in Theoretical Formulation in order to track positions' trajectories.

Considering the movement as a movement in the $y$-$z$ plane, and taking into account the upper and lower segment lengths, the trajectories expected around the 3 axes for the two configurations were:

- $x$-axis: no movement detected, position in this axis must be around 0 cm.
- $y$-axis: position around 0 cm from time 0 to $t_1$ and after $t_2$, position around 24 cm (upper) and 44 cm (lower) during swing phase.
- $z$-axis: position around 24 cm (upper) and 44 cm (lower) from time 0 to $t_1$ and after $t_2$, position around 0 during swing phase.

For Configuration 1, one example of the positions trajectories in every axis are depicted in Figure 4.15 and positions trajectories in 3D are depicted in Figure 4.16. As it can be seen:

- Along $x$ a moving distance of less than 7 cm was detected for the elbow, and a moving distance of less than 14 cm was detected for the wrist, instead of 0 cm expected.
- Along $y$, a moving distance of 21 cm was detected for the elbow, and a moving distance of 39 cm was detected for the wrist, instead of 24 cm and 44 cm expected.
- Along $z$, a moving distance of 14 cm was detected for the elbow, and a moving distance of 30 cm for the wrist, instead of 24 cm and 44 cm expected.

In Configuration 2, the sensors were neither aligned with each other nor with the GB reference frame. After discovering the orientation of the sensors relative to the GB reference frame, one example of the positions' trajectories in the different axes are depicted in Figure 4.17 and the trajectories in 3D are depicted in Figure 4.18. As it can be seen:

- Along $x$ a moving distance of less than 7 cm was detected for the elbow, and a moving distance of less than 19 cm was detected for the wrist, instead of 0 cm expected.
- Along $y$, a moving distance of 23 cm was detected for the elbow, and a moving distance of 34 cm was detected for the wrist, instead of 24 cm and 44 cm expected.
- Along $z$, a moving distance of 16 cm was detected for the elbow, and a moving distance of 30 cm for the wrist, instead of 24 cm and 44 cm expected.

In order to better understand the results, the absolute error for each repetition in each configuration was calculated. This error was calculated based on the expected position for each axis and the one obtained. To summarize the errors, only the maximum error of the elbow and wrist positions for each axis will be presented. The mean value of the elbow and wrist maximum errors for the three repetitions, for each axis and for each configuration is in Table 4.3.

Considering Table 4.3, it is possible to conclude that the errors are higher than the ones described in the preliminary evaluation, so there are additional errors besides the inherent ones.

Therefore, it is possible to conclude that the definition of the GB reference frame was not accurate and the calibration movement should be redefined. The difference between the expected distances and the ones obtained could be explained by wrong execution of the calibration movement. Specifically, when the arm should be perpendicular to the sagittal plane, in the middle of

the swing phase, if the arm was not correctly positioned, the definition of *y*-axis could be incorrect and consequently will mislead the definition of *x*-axis.

One possible solution could be to redefine calibration movements around each axis of rotation for each joint, as the ones described by H. Wang et al in [45]. Considering rotations, the system stops being dependent of the correct alignment of the arm during the calibration movement. H. Wang states that calibrating the upper sensor orientation is slightly different from calibrating the lower sensor, because of the physical constraints due to the anatomical structure of human skeleton.

It is possible to conclude that despite the position errors, the trajectories' representation and the maximum errors are similar for configurations 1 and 2. This indicates that the sensors could be placed in any position and future work could be explored to find a more effective calibration movement that would correctly define the GB reference frame.

Table 4.3: Maximum error (in centimeters) for the elbow and wrist positions for each axis in Configurations 1 and 2.

| Axis | Maximum Error (cm) | | | |
|---|---|---|---|---|
| | Configuration 1 | | Configuration 2 | |
| | Elbow | Wrist | Elbow | Wrist |
| x | 7 | 14 | 7 | 18 |
| y | 3 | 10 | 1 | 10 |
| z | 10 | 14 | 10 | 12 |

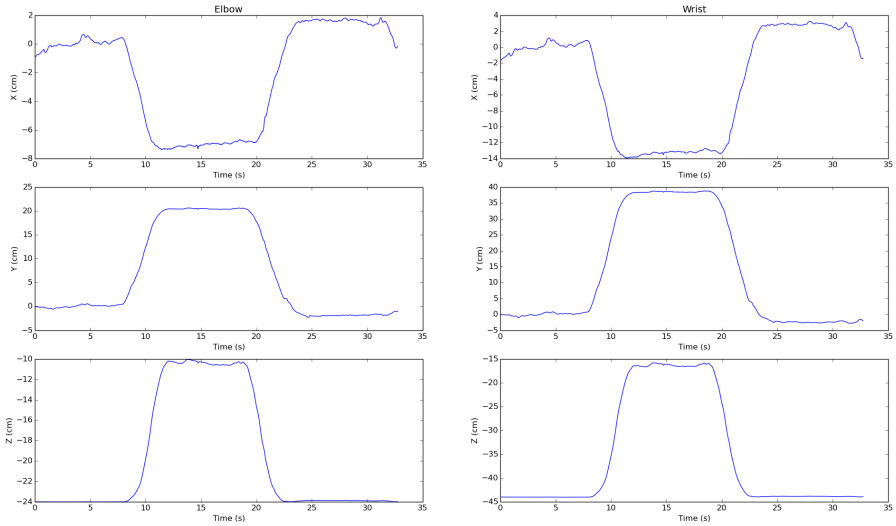


Figure 4.15: Configuration 1 - Positions trajectories in x,y and z axes, for elbow and wrist joints. Positions are represented in cm and time in seconds.

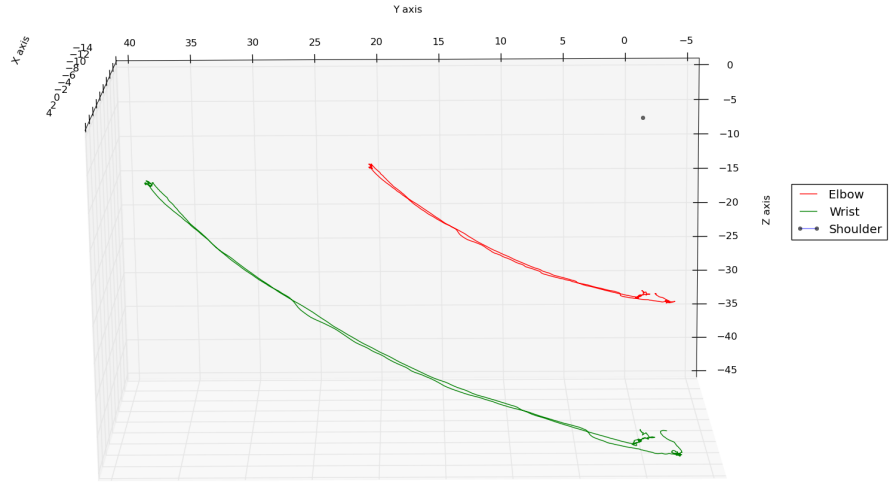


Figure 4.16: Configuration 1 - 3D trajectories (cm) for elbow and wrist joints.

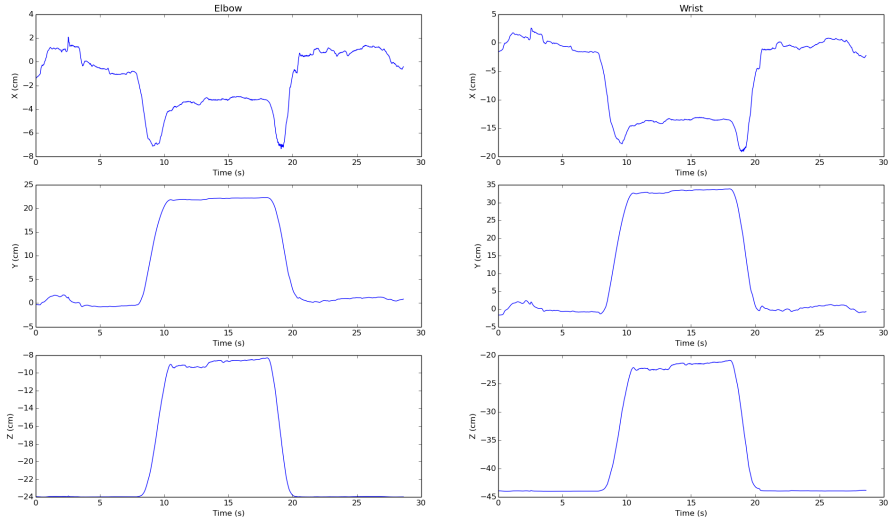


Figure 4.17: Configuration 2 - Positions' trajectories in x,y and z axes, for elbow and wrist joints. Positions are represented in cm and time in seconds.

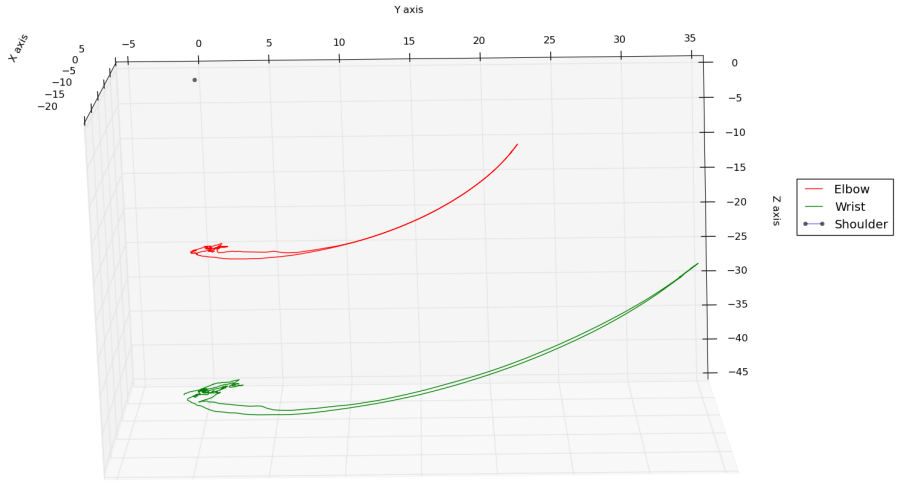


Figure 4.18: Configuration 2 - 3D trajectories (cm) for elbow and wrist joints.

# Chapter 5

# Conclusions and Future Work

Upper limb motion tracking has become an extensive research topic in the human motion tracking studies. This is due to its broad range of applications, including movement evaluation of workers, gaming, human machine interaction and medical rehabilitation. There are many tracking systems available, however, despite this variety of tracking systems, they have some limitations. Additionally, the existing systems are focused on a single application, making it difficult for its re-utilization in other contexts. Therefore, there is a need for an upper limb tracking system that can be used by all people in several different contexts. Thus, the development of an inertial motion tracking system was proposed since it can can be useful for a variety of applications and not specifically or exclusively for any one of them.

In this project, a study has done been regarding upper limb inertial tracking, aiming at improving the current inertial system developed.

Based on current research, the 3DArm system consisted in two IMUs that were placed in the upper and lower arm segment in order to track the elbow and wrist joints, based on EKF sensor fusion and biomechanical constraint of the upper limb. Then, to avoid the burden of manually aligning the sensors with each other, a sensor-to-body frame process was developed.

The 3DArm system was evaluated comparing its performance with the Kinect. In these tests, a maximum mean deviation of 10,60 centimeters and 16,33 centimeters was found for the elbow and wrist joints, respectively. Since these errors were possibly from the alignment of the sensors with each other, a sensor-to-body transformation process was developed in order to overcome this problem.

The sensor-to-body process was based on a calibration movement that calculated the sensor orientation in each segment and to construct the GB reference frame. However, a maximum error of 14 centimeters and 19 centimeters was found for the elbow and wrist joints, respectively. In order to understand the errors of the sensor-to-body frame transformation in the most possibly controllable situation, a preliminary evaluation was performed. This preliminary evaluation concluded that there is about a maximum error of 4 centimeters inherent to this process. Besides the inherent errors described in the preliminary evaluation, the most possible source of these errors was the calibration movement defined, in which it was difficult to ensure that the arm was

completely aligned with the vertical and then perpendicular to the sagittal plane.

Despite the errors presented, the results obtained for the 3DArm system suggest that it can be used to track upper limb motion, and can be a low-cost suitable system for different upper limb tracking applications. Therefore, further development of the project would be of great value.

## 5.1 Future Work

Considering the results obtained in this dissertation, some future work was identified to potentially improve the upper limb motion tracking. The following list details some of future work tasks:

- Implementation of a wearable system that considers both upper limbs.
- Due to the high number of degrees of freedom in the upper limb, the problem of non-rigid movements was not addressed. For example, elbow flexion may accompany forearm supinations or pronations, where the rotation of the muscles nearer to the wrist and elbow joints respectively is not identical. This situation violates the rigidness assumption of the proposed kinematic model and may lead to erroneous measurements. A possible solution is to define a kinematic model that considers the two joint arm movements with more complex patterns and more degrees of freedom.
- Currently, the assumption of a still shoulder joint was kept during arm movements. In a real case, the movements of the upper limb are not restricted to this assumption. In other words, both translation and rotation of the shoulder joint can occur. Therefore, future work could be to develop a trunk model that is an extension of the proposed kinematic model. This approach overcomes this assumption and considers the case of free movements of the shoulder joint.
- The upper limb movement has more movement constraints besides the elbow abduction/adduction. Therefore, more constraints could be fused into the EKF framework. For example, the range of motion of each joint DOF.
- A more thorough research about the effect of the covariance matrices on the EKF sensor fusion could be performed to improve the orientation estimation with biomechanical constraints.
- A more accurate sensor-to-body frame process could be developed. A process that could transform sensor measurements to the GB reference frame without the need of aligning the sensor with each other could substantially improve the accuracy of the 3DArm system, since sensor alignment is a very difficulty task.
- System evaluation based on longer tests in order to evaluate the reliability of the proposed algorithm and evaluate drift progression over time.

- The current tracking system developed could be integrated with other non-visual sensors e.g. potentiometers or laser fibers, etc. In the latter solution, the IMU sensors provide an initial position for the arm and the other sensors work as a "verifier" or "corrector". In due course, the whole tracking system may have more robust performance in a non-rigid circumstance while keeping high accuracy in measurements.

- Accuracy could be investigated by comparing the 3DArm system with more reliable systems than Kinect. For instance, the 3DArm performance could be compared to a commercially available motion tracking such as CODA or Qualisys.

# References


[1] Y. Tian, X. Meng, D. Tao, D. Liu, and C. Feng, "Upper limb motion tracking with the integration of imu and kinect," *Neurocomputing*, vol. 159, pp. 207–218, 2015.

[2] W. A. Latko, T. J. Armstrong, A. Franzblau, S. S. Ulin, R. A. Werner, and J. W. Albers, "Cross-sectional study of the relationship between repetitive work and the prevalence of upper limb musculoskeletal disorders," *American journal of industrial medicine*, vol. 36, no. 2, pp. 248–259, 1999.

[3] G.-Å. Hansson, I. Balogh, K. Ohlsson, L. Rylander, and S. Skerfving, "Goniometer measurement and computer analysis of wrist angles and movements applied to occupational repetitive work," *Journal of Electromyography and Kinesiology*, vol. 6, no. 1, pp. 23–35, 1996.

[4] M. Pasch, N. Berthouze, B. Dijk, and A. Nijholt, "Motivations, strategies, and movement patterns of video gamers playing nintendo wii boxing," 2008.

[5] M. Siddiqui and G. Medioni, "Robust real-time upper body limb detection and tracking," in *Proceedings of the 4th ACM international workshop on Video surveillance and sensor networks*, pp. 53–60, ACM, 2006.

[6] A. Schiele and F. C. van der Helm, "Kinematic design to improve ergonomics in human machine interaction," *Neural Systems and Rehabilitation Engineering, IEEE Transactions on*, vol. 14, no. 4, pp. 456–469, 2006.

[7] H. Zhou and H. Hu, "Human motion tracking for rehabilitation—a survey," *Biomedical Signal Processing and Control*, vol. 3, no. 1, pp. 1–18, 2008.

[8] Z. Luo, C. K. Lim, W. Yang, K. Y. Tee, K. Li, C. Gu, K. D. Nguen, I. Chen, S. H. Yeo, *et al.*, "An interactive therapy system for arm and hand rehabilitation," in *Robotics Automation and Mechatronics (RAM), 2010 IEEE Conference on*, pp. 9–14, IEEE, 2010.

[9] C.-Y. Chang, B. Lange, M. Zhang, S. Koenig, P. Requejo, N. Somboon, A. Sawchuk, A. Rizzo, *et al.*, "Towards pervasive physical rehabilitation using microsoft kinect," in *Pervasive Computing Technologies for Healthcare (PervasiveHealth), 2012 6th International Conference on*, pp. 159–162, IEEE, 2012.

[10] P. Lum, D. Reinkensmeyer, R. Mahoney, W. Z. Rymer, and C. Burgar, "Robotic devices for movement therapy after stroke: current status and challenges to clinical acceptance," 2015.

[11] M. El-Gohary, L. Holmstrom, J. Huisinga, E. King, J. McNames, and F. Horak, "Upper limb joint angle tracking with inertial sensors," in *Engineering in Medicine and Biology Society, EMBC, 2011 Annual International Conference of the IEEE*, pp. 5629–5632, IEEE, 2011.

[12] H. J. Luinge, P. H. Veltink, and C. T. Baten, "Ambulatory measurement of arm orientation," *Journal of biomechanics*, vol. 40, no. 1, pp. 78–85, 2007.

[13] Y. Wang, X. Xu, M. Batalin, and W. Kaiser, "Detection of upper limb activities using multi-mode sensor fusion," in *Biomedical Circuits and Systems Conference (BioCAS), 2011 IEEE*, pp. 436–439, IEEE, 2011.

[14] C. VanPutte, J. Regan, A. Russo, P. Tate, T. Stephens, and R. Seeley, *Seeley's anatomy & physiology*. McGraw-Hill Higher Education, 2013.

[15] J. Hamill and K. M. Knutzen, *Biomechanical basis of human movement*. Lippincott Williams & Wilkins, 2006.

[16] C. L. Taylor, *The biomechanics of control in upper-extremity prostheses*. National Academy of Sciences, 1955.

[17] Z. Zhang, Z. Huang, and J. Wu, "Hierarchical information fusion for human upper limb motion capture," in *Information Fusion, 2009. FUSION'09. 12th International Conference on*, pp. 1704–1711, IEEE, 2009.

[18] H. Zhou, H. Hu, N. D. Harris, and J. Hammerton, "Applications of wearable inertial sensors in estimation of upper limb movements," *Biomedical Signal Processing and Control*, vol. 1, no. 1, pp. 22–32, 2006.

[19] H. Zhou, H. Hu, and Y. Tao, "Inertial measurements of upper limb motion," *Medical and Biological Engineering and Computing*, vol. 44, no. 6, pp. 479–487, 2006.

[20] H. Zhou and H. Hu, "Inertial motion tracking of human arm movements in stroke rehabilitation," in *Mechatronics and Automation, 2005 IEEE International Conference*, vol. 3, pp. 1306–1311, IEEE, 2005.

[21] F. C. van der Helm, "A standardized protocol for motion recordings of the shoulder," in *First conference of the international shoulder group*, pp. 7–12, Citeseer, 1997.

[22] R. Zhu and Z. Zhou, "A real-time articulated human motion tracking using tri-axis inertial/-magnetic sensors package," *Neural Systems and Rehabilitation Engineering, IEEE Transactions on*, vol. 12, no. 2, pp. 295–302, 2004.

[23] S.-W. Lee and K. Mase, "Activity and location recognition using wearable sensors," *IEEE pervasive computing*, vol. 1, no. 3, pp. 24–32, 2002.

[24] H. Zhou, T. Stone, H. Hu, and N. Harris, "Use of multiple wearable inertial sensors in upper limb motion tracking," *Medical engineering & physics*, vol. 30, no. 1, pp. 123–133, 2008.

[25] S. Ayub, A. Bahraminisaab, and B. Honary, "A sensor fusion method for smart phone orientation estimation," in *Proceedings of the 13th Annual Post Graduate Symposium on the Convergence of Telecommunications, Networking and Broadcasting, Liverpool*, 2012.

[26] N. H. Q. Phuong, H.-J. Kang, Y.-S. Suh, and Y.-S. Ro, "A dcm based orientation estimation algorithm with an inertial measurement unit and a magnetic compass," *Journal of Universal Computer Science*, vol. 15, no. 4, pp. 859–876, 2009.

[27] S. O. Madgwick, "An efficient orientation filter for inertial and inertial/magnetic sensor arrays," *Report x-io and University of Bristol (UK)*, 2010.

[28] W. Elmenreich, "Sensor fusion in time-triggered systems," 2002.

[29] C. Perez-D'Arpino, D. Vigouroux, W. Medina-Meléndez, L. Fermín, R. R. Torrealba, J. C. Grieco, and G. Fernández-López, "Development of a low cost inertial measurement unit for uav applications with kalman filter based attitude determination," in *Technologies for Practical Robot Applications (TePRA), 2011 IEEE Conference on*, pp. 178–183, IEEE, 2011.

[30] J. J. LaViola Jr, "A comparison of unscented and extended kalman filtering for estimating quaternion motion," in *American Control Conference, 2003. Proceedings of the 2003*, vol. 3, pp. 2435–2440, IEEE, 2003.

[31] M. I. Ribeiro, "Kalman and extended kalman filters: Concept, derivation and properties," *Institute for Systems and Robotics*, vol. 43, 2004.

[32] R. Faragher *et al.*, "Understanding the basis of the kalman filter via a simple and intuitive derivation," *IEEE Signal processing magazine*, vol. 29, no. 5, pp. 128–132, 2012.

[33] P. S. Maybeck, *Stochastic models, estimation, and control*, vol. 3. Academic press, 1982.

[34] G. Dean, "An introduction to kalman filters," *Measurement and Control*, vol. 19, no. 2, pp. 69–73, 1986.

[35] J. Diebel, "Representing attitude: Euler angles, unit quaternions, and rotation vectors," *Matrix*, vol. 58, pp. 15–16, 2006.

[36] X. Yun and E. Bachmann, "Design, Implementation, and Experimental Results of a Quaternion-Based Kalman Filter for Human Body Motion Tracking," *Robotics, IEEE Transactions on*, vol. 22, 2006.

[37] E. R. Bachmann, I. Duman, U. Usta, R. B. Mcghee, X. Yun, and M. Zyda, "Orientation tracking for humans and robots using inertial sensors," in *Computational Intelligence in Robotics and Automation, 1999. CIRA'99. Proceedings. 1999 IEEE International Symposium on*, pp. 187–194, IEEE, 1999.

[38] M. W. Spong, S. Hutchinson, and M. Vidyasagar, *Robot modeling and control*, vol. 3. Wiley New York, 2006.

[39] H. J. Luinge, *Inertial sensing of human movement*. Twente University Press, 2002.

[40] H. Zhou and H. Hu, "Upper limb motion estimation from inertial measurements," *International Journal of Information Technology*, vol. 13, no. 1, pp. 1–14, 2007.

[41] H. Zhou, H. Hu, and N. Harris, "Application of wearable inertial sensors in stroke rehabilitation," in *Engineering in Medicine and Biology Society, 2005. IEEE-EMBS 2005. 27th Annual International Conference of the*, pp. 6825–6828, IEEE, 2005.

[42] H. Zhou and H. Hu, "Kinematic model aided inertial motion tracking of human upper limb," in *Information Acquisition, 2005 IEEE International Conference on*, pp. 6–pp, IEEE, 2005.

[43] J. Newman, H. Zhou, and H. Hu, "Inertial sensors for motion detection of human upper limbs," *Sensor Review*, vol. 27, no. 2, pp. 151–158, 2007.

[44] C. Chien, J. Xia, O. Santana, Y. Wang, and G. J. Pottie, "Non-linear complementary filter based upper limb motion tracking using wearable sensors," in *Acoustics, Speech and Signal Processing (ICASSP), 2013 IEEE International Conference on*, pp. 963–967, IEEE, 2013.

[45] H. Yang and J. Ye, "A calibration process for tracking upper limb motion with inertial sensors," in *Mechatronics and Automation (ICMA), 2011 International Conference on*, pp. 618–623, IEEE, 2011.

[46] Y. Wang, J. Xu, X. Wu, G. Pottie, and W. Kaiser, "A simple calibration for upper limb motion tracking and reconstruction," in *Engineering in Medicine and Biology Society (EMBC), 2014 36th Annual International Conference of the IEEE*, pp. 5868–5871, IEEE, 2014.

[47] InvenSense, "Mpu-9250." https://store.invensense.com/datasheets/invensense/MPU9250REV1.0.pdf, 2014.

[48] R. G. Valenti, I. Dryanovski, and J. Xiao, "A linear kalman filter for marg orientation estimation using the algebraic quaternion algorithm," 2016.

[49] M. D. Shuster and S. Oh, "Three-axis attitude determination from vector observations," *Journal of Guidance, Control, and Dynamics*, vol. 4, no. 1, pp. 70–77, 1981.

[50] Z.-Q. Zhang and J.-K. Wu, "A novel hierarchical information fusion method for three-dimensional upper limb motion estimation," *Instrumentation and Measurement, IEEE Transactions on*, vol. 60, no. 11, pp. 3709–3719, 2011.

[51] Z. Zhang, "Microsoft kinect sensor and its effect," *MultiMedia, IEEE*, vol. 19, no. 2, pp. 4–10, 2012.

[52] Y.-C. Lai, S.-S. Jan, and F.-B. Hsiao, "Development of a low-cost attitude and heading reference system using a three-axis rotating platform," *Sensors*, vol. 10, no. 4, pp. 2472–2491, 2010.

# Appendix A

# Rotation Matrix $\Rightarrow$ Unit Quaternion

The mapping of a rotation matrix into a quaternion is more complex than the reverse operation. Four different mappings, $q_R^i$, for $i \in 0,1,2,3$, will be defined by [35]:

$$q_R^0(R) = \frac{1}{2}\begin{bmatrix} (1+r_{11}+r_{22}+r_{33})^{\frac{1}{2}} \\ (r_{23}-r_{32})/(1+r_{11}+r_{22}+r_{33})^{\frac{1}{2}} \\ (r_{31}-r_{13})/(1+r_{11}+r_{22}+r_{33})^{\frac{1}{2}} \\ (r_{12}-r_{21})/(1+r_{11}+r_{22}+r_{33})^{\frac{1}{2}} \end{bmatrix} \tag{A.1}$$

$$q_R^1(R) = \frac{1}{2}\begin{bmatrix} (r_{23}-r_{32})/(1+r_{11}-r_{22}-r_{33})^{\frac{1}{2}} \\ (1+r_{11}-r_{22}-r_{33})^{\frac{1}{2}} \\ (r_{12}+r_{21})/(1+r_{11}-r_{22}-r_{33})^{\frac{1}{2}} \\ (r_{31}+r_{13})/(1+r_{11}-r_{22}-r_{33})^{\frac{1}{2}} \end{bmatrix} \tag{A.2}$$

$$q_R^2(R) = \frac{1}{2}\begin{bmatrix} (r_{31}-r_{13})/(1-r_{11}+r_{22}-r_{33})^{\frac{1}{2}} \\ (r_{12}+r_{21})/(1-r_{11}+r_{22}-r_{33})^{\frac{1}{2}} \\ (1-r_{11}+r_{22}-r_{33})^{\frac{1}{2}} \\ (r_{23}+r_{32})/(1-r_{11}+r_{22}-r_{33})^{\frac{1}{2}} \end{bmatrix} \tag{A.3}$$

$$q_R^3(R) = \frac{1}{2}\begin{bmatrix} (r_{12}-r_{21})/(1-r_{11}-r_{22}+r_{33})^{\frac{1}{2}} \\ (r_{31}+r_{13})/(1-r_{11}-r_{22}+r_{33})^{\frac{1}{2}} \\ (r_{23}+r_{32})/(1-r_{11}-r_{22}+r_{33})^{\frac{1}{2}} \\ (1-r_{11}-r_{22}+r_{33})^{\frac{1}{2}} \end{bmatrix} \tag{A.4}$$

Depending on the values of $R$, some of these functions produce complex results. To avoid this, the following composite function is defined, which selects the best of these four, depending on the parameters of $R$. The function $q_R(R)$, is:

$$q_R(R) := \begin{cases} q_R^0(R) if r_{22} > -r_{33}, r_{11} > -r_{22}, r_{11} > -r_{33} \\ q_R^1(R) if r_{22} < -r_{33}, r_{11} < r_{22}, r_{11} > r_{33} \\ q_R^2(R) if r_{22} > r_{33}, r_{11} < r_{22}, r_{11} < -r_{33} \\ q_R^3(R) if r_{22} < r_{33}, r_{11} < -r_{22}, r_{11} < r_{33} \end{cases} \tag{A.5}$$

# Appendix B

# EKF Implementation

The parameters, state and measurement equations necessary to implement the EKF are explained in this Appendix.

In Section 3.5.2 the process model was initially defined as being the system dynamics. The state variables described in equations 3.17 and 3.18 describe a vector rotated by a quaternion operation. The vector rotation operation is defined by:

$$^{B}\mathbf{v} = {}^{A}_{B}\mathbf{R} \times {}^{A}\mathbf{v} \tag{B.1}$$

with ${}^{A}_{B}\mathbf{R}$ (equation 2.28), equation B.1 can be rewritten as a matrix vector multiplication:

$$\begin{bmatrix} {}^{B}v_x \\ {}^{B}v_y \\ {}^{B}v_z \end{bmatrix} = \begin{bmatrix} 1-2q_3^2-2q_4^2 & 2(q_2q_3-q_1q_4) & 2(q_2q_4+q_1q_3) \\ 2(q_2q_3+q_1q_4) & 1-2q_2^2-2q_4^2 & 2(q_3q_4+q_1q_2) \\ 2(q_2q_4-q_1q_3) & 2(q_3q_4+q_1q_2) & 1-2q_2^2-2q_3^2 \end{bmatrix} \times \begin{bmatrix} {}^{A}v_x \\ {}^{A}v_y \\ {}^{A}v_z \end{bmatrix} \tag{B.2}$$

Therefore, state variables $\dot{x}_0$ to $\dot{x}_7$ can be rewritten as:

$$\dot{x}_0 = -\frac{1}{2}({}^{b}w_x^U \times x_1 + {}^{b}w_y^U \times x_2 + {}^{b}w_z^U \times x_3) \tag{B.3}$$

$$\dot{x}_1 = \frac{1}{2}({}^{b}w_x^U \times x_0 - {}^{b}w_y^U \times x_3 + {}^{b}w_z^U \times x_2) \tag{B.4}$$

$$\dot{x}_2 = \frac{1}{2}({}^{b}w_x^U \times x_3 + {}^{b}w_y^U \times x_0 - {}^{b}w_z^U \times x_1) \tag{B.5}$$

$$\dot{x}_3 = \frac{1}{2}(-{}^{b}w_x^U \times x_2 + {}^{b}w_y^U \times x_1 + {}^{b}w_z^U \times x_0) \tag{B.6}$$

$$\dot{x}_4 = -\frac{1}{2}({}^{b}w_x^L \times x_5 + {}^{b}w_y^L \times x_6 + {}^{b}w_z^L \times x_7) \tag{B.7}$$

$$\dot{x}_5 = \frac{1}{2}({}^{b}w_x^L \times x_4 - {}^{b}w_y^L \times x_7 + {}^{b}w_z^L \times x_6) \tag{B.8}$$

$$\dot{x}_6 = \frac{1}{2}({}^{b}w_x^L \times x_7 + {}^{b}w_y^L \times x_4 - {}^{b}w_z^L \times x_5) \tag{B.9}$$

$$\dot{x}_7 = \frac{1}{2}(-{}^{b}w_x^L \times x_6 + {}^{b}w_y^L \times x_5 + {}^{b}w_z^L \times x_4) \tag{B.10}$$

The state variable $\dot{x}_8$ defined in equation 3.19 represents the dot product between the $y$-axis of the lower arm and the $z$-axis of the upper arm. As mentioned in equations 3.14 and 3.15, $Y_t^L$ and $Z_t^U$ also represent vector rotation operations, so they could be defined as:

$$Y_t^L = \begin{bmatrix} 2x_5x_6 - 2x_4x_7 & 1 - 2{x_5}^2 - 2{x_7}^2 & 2x_6x_7 + 2x_4x_5 \end{bmatrix} \tag{B.11}$$

$$Z_t^U = \begin{bmatrix} 2x_1x_3 + 2x_0x_2 & 2x_2x_3 - 2x_0x_1 & 1 - 2{x_1}^2 - 2{x_2}^2 \end{bmatrix} \tag{B.12}$$

This way, state variable $\dot{x}_8$ can be rewritten as:

$$\dot{x}_8 = ((2x_5x_6 - 2x_4x_7) \times (2x_1x_3 + 2x_0x_2)) + ((1 - 2{x_5}^2 - 2{x_7}^2) \times (2x_2x_3 - 2x_0x_1)) + ((2x_6x_7 + 2x_4x_5) \times (1 - 2{x_1}^2 - 2{x_2}^2)) \tag{B.13}$$

In order to linearize and discretize the state equation, equation 3.26 was defined:

$$\Delta x_{k+1} = A_k \Delta x_k + w_k \tag{B.14}$$

The transition matrix $A_k$ is a 9×9 matrix written as follows: each line $i$ and each column $j$ corresponds to the respective state variable ($i$=$j$=0,1,..,9); each pair $ij$ corresponds to the partial derivative of state variable $i$ relative to state variable $j$. Therefore, matrix $A_k$ is defined by:

$$A_k = \begin{bmatrix} 1\Delta t & -\frac{{}^{b}w_x^U\Delta t}{2} & -\frac{{}^{b}w_y^U\Delta t}{2} & -\frac{{}^{b}w_z^U\Delta t}{2} & 0 & 0 & 0 & 0 & 0 \\ \frac{{}^{b}w_x^U\Delta t}{2} & 1\Delta t & \frac{{}^{b}w_z^U\Delta t}{2} & -\frac{{}^{b}w_y^U\Delta t}{2} & 0 & 0 & 0 & 0 & 0 \\ \frac{{}^{b}w_y^U\Delta t}{2} & -\frac{{}^{b}w_z^U\Delta t}{2} & 1\Delta t & \frac{{}^{b}w_x^U\Delta t}{2} & 0 & 0 & 0 & 0 & 0 \\ \frac{{}^{b}w_z^U\Delta t}{2} & \frac{{}^{b}w_y^U\Delta t}{2} & -\frac{{}^{b}w_x^U\Delta t}{2} & 1\Delta t & 0 & 0 & 0 & 0 & 0 \\ 0 & 0 & 0 & 0 & 1\Delta t & -\frac{{}^{b}w_x^L\Delta t}{2} & -\frac{{}^{b}w_y^L\Delta t}{2} & -\frac{{}^{b}w_z^L\Delta t}{2} & 0 \\ 0 & 0 & 0 & 0 & \frac{{}^{b}w_x^L\Delta t}{2} & 1\Delta t & \frac{{}^{b}w_z^L\Delta t}{2} & -\frac{{}^{b}w_y^L\Delta t}{2} & 0 \\ 0 & 0 & 0 & 0 & \frac{{}^{b}w_y^L\Delta t}{2} & -\frac{{}^{b}w_z^L\Delta t}{2} & 1\Delta t & \frac{{}^{b}w_x^L\Delta t}{2} & 0 \\ 0 & 0 & 0 & 0 & \frac{{}^{b}w_z^L\Delta t}{2} & \frac{{}^{b}w_y^L\Delta t}{2} & -\frac{{}^{b}w_x^L\Delta t}{2} & 1\Delta t & 0 \\ a\Delta t & b\Delta t & c\Delta t & d\Delta t & e\Delta t & f\Delta t & g\Delta t & h\Delta t & 1\Delta t \end{bmatrix} \tag{B.15}$$

where $a$, $b$, $c$, $d$, $e$, $f$, $g$ and $h$ are defined as follows:

$$a = 4x_5x_6x_2 - 4x_4x_7x_2 - 2x_1 + 4{x_5}^2x_1 + 4{x_7}^2x_1 \tag{B.16}$$

$$b = 4x_5x_6x_3 - 4x_4x_7x_3 - 2x_8 + 4{x_5}^2x_0 + 4{x_7}^2x_0 - 8x_1x_6x_7 - 8x_1x_4x_5 \tag{B.17}$$

$$c = 4x_5x_6x_0 - 4x_4x_7x_0 + 2x_3 - 4{x_5}^2x_3 - 4{x_7}^2x_3 - 8x_2x_6x_7 - 8x_2x_4x_5 \tag{B.18}$$

$$d = 4x_5x_6x_1 - 4x_4x_7x_1 + 2x_2 - 4{x_5}^2x_2 - 4{x_7}^2x_2 \tag{B.19}$$

$$e = -4x_7x_1x_3 - 4x_7x_0x_2 + 2x_5 - 4{x_1}^2x_5 - 4{x_2}^2x_5 \tag{B.20}$$

$$f = 4x_6x_1x_3 + 4x_6x_0x_2 - 8x_5x_2x_3 + 8x_5x_0x_1 + 2x_4 - 4{x_1}^2x_4 - 4{x_2}^2x_4 \tag{B.21}$$

$$g = 4x_5x_1x_3 + 4x_5x_0x_2 - 8x_5x_2x_3 + 8x_5x_0x_1 + 2x_7 - 4{x_1}^2x_7 - 4{x_2}^x_7 \tag{B.22}$$

$$h = -4x_4x_1x_3 - 4x_4x_0x_2 + 2x_6 - 4{x_1}^2x_6 - 4{x_2}^2x_6 \tag{B.23}$$

The discrete measurement model is $z_k$, defined in equation 3.27 describes the measurement matrix $H_k$ which is a 8×8 identity matrix:

$$H_k = \begin{bmatrix} 1 & 0 & 0 & 0 & 0 & 0 & 0 & 0 \\ 0 & 1 & 0 & 0 & 0 & 0 & 0 & 0 \\ 0 & 0 & 1 & 0 & 0 & 0 & 0 & 0 \\ 0 & 0 & 0 & 1 & 0 & 0 & 0 & 0 \\ 0 & 0 & 0 & 0 & 1 & 0 & 0 & 0 \\ 0 & 0 & 0 & 0 & 0 & 1 & 0 & 0 \\ 0 & 0 & 0 & 0 & 0 & 0 & 1 & 0 \\ 0 & 0 & 0 & 0 & 0 & 0 & 0 & 1 \end{bmatrix} \tag{B.24}$$

Regarding the process and measurement noise covariance matrices, $Q_k$ and $R_k$, respectively, they are related with uncertainties. Since the process noise $w_k$ was considered to be zero, $Q_k$ is a 9×9 zero matrix. The measurement noise covariance matrix $R_k$ represents the level of confidence

placed in the accuracy of the measurements. Assuming the measurements are uncorrelated, $R_k$ is a $8\times8$ diagonal matrix, whose diagonal elements are the variance of individuals measurements. In this case, the variance of individuals measurements was considered to be 0.0001. Therefore, $Q_k$ and $R_k$ are defined as:

$$Q_k = \begin{bmatrix} 0 & 0 & 0 & 0 & 0 & 0 & 0 & 0 \\ 0 & 0 & 0 & 0 & 0 & 0 & 0 & 0 \\ 0 & 0 & 0 & 0 & 0 & 0 & 0 & 0 \\ 0 & 0 & 0 & 0 & 0 & 0 & 0 & 0 \\ 0 & 0 & 0 & 0 & 0 & 0 & 0 & 0 \\ 0 & 0 & 0 & 0 & 0 & 0 & 0 & 0 \\ 0 & 0 & 0 & 0 & 0 & 0 & 0 & 0 \\ 0 & 0 & 0 & 0 & 0 & 0 & 0 & 0 \end{bmatrix} \tag{B.25}$$

$$R_k = \begin{bmatrix} 0.0001 & 0 & 0 & 0 & 0 & 0 & 0 & 0 \\ 0 & 0.0001 & 0 & 0 & 0 & 0 & 0 & 0 \\ 0 & 0 & 0.0001 & 0 & 0 & 0 & 0 & 0 \\ 0 & 0 & 0 & 0.0001 & 0 & 0 & 0 & 0 \\ 0 & 0 & 0 & 0 & 0.0001 & 0 & 0 & 0 \\ 0 & 0 & 0 & 0 & 0 & 0.0001 & 0 & 0 \\ 0 & 0 & 0 & 0 & 0 & 0 & 0.0001 & 0 \\ 0 & 0 & 0 & 0 & 0 & 0 & 0 & 0.0001 \end{bmatrix} \tag{B.26}$$

As it can been seen, despite the index $k$, $Q_k$ and $R_k$ are not $k$-dependent, instead they are constant.

In order to start the EKF, $\hat{x}_0^-$ was set to $[0.5, 0.5, 0.5, 0.5, 0.5, 0.5, 0.5, 0.5, 0]$ and $P_0^-$ to $[100, 100, 100, 100, 100, 100, 100, 100]$.